

University of Southern Queensland
Faculty of Engineering & Surveying

**The Bodywork Package for the USQ's Formula-SAE
Racer**

A dissertation submitted by

Ken Nelder

in fulfilment of the requirements of

ENG4112 Research Project

towards the degree of

Bachelor of Mechanical Engineering

Submitted: October, 2004

Abstract

The University of Southern Queensland has entered a team in the 2004 Formula SAE-A competition. That team comprises nine people, each of whom are designing a different system for the USQ's inaugural entry into the F-SAE-A competition. This project deals with the design of the bodywork. By looking at the solid modelling, Computational Fluid Dynamics (CFD), and manufacturing aspects of this design, I intend to have designed by October, and constructed by December, 2004, a fully functional bodywork package for the vehicle.

Using a solid modelling package, the shape will be developed, then transferred into a CFD software package and analysed. If it is satisfactory, the solid model will be used to create full-size male plugs, which will be used to shape the bodywork.

Factors that will influence the design include its aerodynamic performance in the CFD analyses, its aesthetic appeal (this may invite sponsorship), and its ability to be manufactured. A great aerodynamic design has no use if it cannot be manufactured.

These factors, and more, will be investigated during the course of this project.

University of Southern Queensland
Faculty of Engineering and Surveying

ENG4111/2 <i>Research Project</i>
--

Limitations of Use

The Council of the University of Southern Queensland, its Faculty of Engineering and Surveying, and the staff of the University of Southern Queensland, do not accept any responsibility for the truth, accuracy or completeness of material contained within or associated with this dissertation.

Persons using all or any part of this material do so at their own risk, and not at the risk of the Council of the University of Southern Queensland, its Faculty of Engineering and Surveying or the staff of the University of Southern Queensland.

This dissertation reports an educational exercise and has no purpose or validity beyond this exercise. The sole purpose of the course pair entitled “Research Project” is to contribute to the overall education within the student’s chosen degree program. This document, the associated hardware, software, drawings, and other material set out in the associated appendices should not be used for any other purpose: if they are so used, it is entirely at the risk of the user.

Prof G Baker

Dean

Faculty of Engineering and Surveying

Certification of Dissertation

I certify that the ideas, designs and experimental work, results, analyses and conclusions set out in this dissertation are entirely my own effort, except where otherwise indicated and acknowledged.

I further certify that the work is original and has not been previously submitted for assessment in any other course or institution, except where specifically stated.

KEN NELDER

Q11221429

Signature

Date

Acknowledgments

This project would have been impossible for me if it were not for the invaluable input of so many people.

My supervisors, Mr. Chris Snook and Dr. Ruth Mossad, who have always been able to give some instruction or advice, have been indispensable.

Buchanan Advanced Composites (BAC) have given me immense amounts of support. My thanks go to Norm Watt, Managing Director, Anil Puttaswamy, BAC's resident CNC expert, Martin Rees, engineer, Don Britton for the resin, Bruce Dascombe for his professional advice, and the rest of the boys and BAC.

Also thanks to Vivienne French, Brad Moody and Les Rayner, for their invaluable assistance in the construction of the bodywork, Selvan Pather, for the construction and testing ideas in passing conversation that were so simple, yet so effective, and to David Guscott, Sean Cochrane, and the team at Skelta Sportscars for your experienced views.

To my boss, Cameron Marchant, and my parents for suffering my incessant preoccupation with "my project", instead of with tidiness both in the store and at home.

Without the collective support of these people, this task would have been more than a little out of my reach.

KEN NELDER

University of Southern Queensland

October 2004

Contents

Abstract	i
Acknowledgments	iv
List of Figures	xii
List of Tables	xxiv
Chapter 1 Introduction, Aims and Definitions	1
1.1 What is Formula-SAE?	1
1.2 What is Aerodynamics?	2
1.3 Aims of this project	5
1.3.1 Scope Of This Project	6
1.4 Definitions - Aerodynamic	8
1.4.1 Drag	8
1.4.2 Lift	10
1.4.3 Downforce	11

CONTENTS	vi
1.4.4 Pressure	11
1.4.5 Streamlines	12
1.4.6 Laminar Flow	13
1.4.7 Turbulent Flow	13
1.4.8 Reynolds Number	14
1.4.9 Separation	14
1.4.10 Reattachment	15
1.4.11 Turbulence	15
1.4.12 Boundary Layer	16
1.4.13 Stagnation Point	16
1.5 Definitions - Vehicle-related	17
1.5.1 General	17
1.5.2 USQ Motorsport's F-SAE-A 2004 Entry-specific	19
1.6 Definitions - Computer Related	21
1.6.1 Loft	21
 Chapter 2 Background	 23
 Chapter 3 Overview of Softwares Used	 26
3.1 Chapter Overview	26
3.2 CAE And The FEM	26

3.2.1	Wire Frame Modelling	29
3.2.2	Surface Modelling	29
3.2.3	Solid Modelling	29
3.3	Software Used	31
3.3.1	Solid Modelling Software	31
3.3.2	Geometry Processing Software	32
3.3.3	CFD Software	33
Chapter 4 Methodology - Solid Modelling		34
4.1	Chapter Overview	34
4.2	Solid Modelling - The Chassis Model	36
4.3	Solid Modelling - The Nose Model	40
4.3.1	The First Model	42
4.3.2	The Second Model	47
4.3.3	The Third Model	52
4.3.4	The Fourth Model	55
4.3.5	The Fifth Model	57
4.3.6	The Sixth Model	62
4.3.7	The Final Model	65
4.4	The Centre Section	70
4.5	The Rear End CFD Model	76

4.6	Defeaturing the CFD Model	78
4.7	Exporting The ACIS File	80
4.8	Review Of Solid Modelling	80
Chapter 5 Methodology - Geometry Processing and Mesh Creation		81
5.1	Chapter Overview	81
5.2	The 2-Dimensional Tests	82
5.3	Importing The ACIS File	85
5.4	Cleaning Up The Geometry	86
5.4.1	IGES Files	87
5.4.2	ACIS Files	87
5.5	Adding The Duct	88
5.6	Applying The Meshes	90
5.7	Setting The Boundary Types	91
5.8	Exporting The Mesh File	92
5.9	Review Of Geometry Processing And Mesh Creation	92
Chapter 6 Methodology - CFD		93
6.1	Chapter Overview	93
6.2	Importing The Mesh File	93
6.3	The Grid Menu	94

6.4	The Define Menu	95
6.4.1	Models	95
6.4.2	Materials...	98
6.4.3	Operating Conditions...	98
6.4.4	Boundary Conditions...	99
6.5	The Solve Menu	103
6.5.1	Controls	103
6.5.2	Initialise...	104
6.5.3	Monitors...	106
6.6	Reference Values	108
6.7	Iterate...	109
6.8	The Other menus	109
6.9	2D Experiments	110
6.9.1	Gaining Convergence	110
6.9.2	Gaining Accuracy	115
6.10	The 3D models	117
6.11	Review of CFD	123
Chapter 7 Methodology - Construction		124
7.1	Chapter Overview	124
7.1.1	BAC's Milling Machine	126

7.2	Materials, and Thickness and Fastening	127
7.3	Construction Of The Nose	131
7.4	Construction Of The Centre Section	142
7.5	Review of Construction	145
Chapter 8 Results		146
8.1	Chapter Overview	146
8.2	Solid Models	147
8.3	The CFD Results	150
8.3.1	Contour Plots	150
8.3.2	Vector Diagrams	155
8.3.3	Turbulence	156
8.3.4	Coefficient of Drag	157
8.4	Chapter Summary	157
Chapter 9 Conclusions And Further Work		158
References		160
Appendix A Project Specification		162
Appendix B F-SAE Rules Extracts		165
B.1	Introduction to this Appendix	165

Appendix C Solid Modelling	171
C.1 Introduction to this Appendix	171
C.2 Chassis	172
C.3 Nose	176
C.4 Nose Model Cross-Sections	185
C.4.1 Nose 1	185
C.4.2 Nose 2	188
C.4.3 Nose 2 - redesign	191
C.4.4 Nose 3	194
C.4.5 Nose 4	197
C.4.6 Nose 5	200
C.4.7 Nose 6	202
C.4.8 The Final Model	205
Appendix D Cost Report	208
D.1 Introduction to this Appendix	208

List of Figures

1.1	This is a computer simulation of streamlines (defined later in this chapter) in the flow around a Formula 1 car, coloured with respect to pressure (<i>F1 Racing</i> March 2003).	2
1.2	Vortices producing induced drag on a car (Hucho 1987).	9
1.3	The teardrop is the shape with the lowest drag coefficient (Edgar 2000).	10
1.4	A Porsche 911. Note the aerofoil shape, and the large “Whale-Tail” rear spoiler (Hucho 1987).	11
1.5	Smoke visualisation of streamlines along the centreline of a car in a full-scale wind tunnel (Edgar 2000).	13
1.6	Airflow over the rear end of a car separating at the end of the roof (left), and remaining attached until the bottom of the rear window (right) (Hucho 1987).	14
1.7	Wind-tunnel illustration of clean airflow separation from the top of a cab-spoiler on a truck, then clean reattachment to the top of the trailer (Hucho 1987).	15
1.8	The development of a boundary layer in flow over a flat plate (Fox & McDonald 2003).	16

1.9	Stagnation and separation points in flow over a cylinder (Fox & McDonald 2003).	17
1.10	The chassis members defining the “Kneebox”. Some members have been omitted for clarity.	20
1.11	The cross section sketches and interpolating splines defining the lofted feature of the nose section.	22
3.1	Building a block using Boundary Representation (Snook 2003 <i>a</i>).	31
3.2	Building a block using Constructive Solid Geometry (Snook 2003 <i>a</i>).	32
4.1	The planes defined in Table 4.2.	37
4.2	The two elliptical end section sketches and the centreline for the port front diagonal member. Note also the reference planes shown in light grey.	38
4.3	Trigonometric calculation of the ellipse height for lofting the front diagonal chassis member.	38
4.4	Centreline sketches for (a) the port side of the front roll hoop, (b) the port side of the main roll hoop, and (c) the port upper side impact member.	39
4.5	The completed SolidWorks chassis model.	40
4.6	The first nose model.	43
4.7	The bulkhead sketch, showing the extremities of the chassis bulkhead (the light grey rectangle) and the nose shaper (the light grey circle).	44
4.8	The kneebox sketch, showing the bulkhead sketch in light grey.	44
4.9	The cross-section sketch at the front hoop, showing the separate line segments.	45

4.10	The different faces of the first nose design. Each alternate face is highlighted in green. These faces are produced by SolidWorks, one face for each line segment in the sketches.	46
4.11	Recirculation occurring due to sudden changes in geometry.	46
4.12	A comparison of the bulkhead cross-sections of the first (left) and second nose models.	47
4.13	A comparison of the face join lines between the first (left) and second models, showing the face edges on the second model varying much less than those on the first.	48
4.14	The second nose design.	48
4.15	The mid-life redesign of the second nose model.	49
4.16	The definition of the line segments in the front hoop and the bulkhead and kneebox sketches.	50
4.17	The edges of the redesigned nose were as close as possible to being tangential to the predicted flow.	50
4.18	Front view of the face edges, showing them not bending tangentially to the bodywork surface along their length.	51
4.19	The new nose shaper sketch, made from six line segments, and flat on the bottom.	53
4.20	The floor-level overshoot caused by lofting between two sections whose lowest points are not level.	54
4.21	The fourth nose model.	55
4.22	The separate faces still being created in this model.	56

4.23	The fillet at the edge of the floor panel is not parallel to the z-axis, and so does not follow the rail chassis members correctly.	56
4.24	The fifth nose model. Note the one-piece top panel design.	58
4.25	The bulkhead sketch used to define the shape of the fifth nose model.	59
4.26	The kneebox sketch from the fifth nose model. The bulkhead sketch is shown in grey.	59
4.27	The depression intended to deflect airflow over the driver's head.	60
4.28	The kneebox sketch used to define the depression shown in Figure 4.27.	61
4.29	The first assembly, showing the fit between the nose and the chassis. It includes a very simple motor model. Note that the fit is not perfect, as the top chassis members between the bulkhead and the front hoop protrude through the bodywork	62
4.30	The sketch defining the cut used to round off the nose point.	63
4.31	The rounded nose. This would not comply to the rules, as the radius around the bottom edge is too small.	63
4.32	The bottom edge as created, without the fillet.	64
4.33	The bottom edge with a constant 40mm radius fillet.	64
4.34	The final design, complete with a suspension cutout to clear the wishbones.	65
4.35	The floor of the nose, showing that its edges are not parallel aft of the bulkhead. Also visible is the change in radius of the fillet along the length of the filleted edge	66
4.36	The chassis protruding through the bodywork.	67
4.37	The sketch for the extruded cut outlined in the text.	67

4.38	The extruded cut used to replace the variable radius fillet.	68
4.39	The variation in the radius of the nose fillet.	68
4.40	The straight-edged cut (aft of the bulkhead) merged well with the variable-radius fillet (forward).	69
4.41	$\% \Delta C_D$, as a function of stagnation point height (Hucho 1987).	69
4.42	ΔC_D , as a function of the stagnation point height-vehicle height ratio (Hucho 1987).	70
4.43	The basic early centre section model, using an arbitrary cockpit rim shape.	71
4.44	The base loft feature.	71
4.45	The base loft feature, from the other side from Figure 4.44.	72
4.46	Half of the under side being added.	72
4.47	Rear view of Figure 4.46.	73
4.48	The mirrored part, completing the basic solid model. Note also the highlighted edges. These are to be filleted later.	73
4.49	The definition of the extruded cut used to allow the edges shown in Figure 4.48 to be filleted.	74
4.50	The fillets fully defined, curving around the chassis members.	75
4.51	The sketch used to define the cut to create the plug model.	75
4.52	The completed centre section plug.	76
4.53	The port and starboard plugs assembled to create one model. This will halve the set-up time for the machining operation.	76
4.54	The main hoop sketch to create the rear end of the CFD defeature.	77

4.55	The rearmost sketch to create the rear end of the CFD defeature.	77
4.56	The rear end of the CFD defeature.	78
4.57	The full assembly model, including chassis, motor and firewall.	79
4.58	The defeatured CFD assembly model.	79
5.1	C_D figures for some simple shapes (Fox & McDonald 2003).	83
5.2	The mesh applied to the simple 2D square test model.	83
5.3	An asymmetric wake pattern.	84
5.4	The ACIS file imported. The blue coloured lines indicate correct connectivity with adjacent areas.	86
5.5	The wireframe of the CFD defeatured model. The extra area on the duct floor is used to make meshing the floor easier and faster to re-mesh.	88
5.6	The wireframe of the geometrically-clean car. Note the square bottoms on the tyres.	89
5.7	The triangular mesh as applied to the nose of the car.	91
6.1	The mesh used for the square test.	94
6.2	Dynamic Pressure contours on the square test, showing bunching resultant from incorrect designation of the “Compute from” field.	105
6.3	A similar effect to that shown in Figure 6.3, except using a lengthened duct.	105
6.4	Velocity vectors, coloured by velocity magnitude, of the 2D test.	110
6.5	The convergence plot for the first 2D analysis.	111

6.6	Residual plot for square test, using a combination of the fastest-converging under-relaxation factors.	114
6.7	Residual plot for square test, using the same under-relaxation factors as Figure 6.6, except $\tilde{P} = 0.4$	114
6.8	Residual plot for square test, using final under-relaxation factors.	115
6.9	Deconvergence resulting from the use of a coupled implicit solver scheme.	116
6.10	The final convergence plot for the 2D model.	117
6.11	Static pressure contours over the body of the sedan model.	118
6.12	Static pressure contours from a professional CFD analysis (Edgar 2000).	119
7.1	BAC's milling machine executing its rough-cut.	126
7.2	The surface finish after the smooth cut (to the left of the cutter) is very different from that after the rough cut (to the right).	127
7.3	The locations of the MDF cross-sections, with respect to the front hoop and the bulkhead.	131
7.4	The foam blocks marked out, ready to cut.	132
7.5	Brad Moody cutting the foam blocks on a bandsaw.	132
7.6	The near-failure. Four layers of wet resin allow floating of the parts before it cures.	133
7.7	Each section was mated to a foam block and the resin allowed to cure before continuing.	134
7.8	The blocks added to fill the gaps left by foam blocks that were too small.	135
7.9	130mm of nose cone being cut on the CNC machine.	136

7.10 Vivienne French uses a handsaw to cut away unwanted material before sanding begins.	137
7.11 Comparison of rough-cut and sanded foam.	138
7.12 The partially bogged nose plugs side by side.	139
7.13 Close-up of a patch of bog, showing the eroded foam on each side.	139
7.14 Eroded foam adjacent to the bog around the section 150mm forward of the front hoop.	140
7.15 The light angle shows up eroded foam very well.	140
7.16 Care must be taken to avoid removing good material with the handsaw.	141
7.17 A typical place that has yet to be bogged.	142
7.18 The assembly of the two side panel to form one part that may be machined in one run, thereby halving set-up time.	143
8.1 The SolidWorks chassis model.	147
8.2 The final nose design.	148
8.3 The port side panel.	148
8.4 A full assembly model, including steering, suspension and drivetrain components.	149
8.5 The CFD defeature in its correct colours.	150
8.6 Static pressure contours.	150
8.7 Dynamic pressure contours.	151
8.8 Turbulent Kinetic Energy (TKE, or k).	152

8.9	Turbulence intensity (%).	153
8.10	Turbulence dissipation rate, ϵ .	153
8.11	Vorticity magnitude.	154
8.12	Recirculation occurring due to a change in geometry.	154
8.13	Velocity vectors over the nose.	155
8.14	Velocity vectors over the side of the car.	155
8.15	Close up on the cockpit rim from Figure 8.14.	156
9.1	Wool-tuft testing a VR Commodore (Edgar 2000).	159
9.2	Smoke testing the wake behind an R32 Skyline (Edgar 2000).	159
C.1	The planes defined in Table 4.2.	172
C.2	The two elliptical end section sketches and the centreline for the port front diagonal member. Note also the reference planes, “Bulkhead”, “Kneebox”, “Front Hoop” and “Rail”.	172
C.3	Trigonometric calculation of the ellipse height for lofting the front diagonal chassis member.	173
C.4	Centreline sketch for the port side of the main roll hoop.	173
C.5	Centreline sketch for the port side of the front roll hoop.	174
C.6	Centreline sketch for the port upper side impact member.	174
C.7	The completed SolidWorks chassis model.	175
C.8	The first nose model.	176

C.9	The first nose model in wireframe, showing the many face edges, which will not be parallel to the airflow.	177
C.10	The second nose model. Note the bulges over the bulkhead have been reduced.	177
C.11	The second nose model in front view. Note the curvature of the face edges.	178
C.12	The redesign of the second nose model. Note the slight streamlining of the face edges.	179
C.13	The second model redesign, front view, showing the straighter edges. . .	179
C.14	The bulkhead sketch of the second model. Note the radiating construction lines defining the path for the face edges.	180
C.15	The third model.	180
C.16	The fourth model, showing the one-piece top surface, and the “duck-bill” nose”	181
C.17	The fifth nose model. Note the one-piece top surface.	181
C.18	The sixth nose model. Here, the fillet has been added around the nose point.	182
C.19	The sixth model, using an extruded cut and a revolved solid to round off the nose point.	182
C.20	The final model, showing the one-piece design, variable-radius fillet, and suspension cutouts.	183
C.21	The blisters designed to clear the attachment of the crush zone to the chassis.	183
C.22	Looking inside the final shelled model.	184

C.23 First nose model “nose point” cross section.	185
C.24 First nose model “nose shaper” cross section.	186
C.25 First nose model “bulkhead” cross section.	186
C.26 First nose model “kneebox” cross section.	187
C.27 First nose model “front hoop” cross section.	187
C.28 Second nose model “nose point” cross section.	188
C.29 Second nose model “nose shaper” cross section.	188
C.30 Second nose model “bulkhead” cross section.	189
C.31 Second nose model “kneebox” cross section.	189
C.32 Second nose model “front hoop” cross section.	190
C.33 Second nose model redesign “nose point” cross section.	191
C.34 Second nose model redesign “nose shaper” cross section.	191
C.35 Second nose model redesign “bulkhead” cross section.	192
C.36 Second nose model redesign “kneebox” cross section.	192
C.37 Second nose model redesign “front hoop” cross section.	193
C.38 Third nose model “nose point” cross section.	194
C.39 Third nose model “nose shaper” cross section.	194
C.40 Third nose model “bulkhead” cross section.	195
C.41 Third nose model “kneebox” cross section.	195
C.42 Third nose model “front hoop” cross section.	196

C.43 Fourth nose model “nose point” cross section.	197
C.44 Fourth nose model “nose shaper” cross section.	197
C.45 Fourth nose model “bulkhead” cross section.	198
C.46 Fourth nose model “kneebox” cross section.	198
C.47 Fourth nose model “front hoop” cross section.	199
C.48 Fifth nose model “nose point” cross section.	200
C.49 Fifth nose model “nose shaper” cross section.	200
C.50 Fifth nose model “bulkhead” cross section.	201
C.51 Fifth nose model “kneebox” cross section.	201
C.52 Fifth nose model “front hoop” cross section.	202
C.53 Sixth nose model “nose point” cross section.	202
C.54 Sixth nose model “nose shaper” cross section.	203
C.55 Sixth nose model “bulkhead” cross section.	203
C.56 Sixth nose model “kneebox” cross section.	204
C.57 Sixth nose model “front hoop” cross section.	204
C.58 Final nose model “nose point” cross section.	205
C.59 Final nose model “nose shaper” cross section.	205
C.60 Final nose model “bulkhead” cross section.	206
C.61 Final nose model “kneebox” cross section.	206
C.62 Final nose model “front hoop” cross section.	207

List of Tables

4.1	The reference planes created and the manner in which they were defined. . . .	36
6.1	Under-Relaxation Factor default values	103
6.2	Under Relaxation values for the 2D tests.	109
6.3	Under Relaxation values for the 2D tests.	112
6.4	Summary of variable Define menu settings for the analysis of the SAE car in FLUENT.	120
6.5	Summary of variable Solve menu settings for the analysis of the SAE car in FLUENT.	121
6.6	Summary of reference values for the analysis of the SAE car in FLUENT. . . .	121
6.7	A listing of some known C_D figures (Edgar 2000).	122
7.1	Summary of properties of Aluminium, Fibreglass and Carbon Fibre (densities averaged from (<i>Matweb Website Properties Search</i> 2004))	128

Chapter 1

Introduction, Aims and Definitions

1.1 What is Formula-SAE?

Formula SAE is a competition formed by the Society of Automotive Engineers, for university students to design, construct and run a small, formula-style racing car. It was conceived and has run for years in the USQ as Formula SAE, and now runs also in Britain and Formula Student, and in Australia as Formula SAE-Australia.

The major limitations of the Formula are that the engine capacity must not exceed 610cc, and a 20mm diameter restrictor must be placed in the air intake, upstream from any turbo or superchargers (if used). Other than that, the rules merely define the layout of a Formula-style car (open cockpit, four exposed wheels, not in a straight line, etc.), and provide minimum safety standards.

This year, 2004, the University of Southern Queensland was entered in the Australian competition. A team was formed, calling itself USQ Motorsport, and each team member chose a major system of the car (chassis, engine, driveline, suspension, steering, interior, and exterior bodywork) to design. The team also has a latent designer, who is designing a monocoque chassis to replace the spaceframe chassis and bodywork in a future car,

and a project student manager.

This project deals with the design of the bodywork for the USQ's inaugural entry into the Formula SAE-A competition, from the modelling, aerodynamic and construction standpoints.

1.2 What is Aerodynamics?

Aerodynamics is the study of gas flow, usually air over a body, and is becoming increasingly important in many facets of modern life. It determines how much drag and lift a body generates as it moves through the air, and has been a major factor in aircraft design since the invention of the aircraft, for this reason.

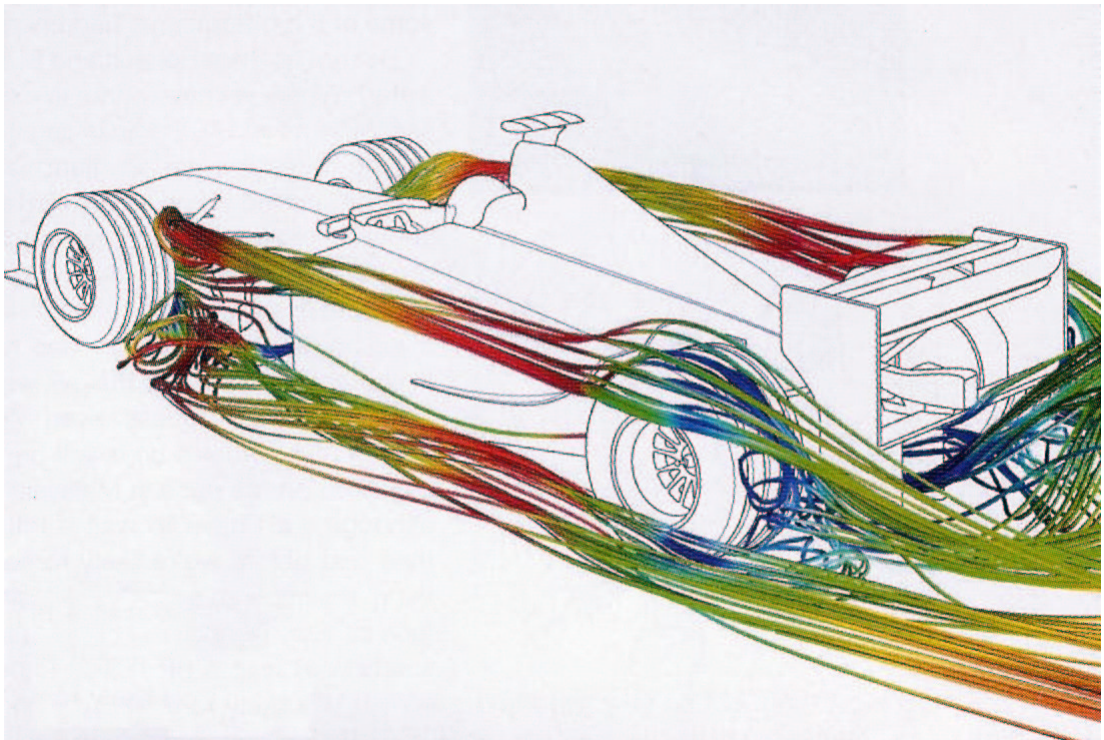


Figure 1.1: This is a computer simulation of streamlines (defined later in this chapter) in the flow around a Formula 1 car, coloured with respect to pressure (*F1 Racing* March 2003).

Latterly, the study of aerodynamics has been applied to automotive design, first in the racing application, then in the design of the personal car.

Lift (or, when turned upside-down, ‘downforce’) can affect the handling characteristics of a car when turning, or in a cross-wind, while drag will slow the car and increase its fuel consumption. In today’s world, every little bit of increased safety and economy is most important.

However, this dissertation focusses on the application of aerodynamics to an open-wheeled, formula-style race car, the aerodynamic requirements of which are different from those of a road car.

The desired outcomes of the aerodynamic design of such a car are:

- Low drag - Drag merely slows the car down and uses more fuel.
- Stability - Predictable and stable handling is paramount, especially when cornering.
- Traction - Higher traction allows faster acceleration, braking and cornering speeds.

Traction is increased by increasing the ‘downforce’ on the car. Downforce follows the same principle as the lift that an aircraft generates to fly, but turns it upside-down, to push the car onto the track. This increases the normal force on the tyres, and therefore traction, without increasing the mass and inertia of the vehicle (Smith 1978).

Stability is also increased via the use of downforce, but by tailoring the amount of downforce that is applied to the front and back wheels. If all the downforce were applied to the front wheels, they would have an immense amount of traction, but the rear wheels would have only a small amount. Thus, when the driver enters a corner at a high speed, the front wheels, with lots of traction, will turn very easily and grip the road well, while the rear wheels will lose traction very easily, and slide straight ahead, instead of following the rest of the car around the corner.

Turbulent airflow over the rear of the car may also cause instability, even in a straight line, as vortex shedding under some circumstances causes a cyclic side-force (Gillespie 1992)¹.

In looking at the application of aerodynamics to a formula-style race car, this disserta-

¹Periodic vortex shedding produces phenomenon called “Von Karman’s vortex street”, for $60 \leq Re_D \leq 5000$. This is of interest if cyclic forces due to such vortex shedding is an issue, but occurs only when the geometry is symmetric, which ours is not, so we will not investigate this. For further reading, see (Hucho 1987), section 2.3.4.1 - *Aerodynamic Noise*, and (Gillespie 1992)

tion is limited (by time) to only the bodywork. Other aerodynamic aids are commonly employed by race teams, such as wings, spoilers, bargeboards, etc., but here, we are confined to only the bodywork. The bodywork is the most fundamental part of the aerodynamic design of the car, and is essential in our case to make the car conform to the relevant rules of the F-SAE-A competition. It includes the general shape of the skin, as well as the undertray (also known as a “floorpan”), side-pods (if any), rear diffuser, and the cockpit rim design.

The aerodynamic design of any motor vehicle, and especially that of a racing car, is equally as important as its mechanical design.

On road cars, the design of even minor elements of the vehicle, such as the wing mirrors, front and rear bumpers and the shape of the fuel tank can have major effects on not only speed, but on fuel economy and, perhaps most importantly from a safety aspect, stability. The air that passes around the side, over the top, and underneath the car exerts pressures on the car that are capable of slowing it down, causing noise and vibration, pushing or sucking it onto the road, and even causing it to become unstable under some conditions². These are all factors which should be taken into consideration when designing a road car, paying particular attention to how they affect the driver and his or her ability to control the vehicle. The driver will want a car that does not have too much wind noise, does not use too much fuel, and is easy to drive around corners and in windy conditions.

However, the area of interest of this project is the aerodynamics of a formula-style race car, to the racing aspects of which the requirements and laws of aerodynamics apply even more directly. A race driver will sacrifice every luxury for more performance, and so will still want a car that accelerates quickly, has a high top speed, and most importantly, remains stable when cornering. A race car requires every small amount of extra power it can possibly get out of the engine, and if half a kilowatt of power is being blown away into the surrounding air (which is effectively what happens when drag is induced), the car cannot then use that power to drive itself forward. In a high-tech

²Some Formula 1 cars routed their exhaust into the low-pressure area at the rear of the underside of the car, which provided slight power gains and reduced drag, but also made the rear end of the car become unstable when the throttle was suddenly closed, greatly increasing the probability of a crash. This practice was soon abandoned.

and high-cost industry where speeds and times are measured to two or three decimal places, losing that amount of power and therefore energy is purely unacceptable.

But what can be done to improve the aerodynamics of a race car? Indeed, what *are* the so-called “aerodynamics” of a car?

Aerodynamics is the science or the study of air flow. The word is frequently used to describe the ease with which a car (or an aircraft) slips through the air. The more easily it moves through the air, the better its aerodynamics are said to be. But this field is much more complex than objects merely “slipping” through air. The science of manipulating, but not overly disrupting the air through which a body moves is extremely complex. Millions of dollars are spent each year by road and race car companies on improving the aerodynamics of their cars.

1.3 Aims of this project

As can be seen in Appendix A, the aims of this project are clearly defined as follows:

1. Research automotive, especially racing aerodynamics, and become familiar with the relevant rules and regulations of F-SAE
2. Review the available software tools for CFD analysis, compare and contrast their capabilities, and use the most appropriate software packages to develop and analyse a simple 2D model of the basic car shape
3. Model the proposed body shape, looking in particular at the airflow over the shape, and the magnitude of its drag
4. Analyse these results, combined with the specifications of the spaceframe design, to develop and analyse a simple model that includes the external shape of the USQ’s Formula-SAE Racer

5. Develop and document techniques for analysing the SAE car with different body geometry

1.3.1 Scope Of This Project

While designing the entire aerodynamic package for this car would be an exceedingly interesting task, it would also be an excessively involving one, and not one which could be fitted into the time available to me. A complete package for a fully competitive race car (such as the one which is the hypothetical aim of the SAE competition) would include a nose, cockpit sides and an engine bay cover, as well as side pods for the radiators (we would use two radiators in such a car), rear diffuser section of the floor panel, front and rear wings with endplates, bargeboards, winglets and keels. However, some of these must be fully designed before others can be started, and the first, most basic of these are the nose and cockpit sides. These are the foundation bodywork parts on which must be built the rest.

A design for front and rear wings would be possible for such an application, if some assumptions were made about the nose shape, or if the nose cone had already been designed. The general feeling among the team members was that at the speeds which the SAE car is expected to reach, downforce from wings would not even become significant, let alone a competitive edge. So before this project was undertaken, a brief preliminary calculation was executed to investigate the feasibility of such a design, using the generally accepted equation for lift:

$$F_L = C_L \frac{1}{2} \rho V^2 A$$

where the coefficient of lift, C_L , is fixed for a certain shape and Reynolds Number (explained in the next section), ρ is the density of the local airflow, V^2 is the relative flow velocity squared, and A is the planar area of the body (i.e., the area of the wing when viewed from the top). Using values of $C_L = 1.6$ (Edgar 2000), $\rho = 1.225 \text{ kg/m}^3$, $V = 20\text{m/s}$ (30m/s being the expected maximum speed), and the planar area of a wing

of appropriate size for this car of about $1m^2$, the lift available from such a wing would be:

$$\begin{aligned} F_L &= 1.6 \times \frac{1}{2} \times 1.225 \times 20^2 \times 1 \\ &= 392N \\ &\Rightarrow 40 \text{ kg downforce} \end{aligned}$$

This sounds promising, considering that this is only the front wing, the rear would be even larger, and the car is expected to weigh only 200-250 kg. However, upon further consideration, it was thought that the maximum *cornering* speed of the car would be around and below 40 km/h (~ 11 m/s), which brings the above calculation down to only 13 kg downforce. Worse, the wings would create a similar drag force to the above figure at 20 m/s, and this would be when we need the least drag to be acting on the car. Additionally, the use of wings on a car like this will only add weight and heighten the centre of mass, making the car accelerate slower, and easier to roll over. So it was quickly decided that in this application, wings would be more of a handicap than an aid, and any future work prospects were promptly dropped.

(For the purposes of the CFD analyses, the velocity used was 16m/s (about 60km/h). Without previous telemetry to give an idea of the time spent in any given speed range, to find out which speed range would be most useful, it was estimated by several members of the USQ Motorsport team that 16m/s would be a useful weighted-average airspeed. The car will not spend enough time above this speed to justify the use of aerodynamics at higher speeds, and the relative airflow is not fast enough at lower speeds to justify any aerodynamic improvements.)

The other aerodynamic aids mentioned above all rely on the major bodywork having been designed, and so will have to wait until such a time as this has been finished before they can be started. So as a result, the field of possibilities for work in the area of aerodynamic design of the USQ's Formula SAE-A racer has been narrowed to the nose cone, cockpit sides and engine bay cover.

The project to design the bodywork for the USQ's Formula-SAE-A racer is also subject to some of the rules of the competition, as set out in the 2003 Formula SAE Rules. The

relevant rules of the competition are compiled in B (for the complete F-SAE-A rules, see (*Formula SAE-A Rules Webpage* 2004)).

So by the end of this project, I aim to have designed, from the aerodynamic, construction and affixation viewpoints, the bodywork for USQ Motorsport's inaugural entry into the Formula-SAE-A competition, abiding by all relevant rules, and to at least have begun to construct it to a standard at which it may be fitted to the car and raced.

In designing the bodywork, I will look at the actual design of the nose and centre-sections (cockpit sides), as these are imperative. If time permits, I will also investigate the feasibility of an engine-bay cover and ducting for the radiator and the engine air intake.

Before embarking on that journey, a few explanations and definitions must be made.

1.4 Definitions - Aerodynamic

To help us to understand this design, the following is a short explanation of terms which are commonly used in the study of aerodynamics, and which will be used in this dissertation.

1.4.1 Drag

The force pulling a moving body in the opposite direction from its motion, attempting to stop the body from moving relative to the air, is called *drag*. Drag is composed of two main types; parasitic drag and induced drag.

Parasitic Drag

Parasitic drag results from the shape and size of the body, and from the mere fact that it is being pushed through the air. It will occur whenever a body is moved through a fluid. Parasitic drag itself is composed of several sub-types, including skin friction

(the friction that results from moving air over a surface) and form drag (the energy transferred to the air in the action of displacing it to move a body through it).

Induced Drag

Induced drag results from turbulence and vorticity imparted to the air by a moving body. Turbulence is essentially eddy currents in the air, which means that the air has velocity, and we know it has mass, therefore, it has kinetic energy (Turbulent Kinetic Energy, denoted by “k” in the CFD analysis). This energy has come from the moving body; i.e., the body is effectively *bleeding* its own kinetic energy to the surrounding fluid. Induced drag is so-called, because it is *induced* by lift. An increase in lift will be accompanied by an increase in vorticity, and so energy bleeding. The vorticity from which induced drag results is shown in Figure 1.2

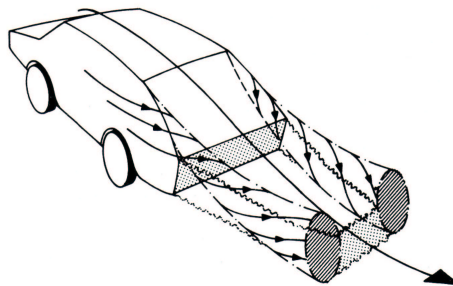


Figure 1.2: Vortices producing induced drag on a car (Hucho 1987).

The magnitude of the drag force (measured in *Newtons*) that will be developed by a body in any given flow conditions is characterised by the non-dimensional parameter, Coefficient of Drag, or C_D . If C_D is known, the drag force, F_D may be calculated using the relationship,

$$F_D = C_D \frac{1}{2} \rho V^2 A$$

where A is the frontal area of the body (i.e., the area of the frontal projection). The effects of every small, body-specific detail that will affect the drag (surface area, roughness, cracks, protrusions, seals and joints, etc.), and of Reynolds Number (explained later) are taken care of in the drag coefficient.

The shape which has the lowest possible C_D is the teardrop (Figure 1.3, (Edgar 2000)).

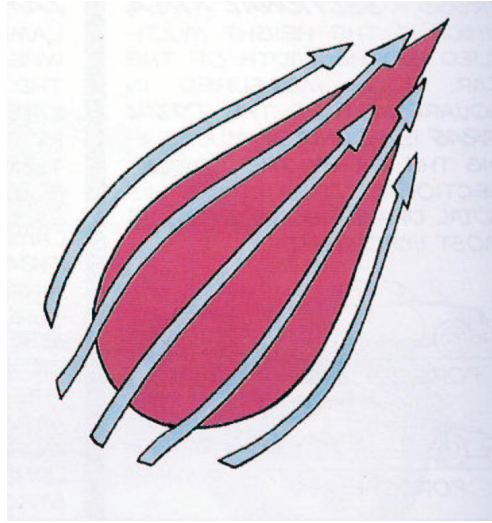


Figure 1.3: The teardrop is the shape with the lowest drag coefficient (Edgar 2000).

1.4.2 Lift

Lift is the force which pulls a body ‘up’ (with respect to the body), which allows an aircraft to fly, lifting the body against the pull of gravity. As described previously, the direct by-product of this is drag, and if lift is increased, so too is drag. Lift is characterised by the non-dimensional parameter, Coefficient of Lift, C_L . Like drag, if C_L is known, lift force can be calculated through:

$$F_L = C_L \frac{1}{2} \rho V^2 A$$

Aerofoils, or aerofoil-like shapes are used to generate lift, although not always to good effect. The Porsche 911 sports car (Figure 1.4) is shaped like an aerofoil, but this creates an upward force which can make the car very unstable at high speeds.



Figure 1.4: A Porsche 911. Note the aerofoil shape, and the large “Whale-Tail” rear spoiler (Hucho 1987).

1.4.3 Downforce

Downforce is effectively lift turned upside-down. It is the force used to great effect by race engineers to increase the traction attainable from the tyres of the race car, without increasing the mass, and therefore inertia, of the car. It pushes the car into the track, and allows it to turn through corners at ludicrous speeds. The wings on a formula-style race car generate the majority of downforce, but race and road cars both produce some downforce by creating a partial vacuum under the car.

1.4.4 Pressure

Pressure is the force caused by fluid particles impacting a body, which is spread over the area of the surface of the body. It is mathematically defined as $Pressure = \frac{Force}{Area}$, and is measured in Pascals (Pa), where one Pascal equals one Newton per square metre. Pressure is usually measured from one of two reference points:

Absolute zero pressure. This gives the total force over the affected area. When this is done, the value is called *Absolute Pressure*, P_{abs} .

Atmospheric pressure (P_{atm}). This gives the nett useable force over the affected area. This is called *Gauge Pressure*, P_g .

These referenced points are mathematically related: $P_{abs} = P_{atm} + P_g$

Pressure can be classified under two main types, Static and Dynamic.

Static Pressure

Static Pressure is “... that pressure that would be measured by an instrument moving with the flow” (Fox & McDonald 2003).

Dynamic Pressure

Dynamic Pressure is that pressure that would be measured by an instrument moving with the body, not with the flow.

The Static and Dynamic pressures add up to give the Total Pressure, so $P_{TOT} = P_{stat} + P_{dyn}$.

1.4.5 Streamlines

Streamlines are defined as: “...lines drawn in the flow field so that at a given instant they are tangent to the direction of flow at every point in the flow field. Since the streamlines are tangent to the velocity vector at every point in the flow field, there can be no flow across a streamline” (Fox & McDonald 2003). That is, a streamline is the line followed by an individual particle which is not moving with respect to the fluid, when the fluid is moving with respect to the body. Streamlines can be illustrated to effect in computer simulations (Figure 1.1) and in wind tunnel tests (Figure 1.5).



Figure 1.5: Smoke visualisation of streamlines along the centreline of a car in a full-scale wind tunnel (Edgar 2000).

1.4.6 Laminar Flow

Laminar flow “...is characterised by smooth motion in laminae, or layers” (Fox & McDonald 2003), and is diagrammatically represented by smoothly-curved or straight, near-parallel streamlines. Adjacent layers of fluid are not mixed, with the exception of diffusion.

1.4.7 Turbulent Flow

In *turbulent flow*, there are no layers, and adjacent fluid ‘elements’ are macroscopically mixed, causing a single streamline to break up into many tangled pieces. This is due to small vortices and random motion of fluid elements with respect to their neighboring elements.

1.4.8 Reynolds Number

The non-dimensional parameter which determines whether a flow field is laminar or turbulent is called *Reynolds Number*. It is defined: $Re = \frac{\rho V D}{\mu}$, where ρ and μ are the density and the absolute viscosity, respectively, of the fluid, V is the relative flow velocity, and D is the characteristic dimension of the body. If the Reynolds Number for a particular fluid is above the critical value (Re_{crit}), the flow is turbulent, while if it is below Re_{crit} , it is laminar. This Re_{crit} depends on the geometry of the flow field and the body.

1.4.9 Separation

Under certain conditions, the flow over a body may become detached from that body. For example, the laminar flow over the upper surface of an aircraft's wing may *separate* from that surface, leaving a near-atmospheric-pressure, recirculating and very turbulent pocket of air in contact with the wing. In this case, this is undesirable, as it reduces lift drastically, but can be used to good effect on a car, for the same reason.

Airflow remaining attached to the upper surface of a car will produce positive lift, which pulls the car upwards, making it hard to drive. The airflow may be deliberately separated from the car in order to reduce lift. This is illustrated in Figure 1.6.

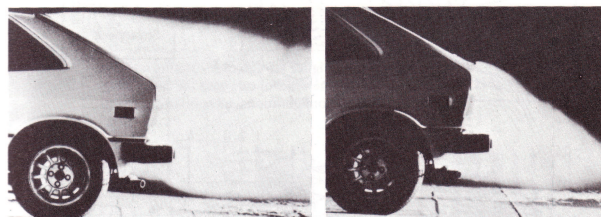


Figure 1.6: Airflow over the rear end of a car separating at the end of the roof (left), and remaining attached until the bottom of the rear window (right) (Hucho 1987).

1.4.10 Reattachment

After a flow has separated from a body, a large, drag-inducing turbulent wake is produced in the space previously occupied by unseparated air. However, through the design of the body geometry, the separated flow may be *reattached* to the body. This allows the resumption of smooth, low-drag, laminar flow, shown in Figure 1.7.

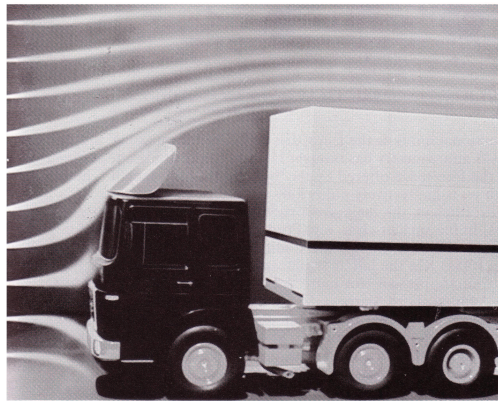


Figure 1.7: Wind-tunnel illustration of clean airflow separation from the top of a cab-spoiler on a truck, then clean reattachment to the top of the trailer (Hucho 1987).

1.4.11 Turbulence

Turbulence is well defined by (A.J. Baker, W.P. Noronha, J.B. Woods 1989) as “the manifestation of a highly persistent small scale motion that substantially changes the continuum appearance of the Stokes and Fourier closure models...”

It manifests itself in the form of eddy currents in the air. This means that the air is moving in small amounts with respect to a reference frame that is moving with the (general) flow, and this motion can be very fast. This results in the bleeding of energy, as described in the section regarding induced drag.

1.4.12 Boundary Layer

The *boundary layer* associated with a viscous fluid flow is that layer adjacent to a stationary surface, in which there exists a shear stress between adjacent particles, and therefore, a velocity gradient extending away from the surface. With reference to Figure 1.8, we can explain that this phenomenon results from the fact that “From the non-slip condition, we know the velocity [of the fluid or a fluid particle] at point A must be zero...[and] at a y location sufficiently far from the plate, say point B, the flow will not be influenced by the presence of the plate” (Fox & McDonald 2003).

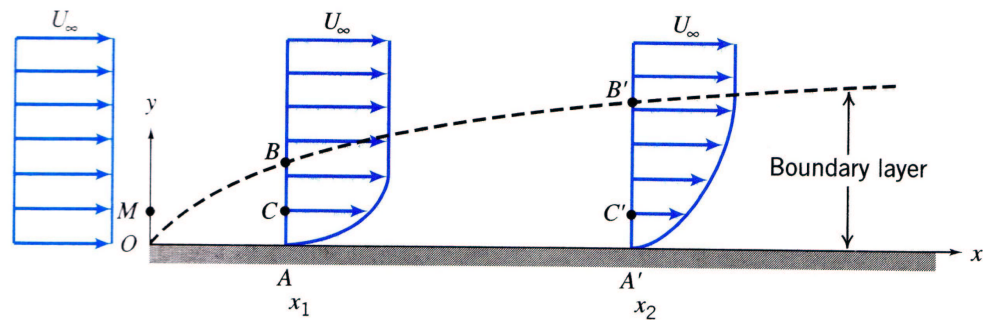


Figure 1.8: The development of a boundary layer in flow over a flat plate (Fox & McDonald 2003).

1.4.13 Stagnation Point

The stagnation point is the point in an airflow at which oncoming air stops moving, or ‘stagnates’, relative to the body (see Figure 1.9). The air above this proceeds to move over the top of the body, while the air below the stagnation point moves under the body, and air to the right and left of the stagnation point move around the side of the body, and combinations thereof. The shape of the body (in the case of a car, the shape of the front bumper or nose cone), in relation to the relative airflow, will dictate the position of the stagnation point.

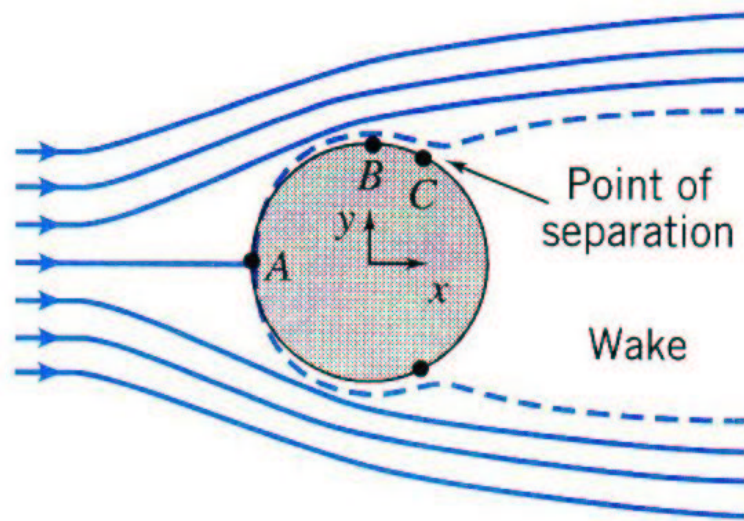


Figure 1.9: Stagnation and separation points in flow over a cylinder (Fox & McDonald 2003).

1.5 Definitions - Vehicle-related

As well as the aerodynamic terms used, there are some terms used with reference to the car itself which must be defined. These are both general (relating to all cars) and specific to our car.

1.5.1 General

Floorpan (or Undertray)

The *floorpan*, or *undertray* of the car is a large, flat panel attached to the underside of the car to smooth the airflow passing under it.

Other Aerodynamic aids

Professional race teams, especially Formula 1 teams, use several other aerodynamic aids.

Bargeboards are small panels placed in front of the radiator intakes, used to smooth the air flow into, and around the sides of, the intakes.

Endplates are panels fitted to the ends of wings in order to prevent vortex generation from the wing tips. Air tends to spill from the high-pressure side to the low-pressure side of the wings, giving itself rotational velocity along an axis parallel to the longitudinal axis of the car. This rotation persists, in the form of a vortex. This vortex can bleed a large amount of energy out of the car, being a major contributor to its total drag.

Sidepods usually provide ducting to a radiator on the side of the race car. This allows the centre of mass to be kept low, and greater manipulation of the local airflow than any other positioning.

A diffuser under the rear end of the car allows the air passing under the car to rise slightly after the car has passed over it, reducing the size of the wake and sometimes increasing downforce.

Winglets are used by Formula 1 teams to smooth the airflow around the car, especially onto the rear wing, and to prevent premature separation from the bodywork.

Port and Starboard

To distinguish the left-hand and right-hand sides of the car, and the frame of reference used, as opposed to using the words "... the left-hand side as viewed from the driver's position", we will use the nautical and aeronautical terms, "port" and "starboard". The "port" side of the car is the left-hand side, when viewed from the driver's perspective, and the "starboard" is the right, so the radiator of this car is on the port side.

Cockpit

The part of a (usually formula-style) racing car containing the driver is usually called the *cockpit*.

1.5.2 USQ Motorsport's F-SAE-A 2004 Entry-specific

The terms which are specific to USQ Motorsport's F-SAE-A 2004 Entry are all related to the chassis. In this report, these terms are used to define the placements of cross-sections and cross-section sketches used in the modelling and construction of the bodywork of the car. Some were defined in the 2003 F-SAE-A rules, while some terms were coined by the author, to name some chassis members from which placement of other entities is referenced.

The Coordinate System

The solid model of the car was defined such that the origin of the coordinate system is in the plane of the main roll hoop, on the centreline of the car, and in the centre (i.e., along the axis) of the floor-level chassis member that runs across the bottom of the main hoop. The positive x-, y-, and z-directions are defined, from the origin, as toward the port-side, towards the top of the roll hoop, and towards the front of the car, respectively.

Bulkhead

Defined by the SAE rules, the bulkhead is the square, non-crushable structure at the front of the chassis, behind which is to remain all non-crushable objects, most importantly, the driver's feet.

Kneebox

The kneebox is the u-shaped structural section of the chassis (shown in Figure 1.10), and the plane in which it lies, parallel to the bulkhead, and 354mm behind it. A reference plane, called “Kneebox” was created here in the solid models of the chassis and nose in order to facilitate their creation.

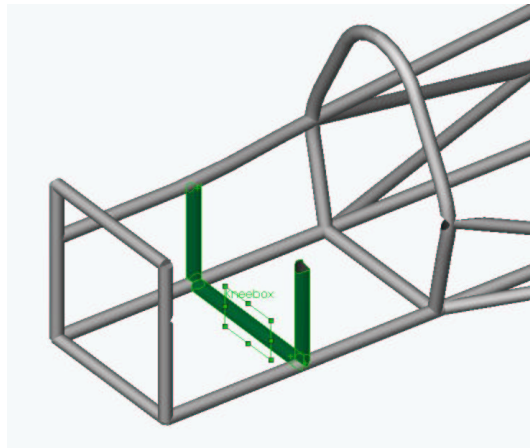


Figure 1.10: The chassis members defining the “Kneebox”. Some members have been omitted for clarity.

Main Hoop

Defined along with the front hoop in the competition rules, the main hoop is that chassis member which protects the driver’s head and neck in the event of a rollover.

Front Hoop

The front hoop is a forward roll hoop, defining the front edge of the cockpit, and prevents the top half of the car’s body from collapsing on the driver’s legs in the event of a rollover.

Rail

The rails are the chassis members which run the entire length of the chassis, along the bottom of the structure. These members were used in the definition of several features in the design of the bodywork, most importantly of which are the fillets along the bottom edges of the original lofted feature.

1.6 Definitions - Computer Related

1.6.1 Loft

A *loft* in SolidWorks (called a “draft” in ProENGINEER, but henceforth shall be referred to as a “loft”) is a method of creating a feature with complex curvature. It uses at least two cross-section sketches (one at the start, one at the end), and optionally, one or more other sketches defining its final shape. The lofts used in this project to create the chassis members used a cross-section sketch at each end, and a centreline sketch, while to create the nose, several cross-section sketches were used, and to create the cockpit sides, a start and an end cross-section and a guide curve were used.

The program creates a shape between the two cross sections which would be created if the sketches were physically cut from a material (such as timber), then a skin stretched over the sections, such that the *maximum* value of the curvature of the skin is a *minimum*.

If only two cross-section sketches are used, the feature is shaped as though the sections had been physically set up, and then a skin of fabric draped over them, then pulled taught.

If more sections are used (such as in the solid model of the nose, shown in Figure 1.11), the skin is shaped as though an infinite number of infinitely thin wires had been attached to the first section at one end, and to the last section at the other end, and curved over all the sections in between such that they just come in contact with them all, but do not bend any more than necessary to do so.

If one or more guide curves are used in either of these situations, the skin is then stretched in or out as required to be in contact with the entire guide curve, but again, such that the maximum value of curvature is kept to a minimum.

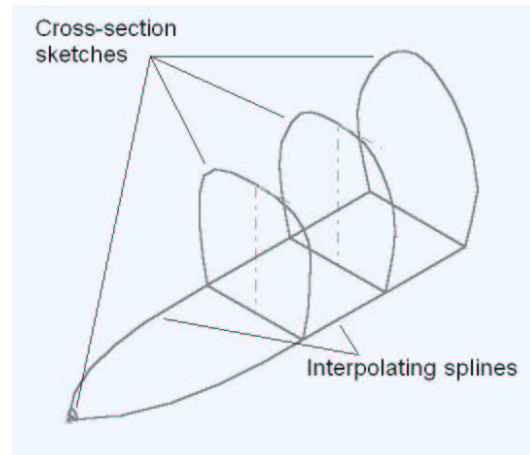


Figure 1.11: The cross section sketches and interpolating splines defining the lofted feature of the nose section.

Chapter 2

Background

Now that we know the definitions of some of the terms used in the study of aerodynamics, it is time to look at the theory behind it; at the concepts that brought us to understand it.

In the 1500's, Leonardo Da Vinci drew many designs of flying machines, effectively pioneering the theory of flight, but he had no way of performing design calculations, and merely drew what he thought *looked* like it would fly. He drew pictures of kites and gliders that were modelled on birds, even drawing them as being constructed with a wing structural design similar to that of a bird.

In the 1700's Daniel Bernoulli (one of at least ten Bernoullis to expand our horizons of mathematics) found the famous relationship,

$$P_1 V_1 = P_2 V_2.$$

In doing this, he opened up the mathematical and theoretical side of aerodynamics, but, being a mathematician, never applied any of his work to practical designs.

The most useful conclusion (to us) of his work was that along a streamline, the relationship,

$$\frac{P_1}{\rho} + \frac{V_1^2}{2} + gz_1 = \frac{P_2}{\rho} + \frac{V_2^2}{2} + gz_2$$

holds (Fox & McDonald 2003). This may be simplified to $P_1V_1 = P_2V_2$. From this stems the vast majority of current aerodynamic theory. Put simply, this relationship states that if the speed of a moving fluid is changed (from V_1 to V_2), the fluid's pressure also changes (from P_1 to P_2), proportionally with the change in speed. More specifically,

$$P_2 = P_1 \times \left(\frac{V_1}{V_2} \right)$$

In 1903, on a beach in Kittyhawk, USA, Orville and Wilbur Wright became the first men to officially fly and control a heavier-than-air vehicle under power. They had pioneered the practical side of flight. The Wright brothers were bicycle mechanics who became interested in flying, and worked in their spare time, in the back of their bicycle shop, on flying machines. They had enough knowledge to put together the work of Bernoulli with what they had observed in nature (watching birds), and test the results.

In the back room of their shop, the brothers designed and constructed a wind tunnel, then designed and constructed some test aerofoil sections, then (perhaps most brilliantly) designed and constructed their own test equipment and instrumentation. They used these to take measurements of, and tabulate, lift and drag forces which are so accurate that modern aerodynamicists, with millions of dollars' worth of wind tunnel equipment, electronic measuring devices, precise manufacturing techniques and computer software, can only improve upon by about one or two percent!

Using the comparisons they made between different aerofoil sections, the Wright brothers selected the best section, then went on to construct an aircraft using this section. They built it from timber, fabric and wire, fitted it with an extremely light car engine, twin chain-driven propellers and a simple control system, and flew it from a rail laid out on Kittyhawk beach.

So was born the application of aerodynamics to flight. However, aircraft remained extremely aerodynamically poor, using twin wings, exposed struts, bracing wires, unretractable undercarriage, and open cockpits.

These aircraft typically had a maximum speed of around 100 miles per hour (87 knots, or 160 km/h). It was not until 1936 that structures and engines had become strong and powerful enough to allow an all-metal covered, cantilever monoplane (single-wing,

not braced or supported by struts) fighter aircraft to be flown. This aircraft was the famous Supermarine Spitfire, and it ushered in a new era of aerodynamic and structural technology. Within years, the maximum speed of military aircraft had jumped to over 380 kts (700 km/h)!

Technology continued to develop, and money continued to be poured into the aerodynamics of military aircraft, but in the 1940's, '50's and 60's, the lessons learned in the aeronautical industry began to be applied to motor vehicles.

About this time, the American car manufacturers began to design and produce a new shape of car; the wide, low, 'saloon' (known in Australia as the 'sedan'), which was different from the 'bug'-like shape of earlier cars. This shape allows the carriage of a large volume of passengers and luggage, while only creating a small turbulent wake, allowing a lower drag coefficient. This translates into lower fuel costs over the life of the car, which is always a desirable result.

Thus, automotive aerodynamic design has developed, such that today, the international benchmark for family car design is such that they produce a negligible wake, have very low drag coefficients (0.30 is a good benchmark level), are very stable in crosswinds, and have barely discernable wind noise.

The racing arena has developed even more quickly to a higher level of technology. Aerodynamicists in professional race teams can spend up to 15 million dollars a year on wind-tunnel testing alone, and have spent similar amounts on computer simulations before even *beginning* to build the wind tunnel model!

This is the area in which this project will work.

Chapter 3

Overview of Softwares Used

3.1 Chapter Overview

Several softwares were used in this project, each to complete a different task. This chapter discusses software in general, the uses of each type of software used, and which specific packages were used.

3.2 CAE And The FEM

Computer-Aided Engineering (CAE) has become and is still becoming an area of great interest and expansion in the world's engineering community. Through the use of such tools, engineers can design parts, structures, machines and anything else that has to be designed, with microscopic accuracy, and with insight into the mechanics of the design which previously were gained with the naked eye, rules of thumb and "engineering judgement".

FEM - As Applied To CFD

The Finite Element Method (FEM) is well described as “...a method used to approximately predict the behaviour of a continuous physical system by solving a finite number of algebraic equations that describe a mathematical model of some equivalent idealised system. The real system is thus represented by a finite number of elements bounded by a mesh or grid” (Snook 2003a).

So a real system may be broken up into a number of small elements, and each element has a set of equations assigned to it. These equations may be any relevant equations, such as stress, heat transfer, or pressure. A typical set of equations (those for stress in three dimensions) is shown below (Snook 2003a):

$$\frac{\partial \sigma_x}{\partial x} + \frac{\partial \tau_{xy}}{\partial y} + \frac{\partial \tau_{xz}}{\partial z} + B_x = 0$$

$$\frac{\partial \tau_{xy}}{\partial x} + \frac{\partial \sigma_y}{\partial y} + \frac{\partial \tau_{yz}}{\partial z} + B_y = 0$$

$$\frac{\partial \tau_{xz}}{\partial x} + \frac{\partial \tau_{yz}}{\partial y} + \frac{\partial \sigma_z}{\partial z} + B_z = 0$$

Some (or all) of these and other equations may be applied to each element, and initial conditions set for certain elements. The equations are then most easily solved in matrix form. In the case of a structural analysis, the deflection of the meshed part under a known load may be calculated using the relationship between force applied and the consequent displacement of the part, using the matrix equation:

$$\{F\} = [K] \times \{d\}$$

where $\{F\}$ is the applied force vector on all nodes, $[K]$ is the stiffness matrix, and $\{d\}$ is resultant displacement vector. Each matrix contains all required information for each node in a mesh. The stiffness matrix contains the “*stiffness influence coefficients*” (Snook 2003a)

This stress analysis is the first type of FEA taught to students. From here, the same principles are applied to other equations. In a CFD (Computational Fluid Dynamics) analysis, the same matrix operations apply, but equations for flow and heat transfer are assigned to each node, instead of those for stress.

Many different mathematical models are used in CFD, each one using a slightly different set of equations. These equations are usually based upon the Navier-Stokes set of equations, but must be altered to account for turbulence. The transport equations used by (A.J. Baker, W.P. Noronha, J.B. Woods 1989) in the analysis on internal flow in a vehicle are:

$$\begin{aligned}
 L(\rho_0) &= \nabla \cdot u & = 0 \\
 L(u) &= \frac{\partial u}{\partial t} + (u \cdot \nabla)u - \nabla \cdot \left(\frac{1+v^t}{Re} \right) \nabla u + \nabla P - \frac{Gr}{Re^2} g & = 0 \\
 L(\theta) &= \frac{\partial \theta}{\partial t} + (u \cdot \nabla)\theta - \nabla \cdot \left(\frac{1}{Pr} + \frac{v^t}{Pr^t} \right) \nabla \theta - s_\theta & = 0 \\
 L(C_A) &= \frac{\partial C_A}{\partial t} + (u \cdot \nabla)C_A - \nabla \cdot \left(\frac{1}{Sc} + \frac{v^t}{Sc^t} \right) \nabla C_A - s_A & = 0
 \end{aligned}$$

The k- ϵ solver in FLUENT, the software package that will be used for the analysis of this car, uses different equations, based on the the turbulence intensity (k) and the turbulence dissipation rate (ϵ). For the standard k- ϵ solver, these are (from the FLUENT online help file):

$$\frac{\partial}{\partial t}(\rho k) + \frac{\partial}{\partial x_i}(\rho k u_i) = \frac{\partial}{\partial x_j} \left[\left(\mu + \frac{\mu_t}{\sigma_k} \right) \frac{\partial k}{\partial x_j} \right] + G_k + G_b - \rho \epsilon - Y_M + S_k$$

for k, and

$$\frac{\partial}{\partial t}(\rho \epsilon) + \frac{\partial}{\partial x_i}(\rho \epsilon u_i) = \frac{\partial}{\partial x_j} \left[\left(\mu + \frac{\mu_t}{\sigma_\epsilon} \right) \frac{\partial \epsilon}{\partial x_j} \right] + C_{1\epsilon} \frac{\epsilon}{k} (G_k + C_{3\epsilon} G_b) - C_{2\epsilon} \rho \frac{\epsilon^2}{k} + S_\epsilon$$

for ϵ . When these equations are matrixised for each node on a mesh and solved, the result will yield the k and the ϵ for each node. From here, many other flow parameters may be calculated.

CAE

CAE encompasses areas of design and manufacture as Computer Aided Drafting (CAD), Computer Aided Design (also called CAD), Computer Aided Analysis (CAA), and Computer Aided Manufacture (CAM). CAM usually involves the use of Computer Numeric Controlled (CNC) machines, to cut complex shapes to very high accuracy, in less time than it would take a human operator.

3.2.1 Wire Frame Modelling

Wire-frame modelling is “the simplest form of modelling to depict shape...[and] only models the edges of an object, with each edge being defined by a line” (Snook 2003*b*). The lines themselves are defined by vertices, and so this form of modelling does not allow the creation of complex shapes. It also cannot contain any information other than the locations of the edges of an object are in space. Such information as surface area, volume, material properties and exact surface definition (where any given point on a given surface is in space, for example, a surface may have edges that form a flat square, but the middle of the surface may bulge out of the plane of the square) are not able to be associated with a wire-frame model.

3.2.2 Surface Modelling

Surface modelling allows three-dimensional visualisation of an object, but cannot be feature-based. The model is composed of surfaces, so if a hole is made through the model, extra surfaces must be added to define the interior of the hole.

3.2.3 Solid Modelling

Solid modelling is the method by which a three dimensional computer model of a part or assembly may be created, with one file (or database) containing all relevant information about the part.

Such information might include:

- Finite Element meshes
- CNC toolpaths
- Exact volume and surface area
- Density (and therefore mass), thermal or electrical conductivity
- Yield strength or ultimate tensile strength
- Manufacturing processes involved
- The order of these processes

The model can be manipulated to allow the operator to view it from every angle, and to see how it interacts with other parts

In this project, a solid model was used to generate a CNC toolpath and to cut a shape from polystyrene foam.

Two sub-types of solid modelling are used: Boundary representation (B-Rep) and Constructive Solid Geometry (CSG).

“B-Rep builds the object by defining the boundaries (surfaces) that bound that object” (Snook 2003*b*). The construction of a block using B-Rep is shown in Figure 3.1.

CSG uses a collection of simple shapes (cubes, cylinders, cones, etc.), and adds or subtracts them using boolean operations. This process is shown in Figure 3.2.

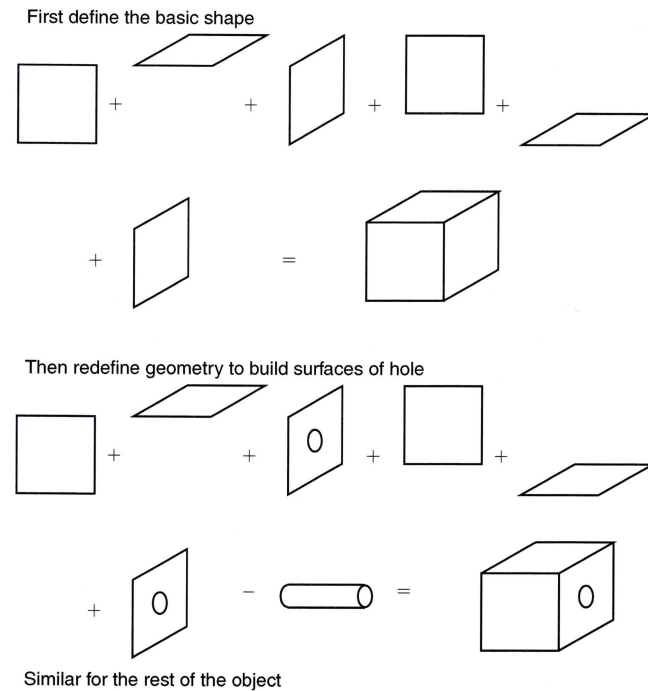


Figure 3.1: Building a block using Boundary Representation (Snook 2003*a*).

3.3 Software Used

In this project, several software packages were used to perform three tasks:

- To create solid models of the bodywork geometry, and from these to create .sat models for importation into the other packages,
- To process the geometry of the .sat models, by creating a finite element mesh around them,
- To perform Computational Fluid Dynamics (CFD) analysis on these meshes

3.3.1 Solid Modelling Software

Two different packages were available for the solid modelling of the parts. These packages were ProENGINEER, and SolidWorks. Having previous experience on both packages, I have found that SolidWorks is a much more user-friendly package to use, and is

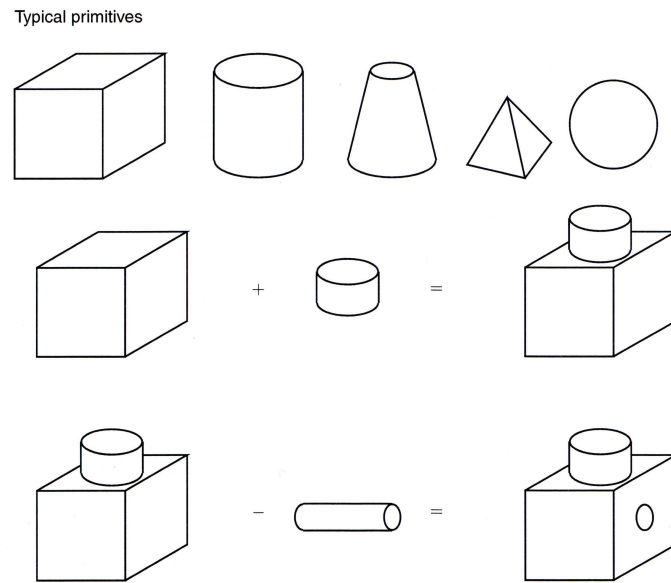


Figure 3.2: Building a block using Constructive Solid Geometry (Snook 2003a).

much easier to learn than ProENGINEER.

It was anticipated that the “loft” feature would be used extensively in this project, so the lofting performance of each package was scrutinised as a major selection criterion. In the event, this was the only selection criterion required to be looked at, as, while ProENGINEER does have a loft function (called a “draft”), it was very hard to learn how to use it. So effectively, SolidWorks was the only solid modelling package that would do what I required. Therefore, this was the package I chose to use.

3.3.2 Geometry Processing Software

The only geometry processing software package available to me for this project is GAMBIT. If I had chosen to use ProENGINEER for the solid modelling, the mesh tool in that package would have been able to create meshes for the CFD software, however, this tool is not specifically designed as a mesh-applying software package, but as a small add-on to a solid modelling package. As a result of this, GAMBIT is a much more powerful and easy to use piece of software.

Initially, .igs files were used to transfer the geometry into GAMBIT. During the course

of the project, however, it was found that .igs files lose the integrity of the original model, and the imported model contains faces and edges that do not meet, and new faces, edges and vertices are created to fill the gaps. This requires a large amount of processing and “cleaning up”, before the mesh can be applied. Contrarily, ProENGINEER’s mesh tool will operate directly on the .prt file, therefore requiring no cleaning up.

However, the amount of geometry cleaning up required reduced very quickly with improved model design and with increased experience on the software, and became a relatively small problem. Then, on advice from Mr. Chris Snook, ACIS files (.sat) were used. This filetype retains great accuracy (in the final CFD model, all points were accurate to within 10^{-5} m), and when imported into GAMBIT, the model retained its edge connectivity.

GAMBIT is able to create geometry itself, and it was suggested that the car’s geometry be created here, but this option was simply impossible for the shapes that are being used. The nose cone of the SAE car has a complex curvature to it, which is impossible to create in a surface modelling program such as this, as it has no way to constrain the angle at which a surface leaves the edge defining it, relative to a plane, nor to define how and where the curved surface bulges (over the bulkhead of the chassis, in this case).

3.3.3 CFD Software

Several packages capable of CFD Analysis are available, including ANSYS 5.0 and FLUENT. ANSYS’s CFD capability is provided by the FLOTRAN CFD addon, but again, this is just an addon tool, not a dedicated software package like FLUENT, and therefore not as powerful or easy to use. I have ready access to FLUENT V6 and professional help at USQ, and after a few hours of tutoring, have found FLUENT to be a wholly acceptable package to use.

So these are the three packages that will be used in the design and analysis of the bodywork for the USQ’s Formula SAE-A car.

Chapter 4

Methodology - Solid Modelling

4.1 Chapter Overview

Now that we have an understanding of what solid modelling is and how it may be used, we may now outline the methodology that has been developed to design the solid model of the SAE vehicle. It is hoped that this methodology may be followed and used in the future to build upon the developments that have occurred in the past year, to improve on the design in a shorter time.

By far the most time-consuming facet of this project was the computer modelling and simulation. This chapter deals with the methodologies that were developed and used to construct, mesh and analyse the models.

Wind-tunnel testing of scale models of the car would have been very interesting and helpful, but the wind tunnel available at USQ has a test section of $300 \times 300 \times 600mm$, and it would be much simpler to model the car in a solid modelling program, than to design and construct an accurate enough scale model. Computer simulation also costs less than constructing a scale model, then running a wind tunnel, if the required software is already accessible. It is hoped that in future years, some wind-tunnel work can be done.

As stated previously, three software packages were used extensively in this project:

- SolidWorks - Used for the creation of solid models
- GAMBIT - Used for the generation of meshes
- FLUENT - Used for the CFD analysis

The steps taken in the computer-aided design of the bodywork of the USQ's F-SAE racer are as follows:

1. Familiarise myself with SolidWorks, GAMBIT, and FLUENT software packages,
2. Construct solid models of the car's chassis and bodywork,
3. Import this body into GAMBIT, create a 'duct' around it, and apply boundary conditions, constraints and meshes to these entities,
4. Analyse this model in FLUENT,
5. Analyse the results of the test, especially turbulence, drag and lift magnitudes on the body,
6. Improve the model, if required,
7. Repeat until the model satisfies our needs,
8. Use this computer model to construct a full-scale model of the outside of the car,
9. Use this physical model to shape the bodywork from fibreglass.

The following methodologies were developed for each of the major steps in the creation of the bodywork for the car.

Solid models of the chassis and bodywork were created in SolidWorks. A chassis had already been created in ProENGINEER, but as SolidWorks was being used to create the body, a model in that format was required. It would have been possible to import the ProENGINEER model in IGES, Parasolid, or ACIS format, but this would not facilitate easy modification later.

Table 4.1: The reference planes created and the manner in which they were defined.

Plane Name	Definition
“Main Hoop”	Renamed from “Front”
“Floor”	Renamed from “Top”
“Front Hoop”	Offset parallel to, and 725mm in front of, “Main Hoop”
“Bulkhead”	Offset 1421mm in front of “Main Hoop”
“Kneebox”	Offset 354mm behind “Bulkhead”
“Rear Box 1”	Offset 600mm behind “Main Hoop”
“Rear Box 2”	Offset 400mm behind “Rear Box 1”
“Level 1”	Offset 250mm above “Floor”
“Level 2”	Offset 383mm above “Floor”
“Top”	Offset 1108mm above “Floor”
“Rail”	Offset 191.5mm to the port side of “Right”
“Midplane”	Offset 317mm to the port side of “Right”
“Outside Edge”	Offset 450mm to the port side of “Right”

4.2 Solid Modelling - The Chassis Model

The creation of the chassis model was conducted using measurements taken off the actual chassis that had been created for this F-SAE car by Chris Baker, not off his design, for the reason that this would take into account any inaccuracies in its construction (although these were expected to be negligible) and post-design changes.

As well as the “Front”, “Top” and “Right” planes which are automatically created in any SolidWorks part, a series of reference planes was created, as shown in Table 4.2, and pictorially in Figure 4.1 (all of the following figures are also shown in Appendix C).

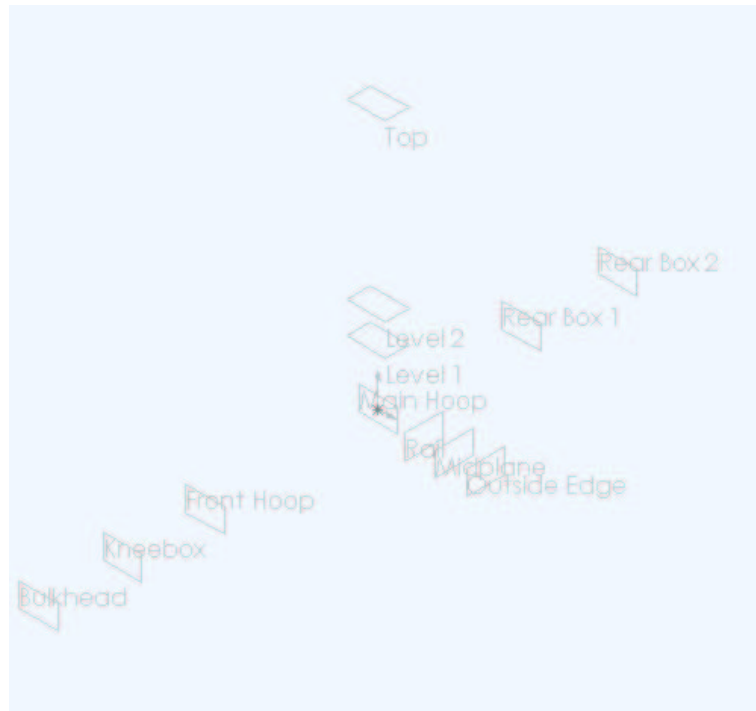


Figure 4.1: The planes defined in Table 4.2.

On these planes were drawn circles and ellipses, from which were lofted or extruded the pipe sections to construct the computer model of the port side of the chassis. This side was then mirrored to create the whole model. Circles were used to define the shape of members which run perpendicular to the plane on which the section was drawn, but for those members not normal to any plane, ellipses were sketched on a relevant plane.

For example, the diagonal member between the bulkhead and the kneebox was drawn using an ellipse at each end (sketched on the “Bulkhead” and “Kneebox” planes), and a centreline on the “Rail” plane from the centre point of one ellipse to the centre point of the other (Figure 4.2). The angle from the member to the horizontal is 29.71° , so the ellipses have the dimensions 32mm wide (all members were 32mm in diameter) by $h = \frac{32}{\cos(29.71)} = 36.84\text{mm}$ high. This results in the cross section perpendicular to the centre line being a circle of diameter 32mm, as shown in Figure 4.3.

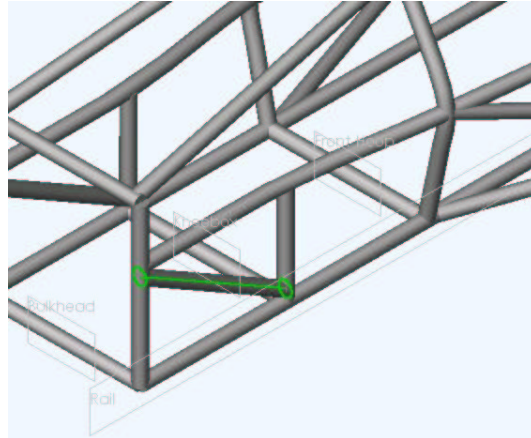


Figure 4.2: The two elliptical end section sketches and the centreline for the port front diagonal member. Note also the reference planes shown in light grey.

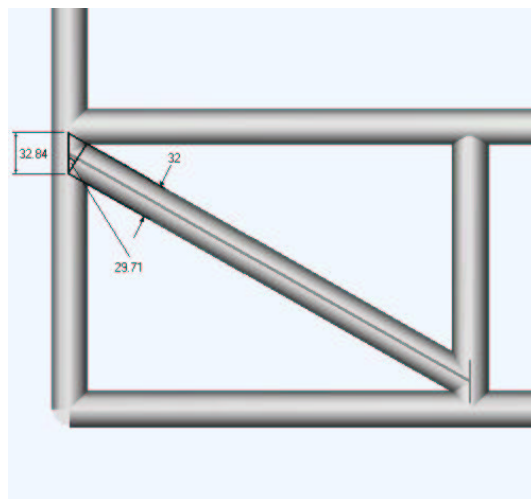


Figure 4.3: Trigonometric calculation of the ellipse height for lofting the front diagonal chassis member.

Members that have been bent into shape (the main and front roll hoops and the upper side impact member) were constructed in the same way, but a curved centreline sketch drawn on the relevant plane (Main Hoop, Front Hoop and Level 1, respectively) defined the curved path of the loft. This can be seen in Figure 4.4.

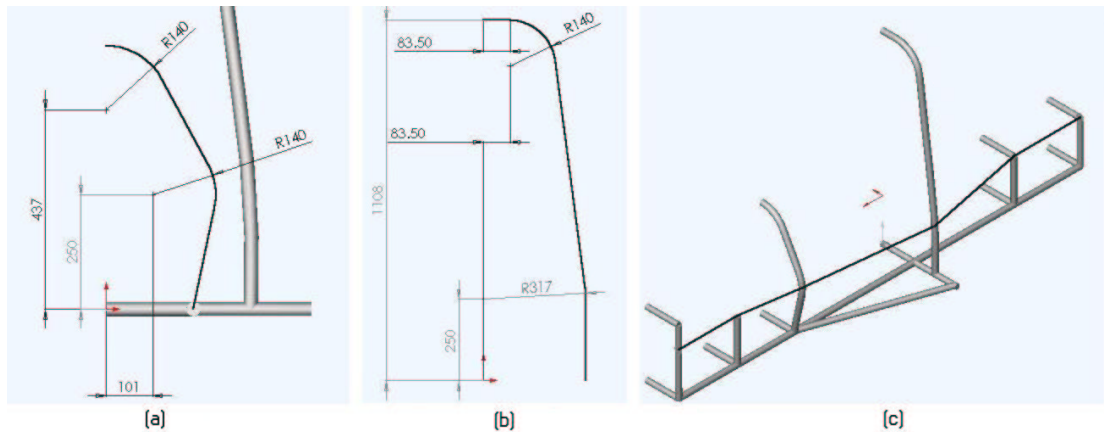


Figure 4.4: Centreline sketches for (a) the port side of the front roll hoop, (b) the port side of the main roll hoop, and (c) the port upper side impact member.

This created the chassis model, as shown in Figure 4.5. Creating this model was without problem, except that many of the straight members were created using lofts, instead of extrusions. This was merely because I chose to use this to expand my personal knowledge of modelling in SolidWorks. The problem arises when the model is rebuilt. A loft needs three sketches (if a centreline is included), and so takes more memory and time to rebuild, so the rebuild time was long and the file size was large. The computer on which I was working began to shut down SolidWorks sometimes when the model was rebuilt. However, in the event of a successful rebuild, the end result is the same.

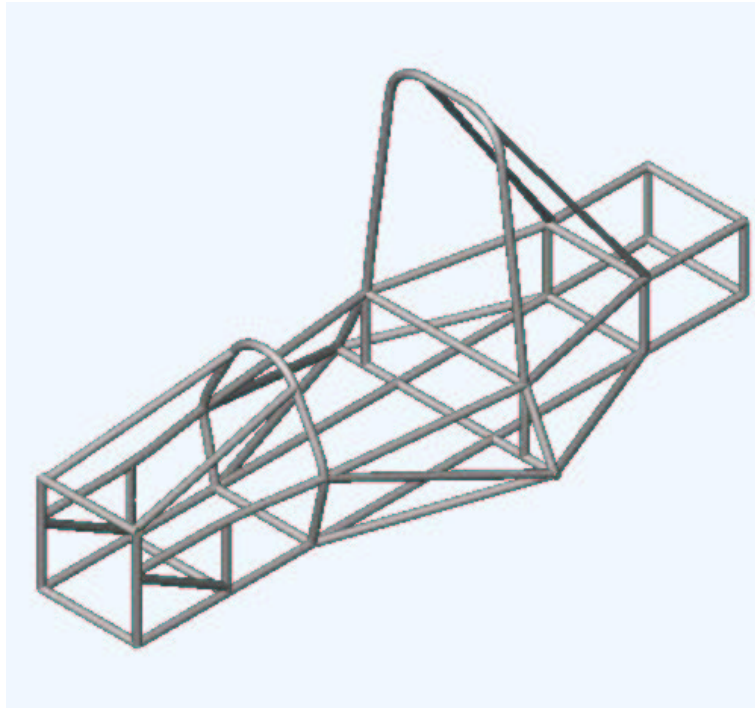


Figure 4.5: The completed SolidWorks chassis model.

4.3 Solid Modelling - The Nose Model

The solid model for the nose of the car was the one most concentrated on. The lessons learned from this were able to be applied to the centre and rear sections. It went through many design iterations, which are shown in Appendix C.

For the nose model, the required reference planes were different from those of the chassis. The “Bulkhead”, “Kneebox”, “Front Hoop” and “Main Hoop” planes remained the same, but all the others were deleted, and two more were defined: “Nose Point” was defined offset 2220mm in front of “Main Hoop”, and “Nose Shaper” defined 20mm behind the “Nose Point” plane.

The *basic* definition of each iteration of the nose model was identical, but differed only in cross section sketch shape, number of line segments in each sketch, and type and number of lofts used to create each model.

At the beginning of the project, lofted surfaces were used, since the final product was

to be hollow, and the skin was to be very thin. However, this produced two main problems. These were that SolidWorks cannot mirror surfaces (only solid objects), and that when imported to GAMBIT as an .igs file, the resulting GAMBIT model is very “messy”. That is, the surfaces do not meet, and small edges are produced to fill the spaces. This problem occurs in any .igs model, but in my experience, it appears to be more pronounced if there are only surfaces, and no solid parts to the original model.

This requires a large amount of processing, involving deleting surfaces and lines. Herein lies the problem: when a curved surface is deleted, the model loses the curvature of that face. The face is imported in a certain shape, in this case, the top edge of the face which had to be deleted was normal to the y-z plane, and the bottom edge propagated upward and outward (away from the y-z plane) at an angle of approximately 15° . If it is deleted, the lines may easily be redefined, but GAMBIT cannot recreate the original face, constraining the top edge to be normal to the y-z plane. Furthermore, GAMBIT requires that the points defining the lines which are being used to define a new face *must* be coplanar. This is not a problem when there are only three points, but very rarely in an application such as this will there be three required points and will these points be coplanar.

This did occur in the early stages of this project, and when the face was redefined in GAMBIT, the finished product would have had a triangular cross-section. Unfortunately, no way could be found to keep the face as it was. This is the reason I switched to using solid parts and the shell feature.

Once the potential of creating a “shell” feature in a solid part was discovered, base and boss lofts were used exclusively.

Each model was lofted between five main cross sections (some models went further behind the front hoop, to the main hoop, but this practice was abandoned). The cross section sketches, as shown in Appendix C were:

1. Nose Point1 - a sketch containing a point at a specified distance above the “floor” plane, sketched on the “Nose Point” plane, and used as the convergence point for the entire nose,

2. Nose Shaper1 - sketched on the plane of the same name (20mm behind the Nose Point1 sketch), defining the general shape of the nose over the rest of its length,
3. a Bulkhead sketch - to define the shape of the nose as it passes over the chassis bulkhead,
4. a Kneebox sketch, and
5. a Front Hoop sketch - to do the same as the Bulkhead sketch.

From the bulkhead sketch rearwards, all sketches were drawn with a flat underside, 16mm below the “Floor” plane. The origin in the chassis model is in the centre of the frame member that runs across the bottom of the main roll hoop, and that member has a 16mm radius. This places the top face of the floor pan at 16mm below the origin of the chassis part. This affected the nose model merely because it negates the need to transpose any mates (in the chassis-nose assembly model) or measurements to allow for a 16mm offset in the z-direction.

As an example to illustrate the last point, the top of the port side of the bulkhead in the chassis model is at the x,y,z coordinates [207.50 , 399 , 1421], but if the bottom edges of each cross section sketch in the nose model were aligned with the origin (and therefore with the “Floor” plane), I would have to convert the y value of 399 to a value of $399 - 16 = 383\text{mm}$ before I could use that value in the nose model. This in itself is not hard, but it lends itself very well to human errors such as forgetting to execute the transposition.

4.3.1 The First Model

The first model (Figure 4.6), aside from being described as “hideously ugly”, is not a very practical design. The flat, slab-sides offer no rigidity, meaning that more fasteners or more fibreglass than necessary would have to be used, and a quick inspection of the geometry shows that a streamline from the nose point will follow external curves that are smaller than they need to be (creating a steeper pressure gradient, promoting turbulent flow to occur sooner).

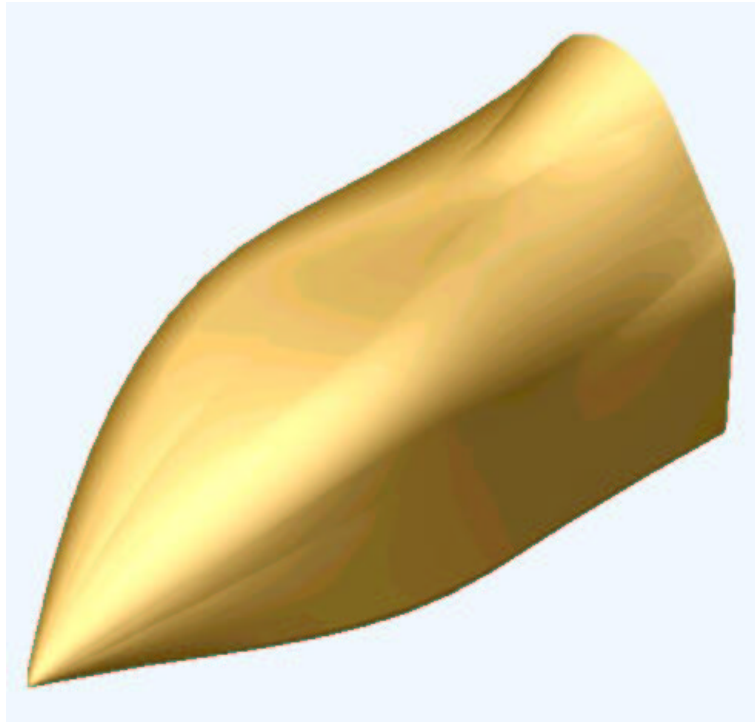


Figure 4.6: The first nose model.

The design requirements at this stage (which were refined later) were to fit the bodywork over the chassis as closely as possible, in the simplest possible basic shape, while keeping the nose as short as possible (to reduce material used, thereby reducing weight). The decision to use a square cross section, with rounded corners was based on the fact that this keeps the bodywork tightly packed around the chassis (which is of square cross-section), minimising frontal area. So the cross section at the bulkhead was defined such that the skin would run parallel to the vertical chassis members, 30mm outboard, and curve over the top, to a flat upper surface. The radius of curvature was purely arbitrary. The section level with the kneebox was given sides and a bottom which follow the bulkhead sketch, but the top corner curves were of greater radius, and the top surface was higher. These are shown in Figures 4.7 and 4.8. The shape for the front hoop section followed the exact outline of the front hoop member in the chassis model (Figure 4.9). This sketch contained eight line segments (shown in green).

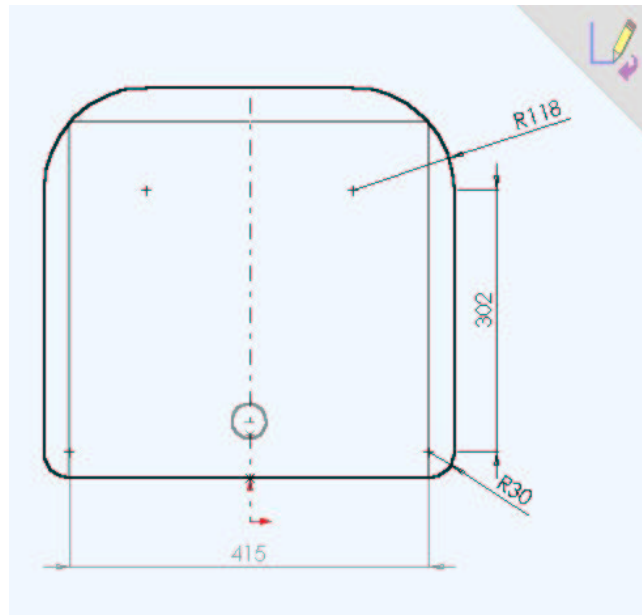


Figure 4.7: The bulkhead sketch, showing the extremities of the chassis bulkhead (the light grey rectangle) and the nose shaper (the light grey circle).

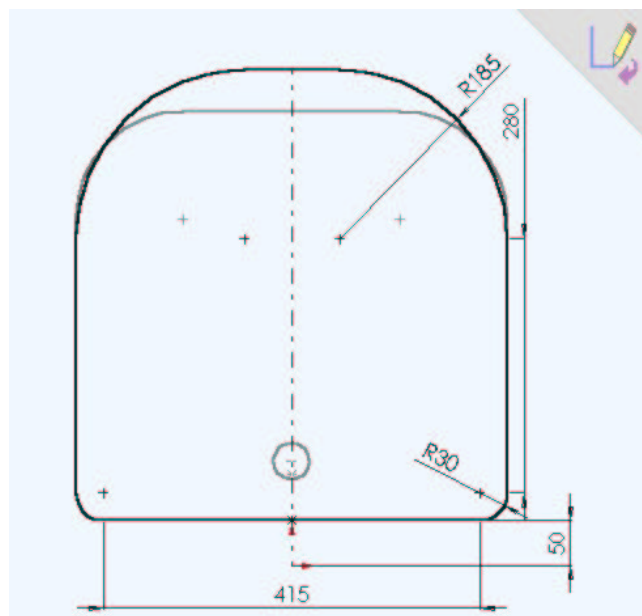


Figure 4.8: The kneebox sketch, showing the bulkhead sketch in light grey.

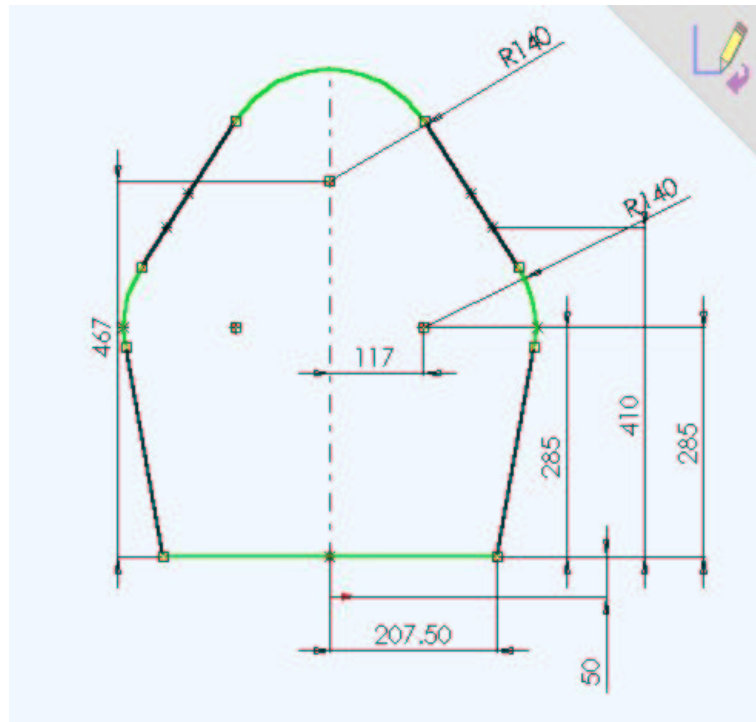


Figure 4.9: The cross-section sketch at the front hoop, showing the separate line segments.

However, this produced a separate face for each line segment in the sketches (line segments are illustrated in Figure 4.9). Lofting between sections in SolidWorks requires that the same number of line segments exist in each sketch (this is learned by experience with the software). If that is not the case, the loft may still solve, but the finished part will appear warped. To prevent the loft from warping, the same number of line segments were placed in each cross section. This number was dictated by the “Front Hoop” sketch, which, as mentioned, tightly follows the outside of the front roll hoop, and has eight line segments.

The top horizontal sections of the bulkhead and kneebox sketches were of different lengths, and this gave rise to the strangely shaped faces shown in Figure 4.10). By inspection, it can be seen that the edges of the faces will not even approximately follow the streamlines in the airflow, and this is not aesthetically attractive. That sounds only a small problem, but one of the concerns of this project is to make an attractive car, to invite sponsorship.

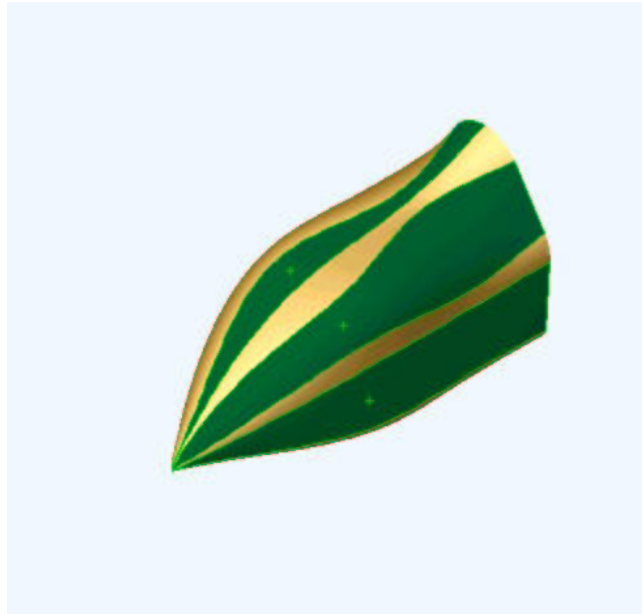


Figure 4.10: The different faces of the first nose design. Each alternate face is highlighted in green. These faces are produced by SolidWorks, one face for each line segment in the sketches.

If the car were able to travel at a higher speed (this car is not expected to exceed 110km/h), another more important concern would be the edges between the faces of this model not being parallel to the streamlines for an aerodynamic reason. The faces do not meet tangentially; that is, the line along which the faces meet can be seen, because they meet at an angle. If this edge is not parallel to a streamline when the car is driving, these edges will promote recirculation zones. However, at the speeds expected from this car, these zones will be negligible.

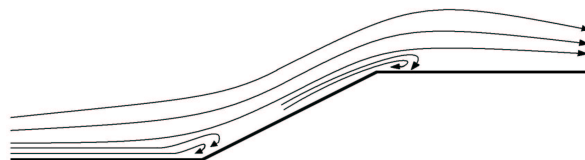


Figure 4.11: Recirculation occurring due to sudden changes in geometry.

4.3.2 The Second Model

The second model was only a minor redesign of the first, incorporating a streamlining of the face edges. This was achieved, as shown in Figures 4.12 and 4.14, through a change in the definition of the bulkhead sketch, as well as a redefinition of the “Nose Shaper” plane, from 20mm behind to 10mm behind the “Nose Point” plane. This was intended to reduce the angle at the point of the nose. Attempts were made to use the “Nose Shaper1” sketch to define the curvature of the point, but this was not the best way to do that. It does not allow the radius of curvature of the very foremost part of the bodywork to be measured, and this is required. As stated in F-SAE Rule 3.3.7, “Frontal Impact Protection → Others”, there is a requirement of a forward facing radius of “...at least 38mm (1.5 inches)... extend[ing] to at least 45 degrees relative to the forward direction, along the top, sides and bottom of all affected edges” (*Formula SAE-A Rules Webpage 2004*)

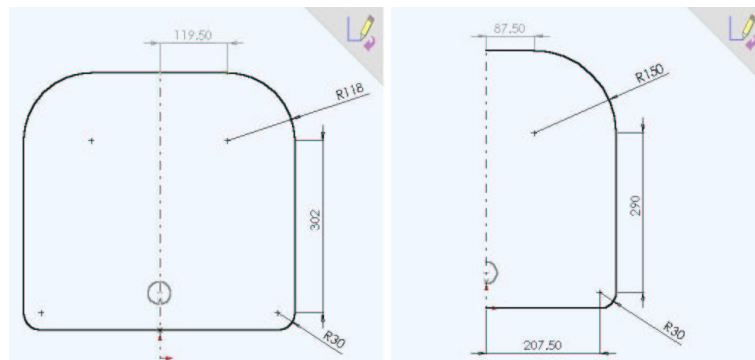


Figure 4.12: A comparison of the bulkhead cross-sections of the first (left) and second nose models.

It should also be noted that this model was constructed on one side only (i.e., only the port side of the nose was modelled). This was intended to simplify the model for use in the CFD analysis. (To halve the size of the mesh when analysing a shape using FEA or CFD software, a model is usually cut along any planes of symmetry. These models are symmetrical about the “Right” plane. The practice of creating only half a model was later abandoned in favour of creating a “Symmetry Cut” feature at the end of the creation of the full model.)

The change in radius of the top curve of the bulkhead sketch from the first to the second model results in the same general shape, but much less pronounced bulges, a comparison of this from the first model is shown in Figure 4.13, and the new model is seen in solid form in Figure 4.14. Also visible here is the increased included angle in the nose point, which results in a smoother curve forward of the bulkhead.

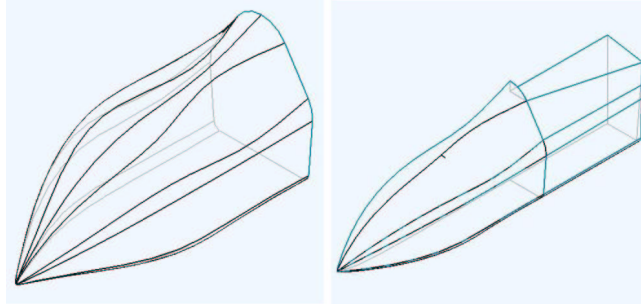


Figure 4.13: A comparison of the face join lines between the first (left) and second models, showing the face edges on the second model varying much less than those on the first.

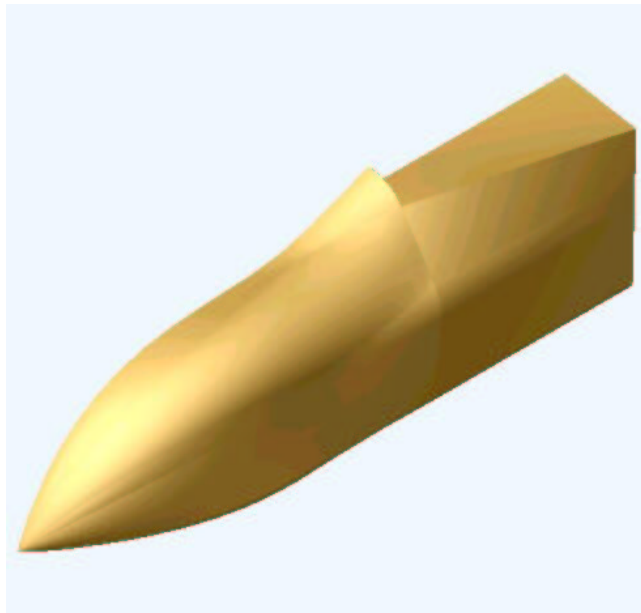


Figure 4.14: The second nose design.

The second model was refined mid-life (Figure 4.15), by a different definition of the bulkhead and kneebox cross sections. In these sketches, construction lines were drawn (see Figure 4.16), constrained at one end to the “Nose Point1” sketch, and at the other

end, to the ends of two joined line segments in the “Front Hoop1” sketch. The line segments in the “Bulkhead1” and “Kneebox1” sketches were constrained to start and finish at these construction lines. This had the effect of creating straight-edged faces (when viewed from the front), shown in Figures 4.17 and 4.18, which will not follow the streamlines in the airflow *exactly*, but is much closer than the previous design, thereby reducing the propensity to set up recirculation zones, and makes this model look much better.

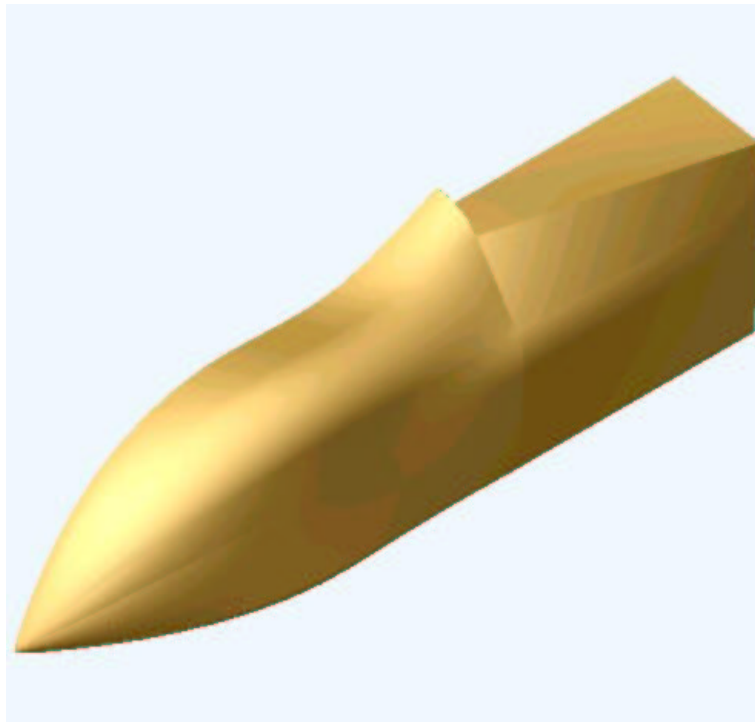


Figure 4.15: The mid-life redesign of the second nose model.

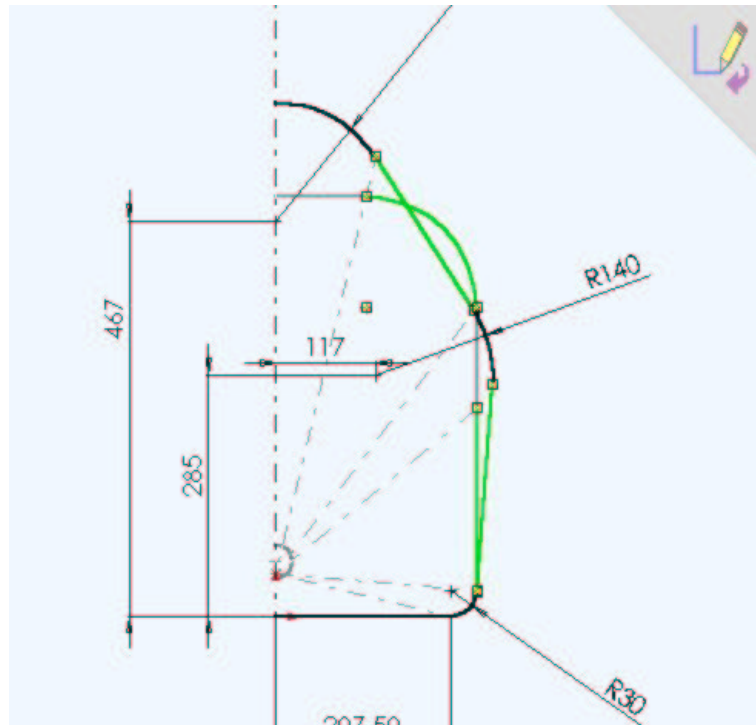


Figure 4.16: The definition of the line segments in the front hoop and the bulkhead and kneebox sketches.

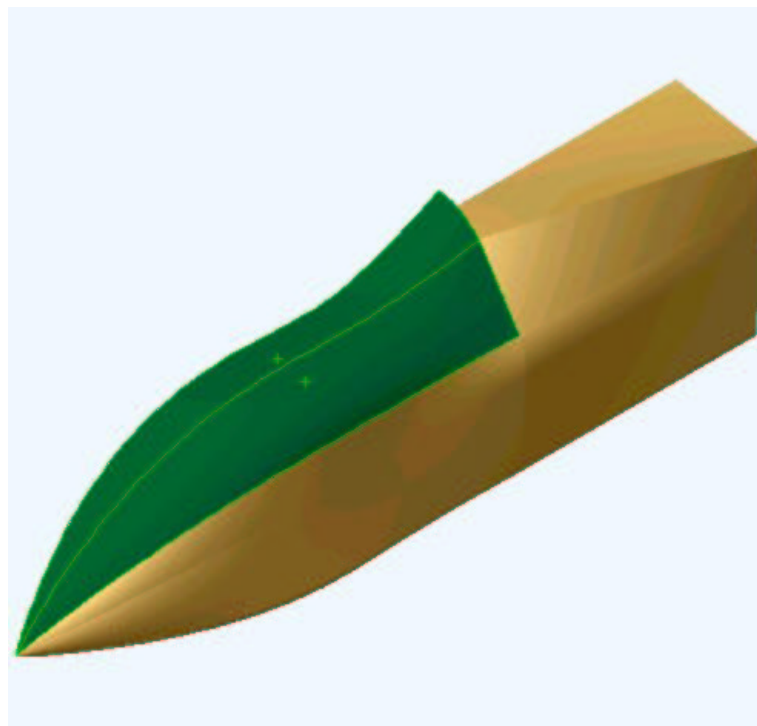


Figure 4.17: The edges of the redesigned nose were as close as possible to being tangential to the predicted flow.



Figure 4.18: Front view of the face edges, showing them not bending tangentially to the bodywork surface along their length.

As can be seen from Figures 4.15 and 4.16, the new method of defining the bulkhead and kneebox sections means that these two sections were congruent, creating the flat (in the z-direction) section on the top of the nose between these two sections. This (again, by inspection) will cause a pressure gradient up the centreline of the car that first decreases sharply, then increases sharply until it reaches the front hoop. Changing the pressure like this will always create a greater disturbance to the airflow than required (much like the head loss from placing multiple venturis in a pipe).

After this, one of the design intents for the nose was refined to be to create the most gradual pressure gradient possible. This would be achieved by using the most gradual curvature possible.

A cockpit side section was added to the rear of the second model. This is shown in Figures 4.14 and 4.15, in which it can be seen that the cockpit rim is a straight edge. This is simply because at the time, no cockpit rim member (part of the chassis) had been designed. It was planned that when that member was added to the chassis, the

cockpit rim shape could be created in this model.

This centre-section design would allow the side-impact chassis members to protrude through the bodywork (Figure 4.29), but also at the time, the design incorporated low-down sidepods, which were to fit over the protruding chassis members. The pods were later abandoned, requiring a redesign of the centre section of the car.

4.3.3 The Third Model

The third nose model involved three changes over the second:

- A 200mm stretch, via the redefinition of the “Nose Point” plane to 2120mm (from 1920mm) forward of “Main Hoop”,
- The “Nose Point1” sketch being placed level with the floor,
- A redesign of the “Nose Shaper” sketch, as shown in Figure 4.19

The “Nose Shaper” plane remained 10mm behind the “Nose Point” plane.

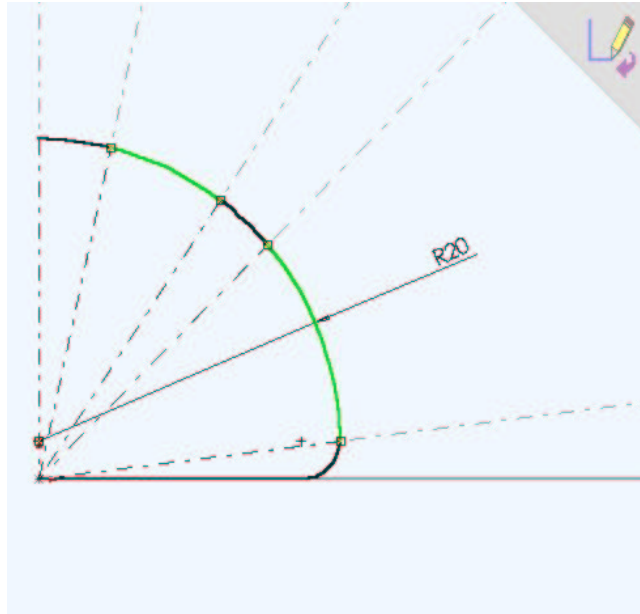


Figure 4.19: The new nose shaper sketch, made from six line segments, and flat on the bottom.

The “Nose Shaper1” sketch in this model was constructed from the construction lines described in the redesign of the second model. A 20mm radius circle was constrained such that its centre was coincident with the (vertical) centreline, and the right-hand (as we view it from the front, i.e., the port side) constrained tangent to a small circle which itself was tangent to the floor line. From here, the circles were trimmed and constraints were placed such that the point at which the 20mm circle met the smaller circle was coincident with the bottom construction line, and horizontal with its centre. Once this was fully defined, the 20mm circle was split at each construction line to produce the sketch shown in Figure 4.19.

This redesign was intended to flatten the underside of the nose, while containing as many line segments as the front hoop sketch, to prevent the loft from warping, as described earlier. The requirement for this was derived from the competition rule 3.2.1: “Ground Clearance”, stating that “ground clearance must be sufficient to prevent any portion of the car (other than tires) from touching the ground during track events.” From this, the relevant members of the USQ Motorsport team decided on an arbitrary ground clearance of 65mm. This would allow the regulation ± 1 inch (25mm) of suspension travel, with a 40mm safety margin at the axle. However, if the suspension

moves through 25mm, and the car pitches (the nose moves up or down) at the same time, the change in ride height will be different at any point that is not level with the axle. Consequently, if the bodywork in front of the front axle extends below the 65mm decided upon, and the front suspension is fully compressed at the same time as the car undergoes a forward pitch (the nose points down), the safety margin is reduced.

Placing the nose point sketch above the level of the floor of the car, as previously practiced, requires that the bottom surface of the lofted feature generated from that sketch must extend downwards before passing the bulkhead sketch. By the nature of a SolidWorks loft, this usually results in the curve defining the bottom surface of the feature “overshooting” the floor level and extending below it, before retreating upwards to join the floor (shown in exaggerated fashion in Figure 4.20).

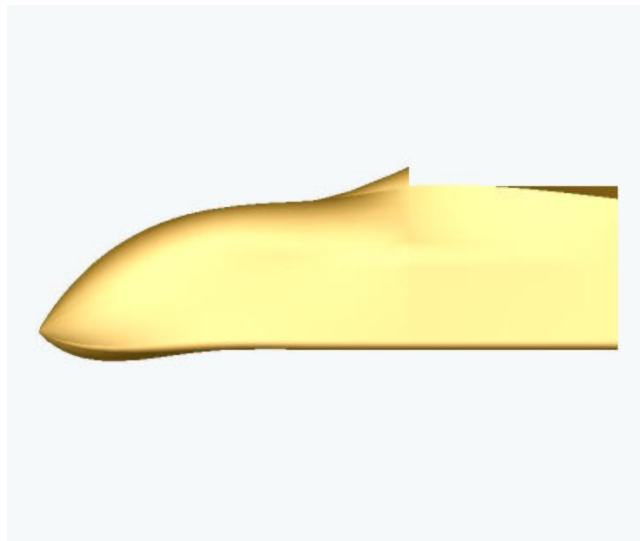


Figure 4.20: The floor-level overshoot caused by lofting between two sections whose lowest points are not level.

In this model, the point sketch and the bottom edges of all other sketches are placed level with the floor of the car, creating a completely flat underside. This not only results in the elimination of the overshoot of the floor below the 65mm ground clearance, but also eliminates the rounded boat-like underside of the forward nose (also visible in Figure 4.20).

The 200mm stretch of this model was found to create a more gradual curve up the centreline of the body than the original length. This was one of the design aims decided upon earlier. Additionally, this increase in length will produce an increase in surface area on which sponsorship logos may be placed. Increasing signable area to increase sponsorship was a major design aim from the beginning of the project.

4.3.4 The Fourth Model

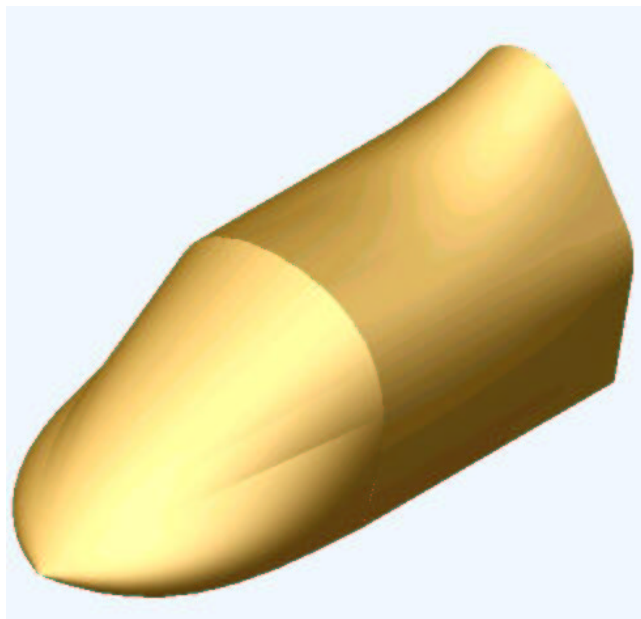


Figure 4.21: The fourth nose model.

The fourth nose model showed a large advance in the design of the nose model. Learning how to use the “spline” tool in SolidWorks was instrumental here. The use of the spline allows a smooth cross section to be defined at multiple places along the intended loft. This means that “hard” edges (that do not meet tangentially) can be almost eliminated.

Unfortunately, this model still used a number of line segments for each sketch. As shown in Figure 4.22, this still leaves us with several faces. However, this was not the problem intended to be solved here. This model was constructed in an effort to prevent the undersurface of the forward nose from extending outboard of the fillets. As shown in Figure 4.23, the floor of the third model (bounded by the in-built fillet at the side)

extends outboard of the rail in the chassis ¹.

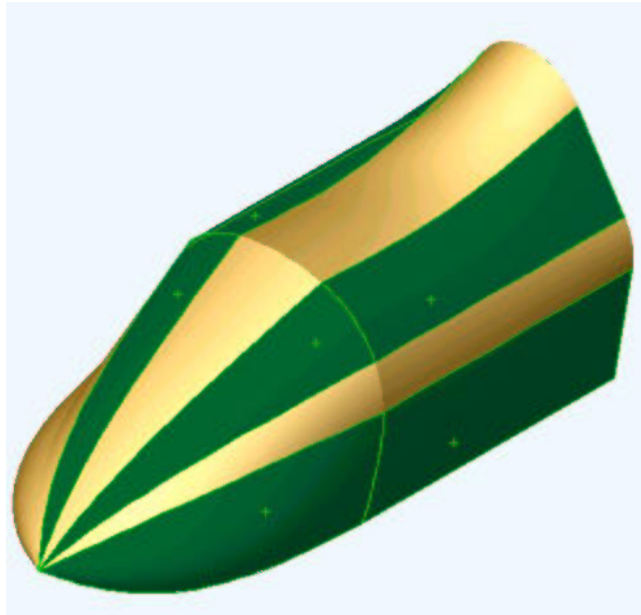


Figure 4.22: The separate faces still being created in this model.

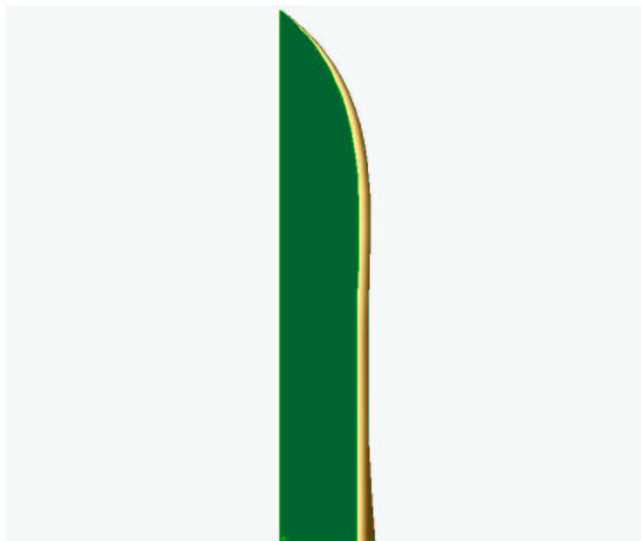


Figure 4.23: The fillet at the edge of the floor panel is not parallel to the z-axis, and so does not follow the rail chassis members correctly.

So the intent for the fourth model was to use two lofted surfaces, and use the **Start/End Tangency** feature in SolidWorks to constrain the rearmost edge of the foremost loft

¹The rail is the length-wise member which runs from the bottom corner of the bulkhead to the bottom corner of the rearmost box, along the “Rail” plane , shown in Figures 4.5 and 4.1.

to be tangential to the forward edge of the adjacent loft.

Unfortunately, this attempt was fruitless, as the only effects that applying an end tangency constraint had were to *slightly* reduce the “duckbill” bulge, and to round off the edge between the two lofts. Neither of these outcomes were anywhere near the desired outcome, making this model an apparent loss.

However, out of this model came a major breakthrough. As discussed at the beginning of this section, the “loft” feature was used successfully to define a smooth cross section. This ability was used to effect in the next model.

This model was very different from the preceding models, the most striking difference (apart from the hard edge between the two loft sections) coming from the fact that this model contained an elliptic nose shaper. This produced the strange “duckbill” shape, and the sides of the nose in front of the bulkhead bulged outwards. This would make removal of the finished product from a male plug very hard. By inspection, one can see that it will also create a turbulent zone along the sides of the car from the bulkhead rearwards, but serves no positive purpose. This problem could have easily been fixed by redefining the “Nose Shaper1” sketch to be narrower in the y-direction. This was manifested in the following models.

4.3.5 The Fifth Model

Using the lesson learned in the construction of the fourth model, the fifth model (Figure 4.24) represented the greatest advance in the model design so far. The advance was that, using the “spline” feature, a single line segment was used to define the upper surface of the nose, and therefore, a single surface was lofted here. The use of a single line segment is illustrated in Figures 4.25 and 4.26. ²

A slight problem still remained, though. The “Front Hoop1” sketch still contained eight line segments, so at the rear of the model, the lofted section was defined by a sketch

²These sketches were constructed using splines which are not fully defined (shown in blue). The two endpoints and three interpolation points *are* fully defined, but the gradient of the ends of the spline is not. The default condition that produces a spline of least curvature is invoked here (tested using the **Inspect Spline Curvature** tool).

containing eight segments, while the front end was defined by a sketch containing only three (one segment for the floor, one each for the fillets, and one for the upper surface). Making this one part would warp the loft, as discussed earlier, so it was decided to construct this model from two lofts.

To do this, the first loft was constructed over the usual “Nose Point1”, “Nose Shaper1”, “Bulkhead1” and “Kneebox1” sketches. Then the (three-segment) “Kneebox1” sketch was used (using the **offset entities** tool) to create an eight-segment “Kneebox2” sketch. The entities in the first kneebox sketch were offset to another sketch, then the construction geometry used in the redesign of the second model was used again to split the spline. This left the spline not fully defined (Figures 4.25 and 4.26), but the general shape remained, and it was considered that this was accurate enough for the purposes of a “proof of concept” model such as this. Full definition of this spline would come later.

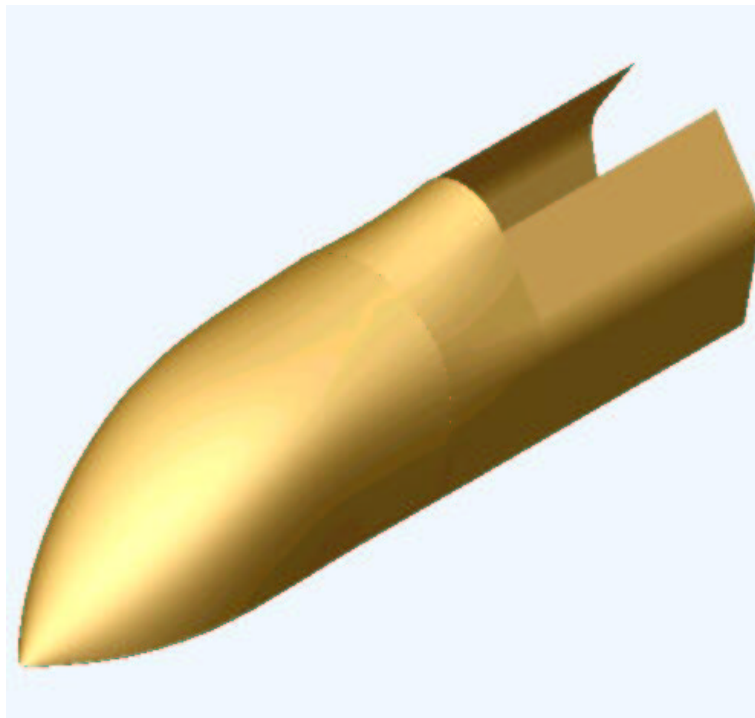


Figure 4.24: The fifth nose model. Note the one-piece top panel design.

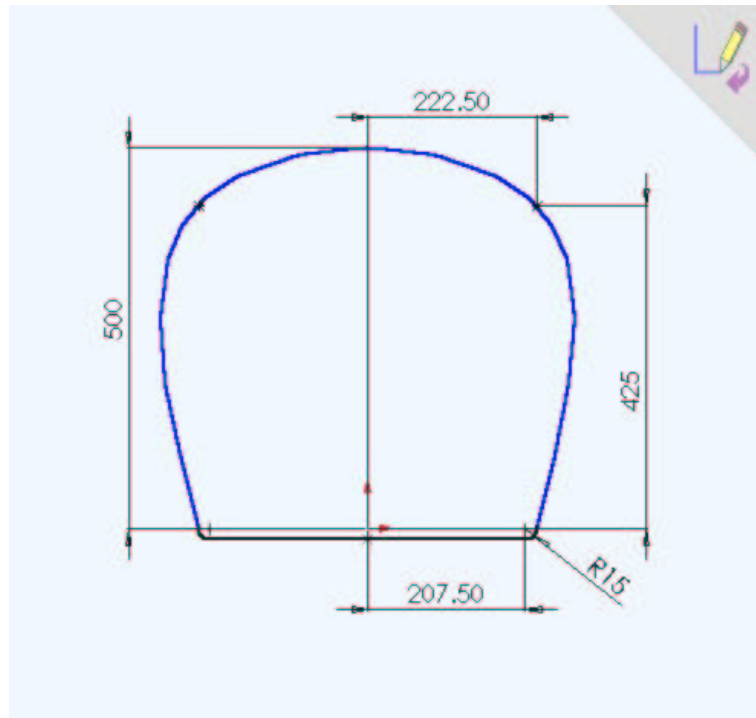


Figure 4.25: The bulkhead sketch used to define the shape of the fifth nose model.

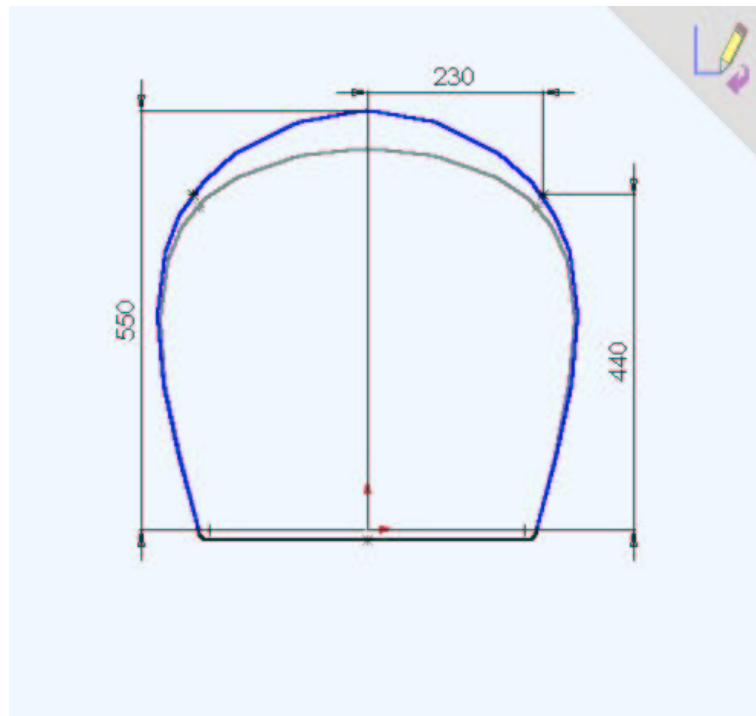


Figure 4.26: The kneebox sketch from the fifth nose model. The bulkhead sketch is shown in grey.

This model, although being a great step forward in the design, was also still being held back: lofted surfaces were still being used, and therefore filleting was impossible (filleting surfaces is possible, but SolidWorks 2001 cannot fillet the point of the nose). Because of this, the fillet along the bottom edge had to be created in the definition of the original loft, not added later, as is the usual practice with feature-based modelling software.

It was considered possible that once CFD analysis had begun, a requirement for a modification to the bodywork to more vigorously deflect the oncoming airflow to be deflected over the top of the driver's helmet *might* be discovered. This principle is used to effect on modern road motorcycles to reduce wind buffet on the rider at highway speeds.

With this in mind, a mid-life redesign of this model was executed, but soon abandoned as a permanent fixture (it may very easily be reintroduced to the final model, if required). This change was the addition of a small dip in the top surface of the model, level with the kneebox, as shown in Figure 4.27, and the spline used for the definition of which is shown in Figure 4.28.

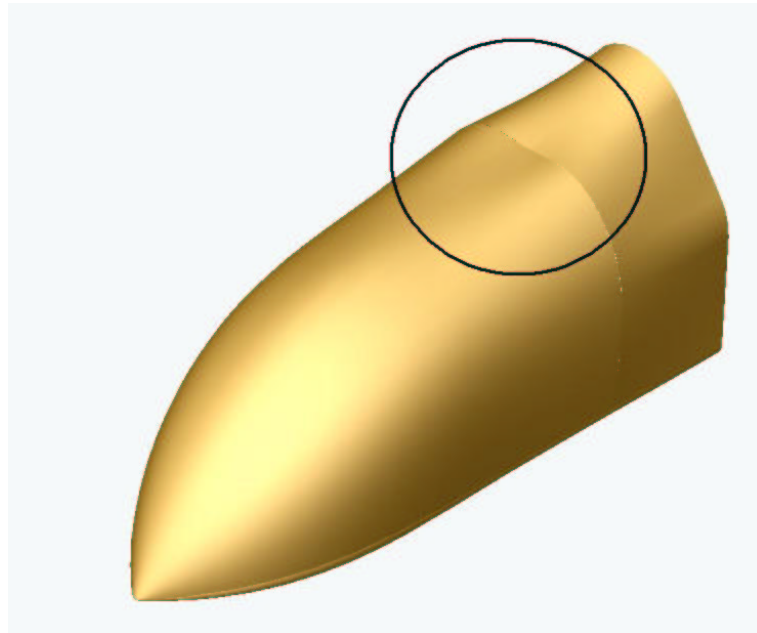


Figure 4.27: The depression intended to deflect airflow over the driver's head.

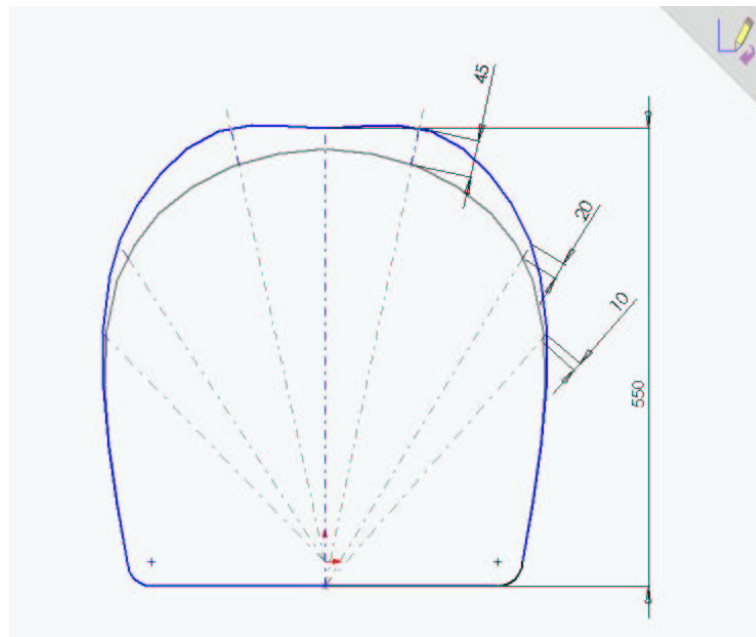


Figure 4.28: The kneebox sketch used to define the depression shown in Figure 4.27.

This redesign was intended to increase the gradient at which the airflow leaves the bodywork at the front roll hoop, thereby spitting the airflow over the top of the driver's head. No CFD had been done at this stage, but if it were found that such a mechanism were required, this model proved the ability and developed the method by which to do it.

The fifth nose model was used to construct the first assembly of parts. This is shown in Figure 4.29. This was used to check the fit between the nose model and the chassis.

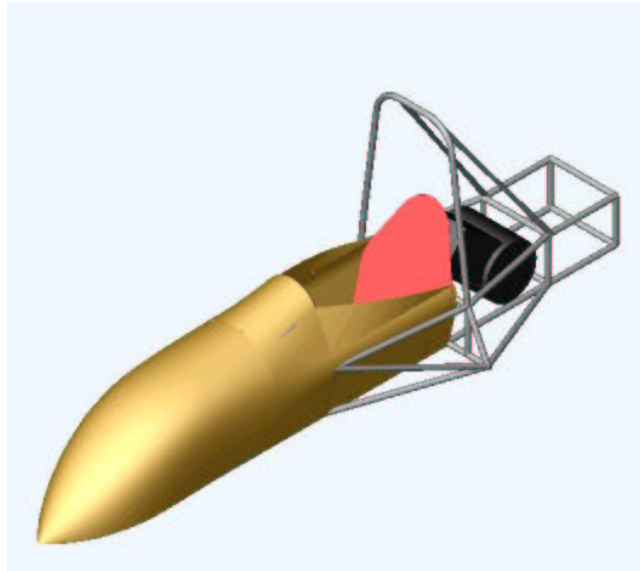


Figure 4.29: The first assembly, showing the fit between the nose and the chassis. It includes a very simple motor model. Note that the fit is not perfect, as the top chassis members between the bulkhead and the front hoop protrude through the bodywork

4.3.6 The Sixth Model

The sixth design iteration of the nose model introduced the solid model, as opposed to the model constructed from surfaces, and the first attempts at rounding the point of the nose, as required in Rule 3.3.7.

As an effective method of filleting the entire edge along the bottom of the model from end to end had not been discovered yet, the solid loft was defined using sketches similar to those from previous models (modified slightly to produce a cross-sectional shape with flatter sides and top, half way between the first model's rectangular section and the fourth model's round section), including the rounded bottom corner. Creating the fillet was not the design intent of this model, rather to find a way to round the nose.

With this in mind, the model was created as before, then a cut extruded (Figure 4.30) to take 20mm off the very front of the nose, and the space replaced with a revolved dome. This produced the geometry shown in Figure 4.31

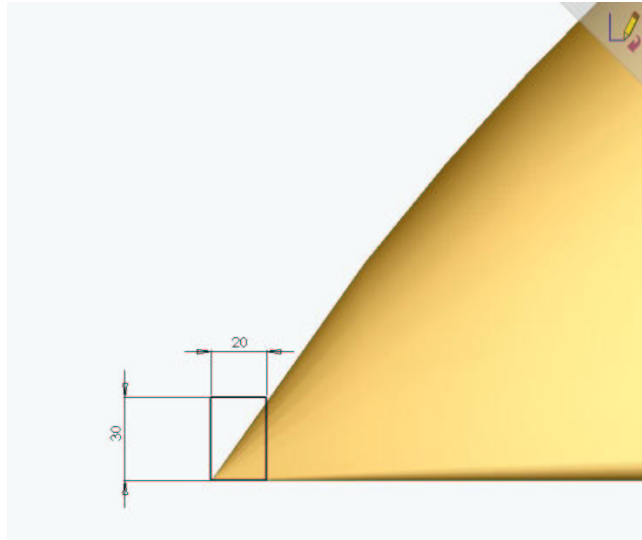


Figure 4.30: The sketch defining the cut used to round off the nose point.

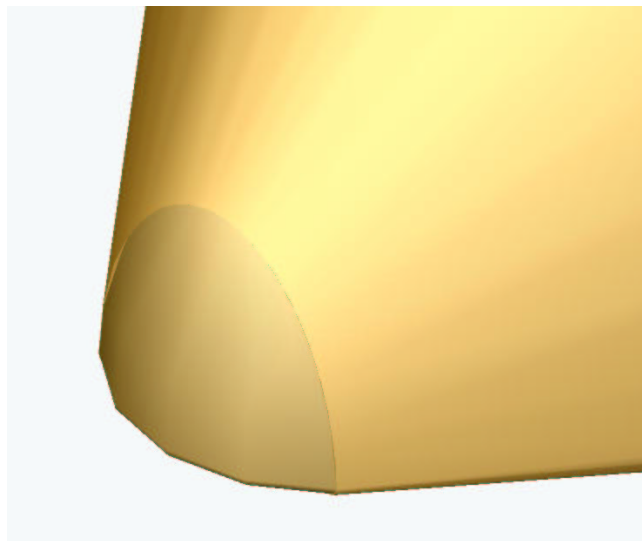


Figure 4.31: The rounded nose. This would not comply to the rules, as the radius around the bottom edge is too small.

This trial was deemed an unsatisfactory method by which to round the nose, as it rounds only the sides and top of the nose point, and not the bottom edge. This would result in disqualification from the F-SAE competition under the “Frontal Impact Protection - Others” ruling. This method is also far more complex than one would expect from experience in solid modelling.

After some redefining of the fillet radius, and the body geometry (to increase the included angle in the nose point), it was found that an edge fillet could be made to work. So, in anticipation of using this tool, the sketches defining the lofted sections were redefined to omit the rounded bottom edge, leaving it a “hard” edge (Figure 4.32). Subsequently, this hard edge was filleted to a constant radius of 40mm (Figure 4.33).

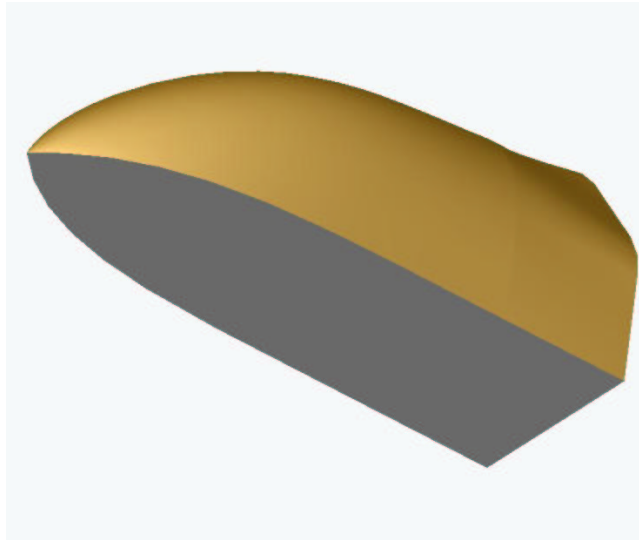


Figure 4.32: The bottom edge as created, without the fillet.

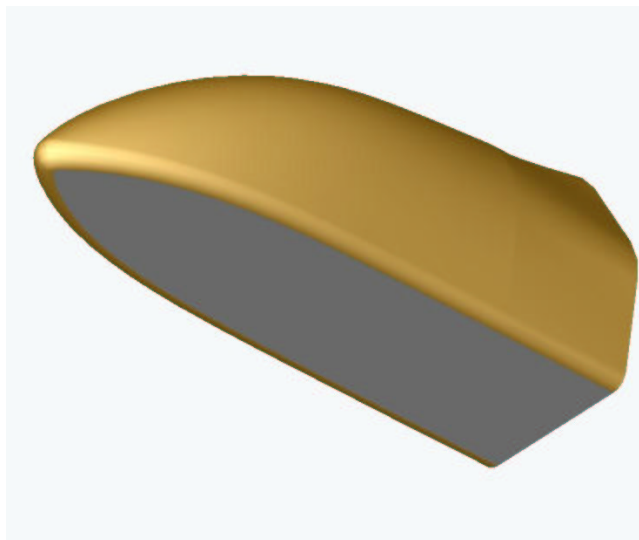


Figure 4.33: The bottom edge with a constant 40mm radius fillet.

The use of the fillet represented another large advance in the design of the solid model, but again, was held up by the fact that the fillet radius around the chassis rail was

required to be 16mm (the outer diameter of the steel tube used), while at the point of the nose, to be 40mm (slightly greater than the 38mm specified in Rule 3.3.7).

Investigations into the use and limits of use of the **Variable Radius Fillet** tool had been occurring for some time, but to date had been returning only error messages. Now, upon slight modification of the model to increase the included angle in the very point of the nose, the use of the variable radius fillet was successfully demonstrated, and used to great effect in the next, and final, model.

It was at this stage that it was decided that the bodywork did not have to remain in contact with the chassis for the entire perimeter of the front roll hoop. It would be wholly acceptable to leave a gap between the hoop and the bodywork, which may be left as-is, or plugged later to reduce vibration. This idea was used also to great effect in the final model.

4.3.7 The Final Model

The final final model is, as can be seen in Figure 4.34, *completely* different from the initial design. Incorporating a single lofted section, with a total of two faces (top surface and floorpan), it demonstrates the intended use of a feature-based solid modelling program. The original loft was featured with a variable radius fillet (from 16mm at the rear end to 40mm at the front), then shelled to create the final model.

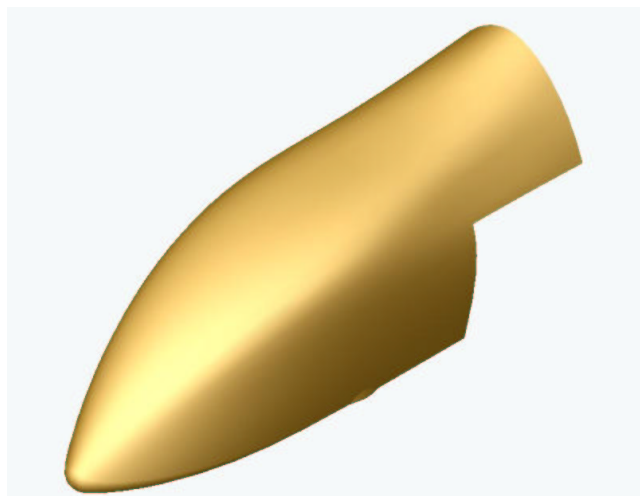


Figure 4.34: The final design, complete with a suspension cutout to clear the wishbones.

But the modelling did not stop here. Upon inspection of the fillet, it was found that the bottom edge, where the fillet joins the floorpan, is not a straight line, but curves in towards the centreline of the car, and the chassis protrudes from the bodywork near the bulkhead. This is because the variable radius fillet begins at the front hoop, at a radius of 16mm, and linearly expands to 40mm at the nose. This means that at the bulkhead, which 46.6% of the way from the front hoop to the nose point, the radius of the fillet is $40 - 16 \times 0.466 + 16 = 27.17mm$. The ends of the curve, when viewed in cross-section, are tangential to the neighboring surfaces, so the surface of the fillet must progress inside that of a fillet of a smaller radius. This is shown in Figure 4.36.

The variable radius fillet was suppressed, and an extruded cut, very much like a 16mm radius, created from the bulkhead plane, and extruded backwards “Through All”. From here, the suppressed fillet was redefined to apply to the edge that was left after this extruded cut was taken, and unsuppressed. This had the effect of creating a fillet of 16mm radius from the front hoop to the bulkhead, then linearly varying to a 40mm radius at the very point of the nose.

Illustrations of this can be seen in Figures 4.35, 4.36, 4.37, 4.38, 4.39 and 4.40,



Figure 4.35: The floor of the nose, showing that its edges are not parallel aft of the bulkhead. Also visible is the change in radius of the fillet along the length of the filleted edge

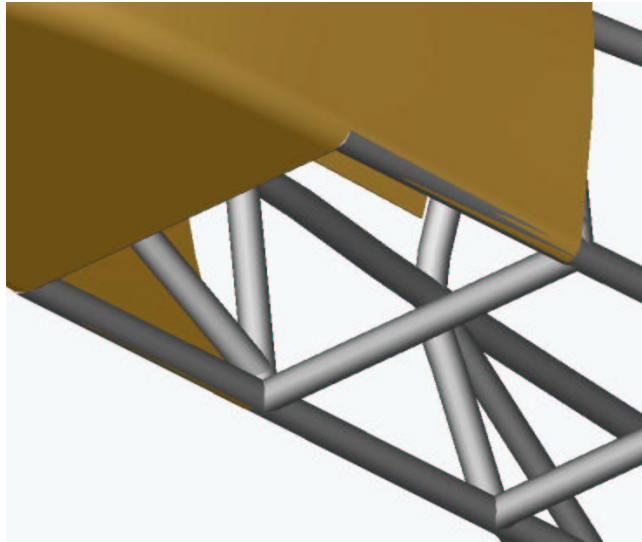


Figure 4.36: The chassis protruding through the bodywork.

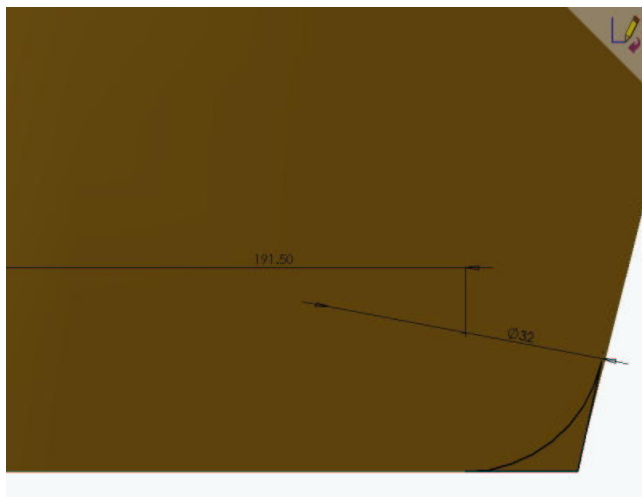


Figure 4.37: The sketch for the extruded cut outlined in the text.

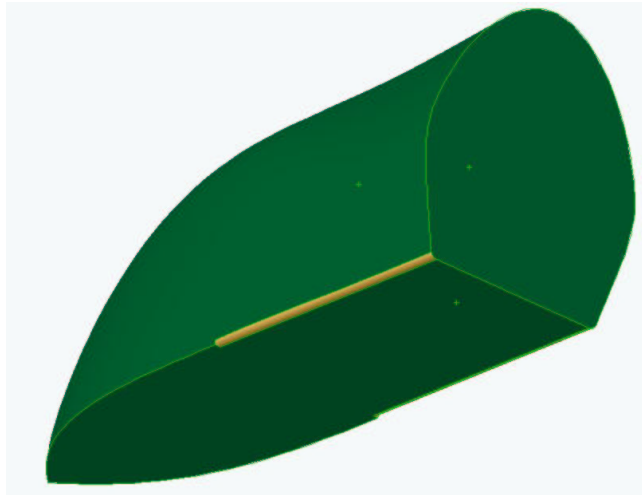


Figure 4.38: The extruded cut used to replace the variable radius fillet.

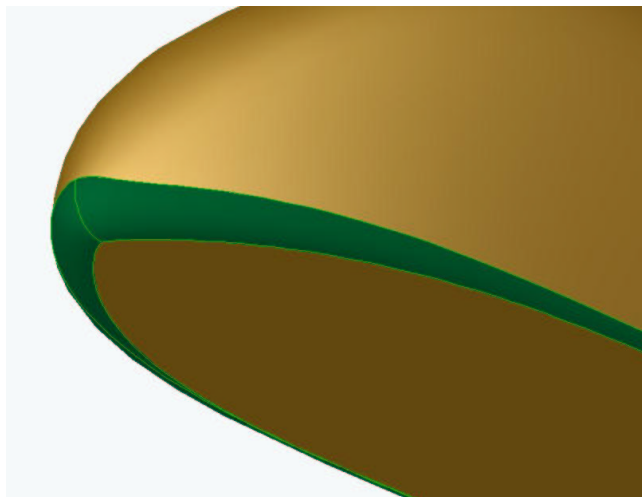


Figure 4.39: The variation in the radius of the nose fillet.

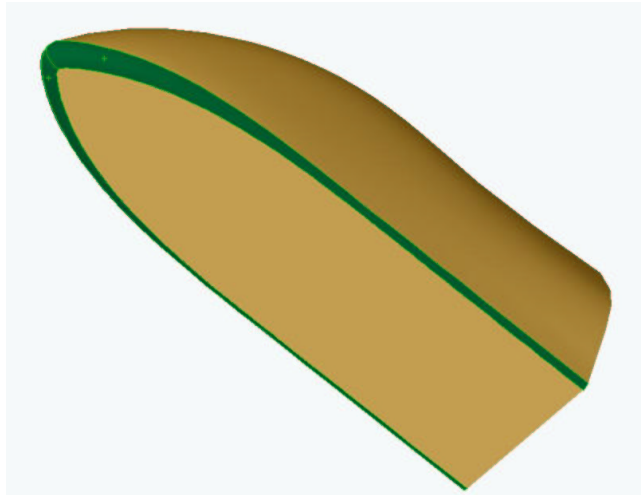


Figure 4.40: The straight-edged cut (aft of the bulkhead) merged well with the variable-radius fillet (forward).

The very front of the variable radius fillet could have been higher off the ground, in order to make the nose shorter and lighter. However, as previously discussed, the nature of lofting in SolidWorks makes this hard, but also, Figures 4.41 and 4.42 show the effect of raising the stagnation point on the nose of a car. It is clear from this that the lower the stagnation point, the better.

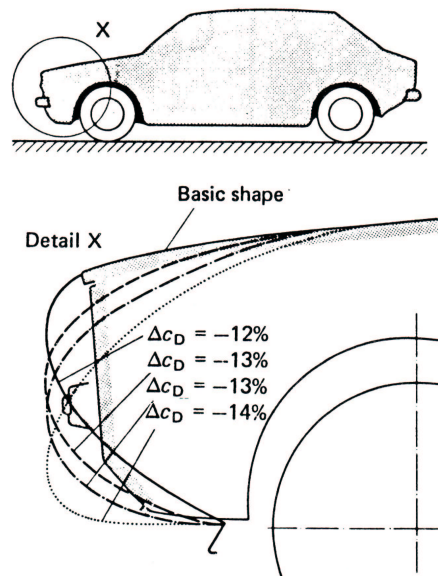


Figure 4.41: $\% \Delta C_D$, as a function of stagnation point height (Hucho 1987).

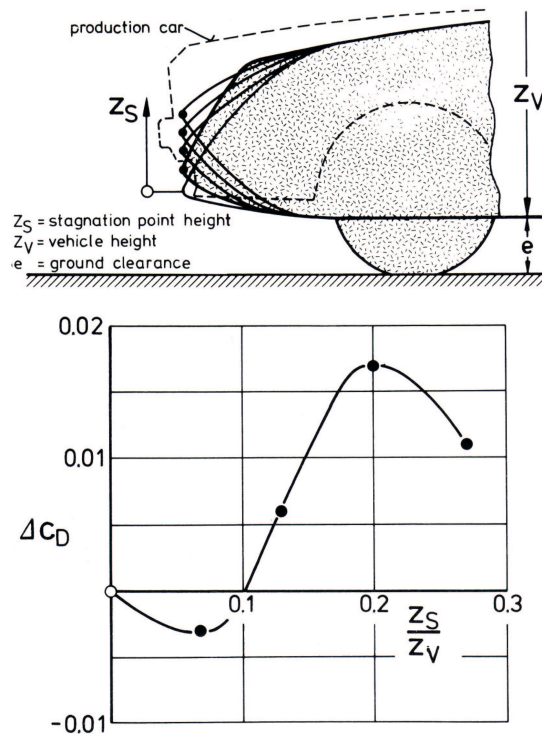


Figure 4.42: ΔC_D , as a function of the stagnation point height-vehicle height ratio (Hucho 1987).

4.4 The Centre Section

The centre section was the easiest part of the car to design. No work was done on this part until very late, as it was anticipated that after the team obtained a seat, another chassis member could be placed around the back of the seat, to define the cockpit rim, then the side panels could be moulded around this member. So not much design was done of this section until it was decided not to wait for the seat, but to cut the cockpit sides down to the level of the upper side impact chassis member.

The early model, assuming an arbitrary cockpit rim shape can be seen in Figure 4.43. The cockpit rim shape was created in a 3D sketch as a spline from one of the spline interpolation points in the front hoop sketch (imported from the nose model), to the point on the Main Hoop plane with the (x,y) coordinates, (288.10 , 603.49) (this was a

geometrical entity in the “main hoop2” sketch), and constrained to be normal to the x-y plane at both ends.

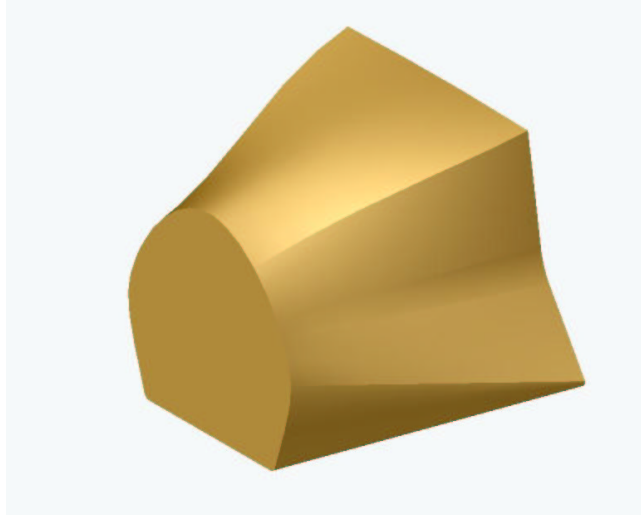


Figure 4.43: The basic early centre section model, using an arbitrary cockpit rim shape.

This spline was then used as a guide curve for the lofting of the section between the upper sketch of the front hoop and the main hoop sketch (Figures 4.44 and 4.45).

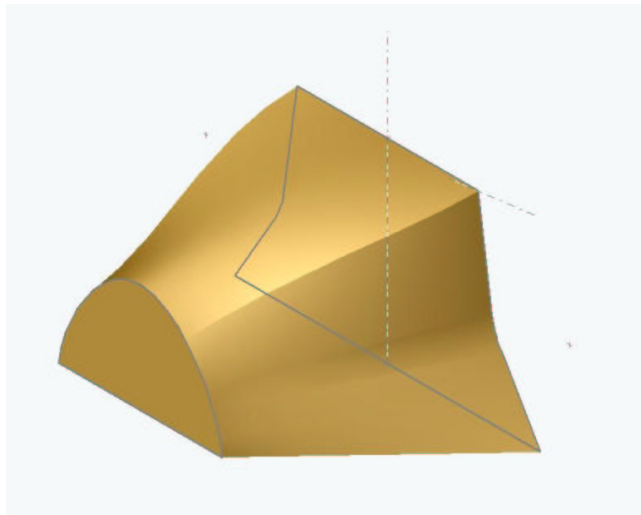


Figure 4.44: The base loft feature.

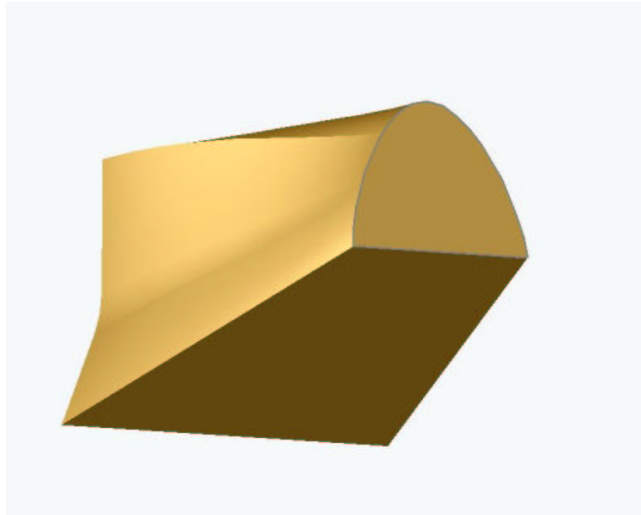


Figure 4.45: The base loft feature, from the other side from Figure 4.44.

Figures 4.46 and 4.47 show the bottom half being attached to the model, by the use of another loft. This loft was then mirrored, to produce Figure 4.48. The highlighted edges in Figure 4.48 were attempted to be filleted, however, SolidWorks is not able to do this when the two edges meet at a vertex. So, the front hoop plane was redefined to be 60mm forward of its actual position, and a 60mm cut extruded off the rear end of the model (Figure 4.49). This made the edges able to be filleted.

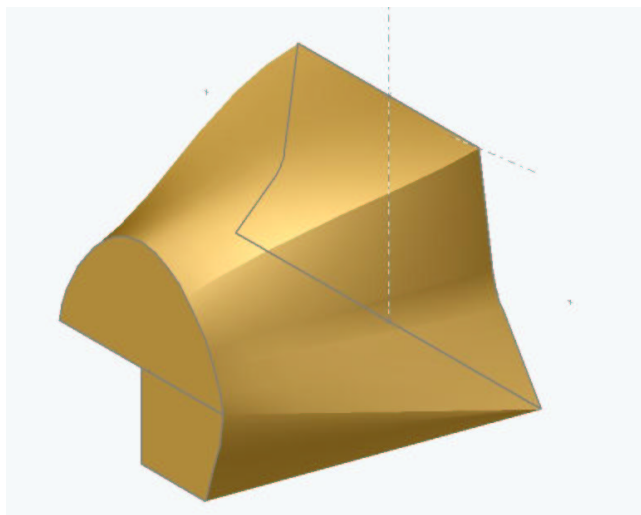


Figure 4.46: Half of the under side being added.

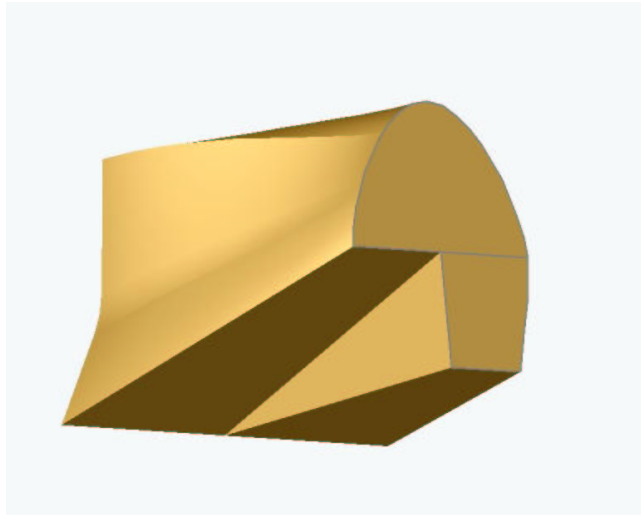


Figure 4.47: Rear view of Figure 4.46.

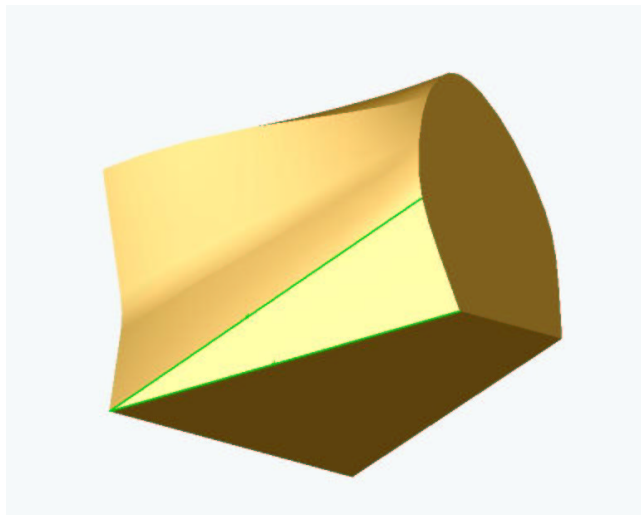


Figure 4.48: The mirrored part, completing the basic solid model. Note also the highlighted edges. These are to be filleted later.

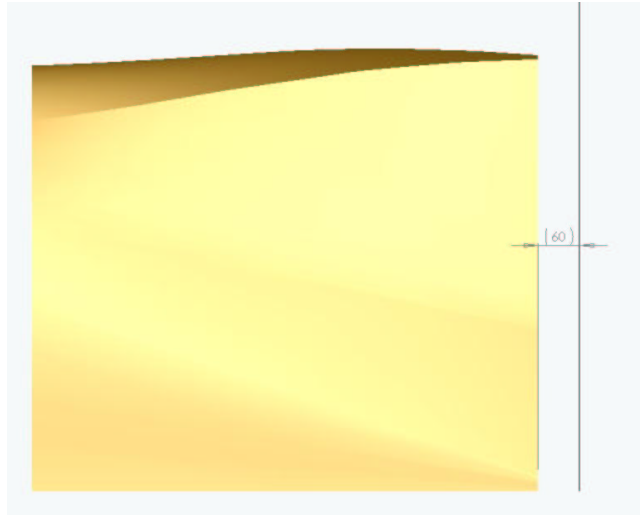


Figure 4.49: The definition of the extruded cut used to allow the edges shown in Figure 4.48 to be filleted.

After the decision was made not to wait for the seat, but to use the upper side intrusion member to shape the bodywork, the model was cut off above 266mm (the height of the upper surface of the member). The six exposed edges were then filleted (Figure 4.50).

This was a relatively simple formulation of a part, but after the experience gained on the nose model, this took much less time than expected.

From this solid model, a plug model was required for entry into the CNC milling machine and (BAC) in order to cut the plugs.

Keeping the amount of material removed to a minimum in a CNC operation reduces the machining time for that operation. The maximum depth of cut for BAC's machine is 250mm, and it cannot undercut (it is a three-axis machine), so a plug model which was no more than about 250mm, but takes up as much space inside a rectangular prism bounding the required part, while not containing an undercut, was required. In order to make this, a new plane had to be defined. To define the plane, and 3D sketch was constructed, as shown in Figure 4.51, using four straight lines. The corners were constrained to be coincident with the edge that they lie on, three of the corners constrained coincident with the ends of the fillet sections near them, and each pair of opposite edges were constrained to be parallel to each other. This fully defined the

sketch in a plane, allowing the creation of another datum plane in the plane of the sketch.

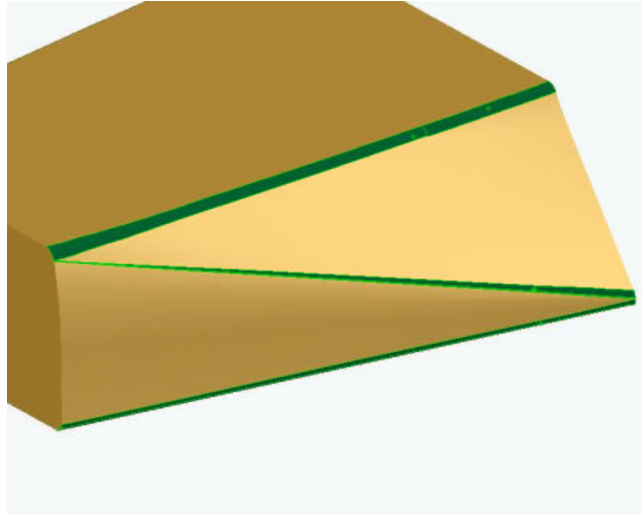


Figure 4.50: The fillets fully defined, curving around the chassis members.

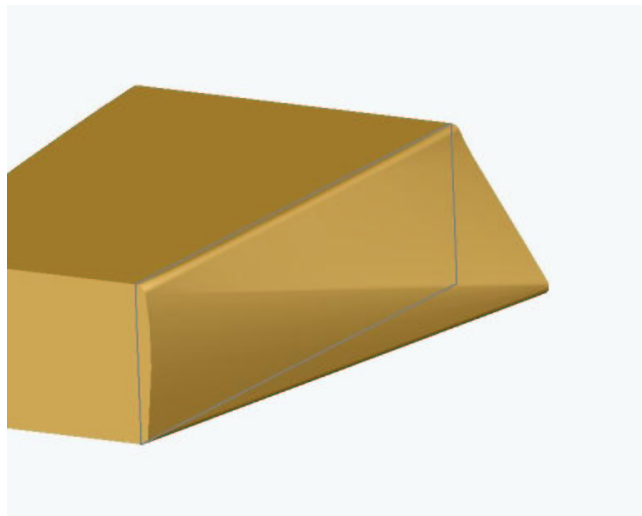


Figure 4.51: The sketch used to define the cut to create the plug model.

This new datum plane was used to extrude a cut to remove all material of the inboard side of the plane, and shown in Figure 4.52.

This fully created the plug model for the port side panel, and the starboard plug was merely a mirror image of this. The two models were assembled together in an assembly, so that they could be cut concurrently. This assembly is shown in Figure 7.18.

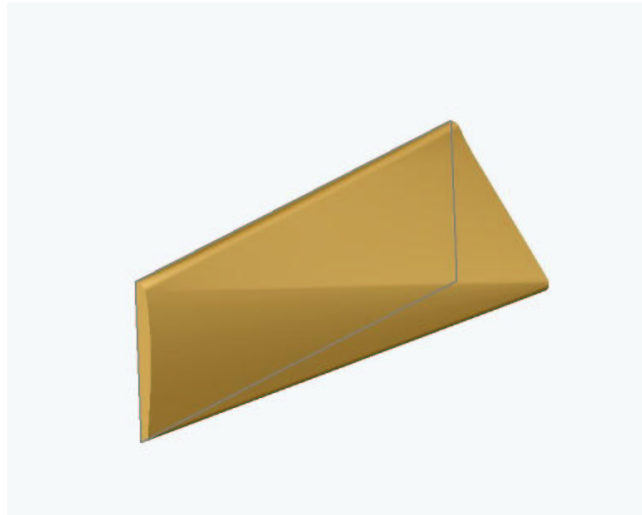


Figure 4.52: The completed centre section plug.

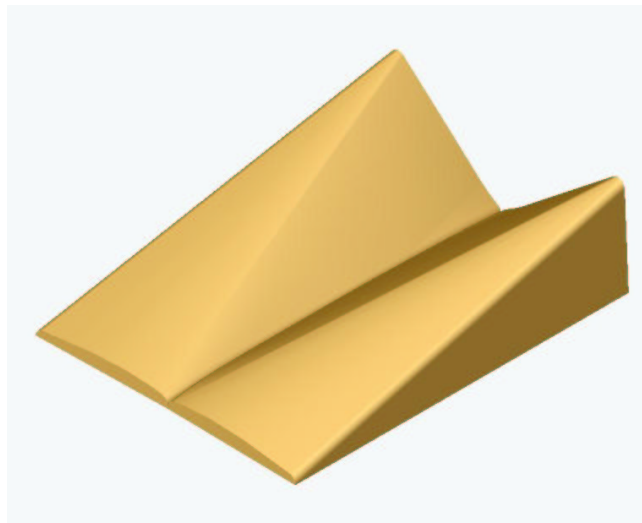


Figure 4.53: The port and starboard plugs assembled to create one model. This will halve the set-up time for the machining operation.

4.5 The Rear End CFD Model

The CFD analyses will require another section attached to the car, to simulate the rear end, aft of the main hoop.

The flow through this area on the actual car will be very turbulent, and there will be no

flow attachment anywhere, so a simple shape that promotes this kind of flow regime is required. The shape shown in Figure 4.56 was constructed by lofting between two cross sections, as shown in Figures 4.54 and 4.55. The sketch in Figure 4.54 was converted from the rear edge of the centre section, with the top half added arbitrarily, in order to simulate the firewall and driver's head.

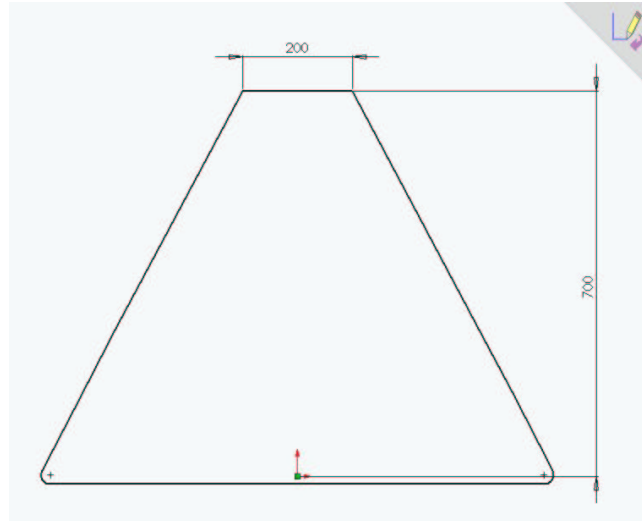


Figure 4.54: The main hoop sketch to create the rear end of the CFD defeature.

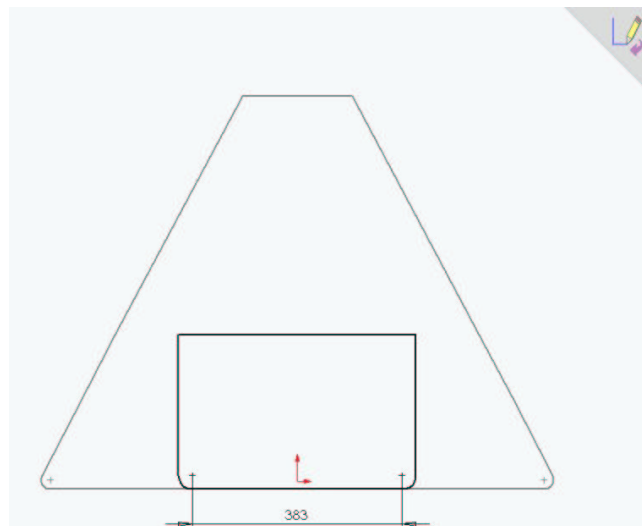


Figure 4.55: The rearmost sketch to create the rear end of the CFD defeature.



Figure 4.56: The rear end of the CFD defeature.

4.6 Defeaturing the CFD Model

When finite-element analyses are performed, the part that is being analysed is usually “defeatured”. This means that many of the small features that will not make a significant contribution to the final outcome are taken away. If they were not omitted, the mesh around these small features would be incredibly small, and therefore, the size of the whole mesh in terms of number of elements would be incredibly large. This increase in mesh size is not warranted by the negligible (if any) increase in accuracy of the simulation.

So the process of defeaturing the car was undertaken. The blisters covering the bulkhead screws were suppressed, as were the cutouts and the shell feature in the nose. The chassis was not included in this model, and the centre section side panels were replaced by the original part, with all features suppressed after the horizontal cut at 250mm, and the subsequent fillets. All other assembly members were omitted. So the model was defeatured from that seen in Figure 4.57, to that seen in Figure 4.58.

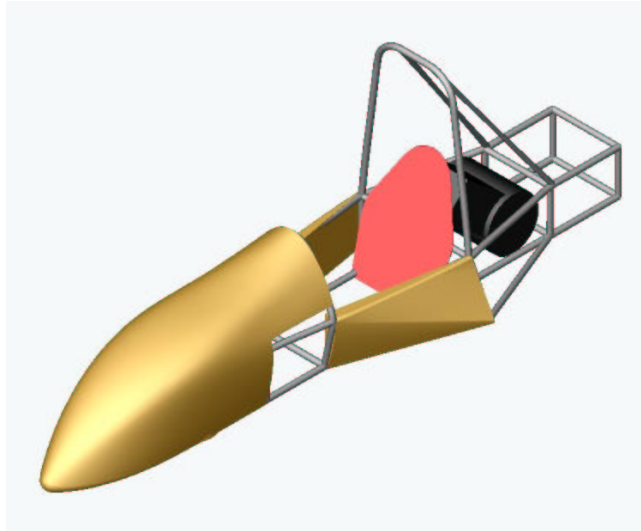


Figure 4.57: The full assembly model, including chassis, motor and firewall.

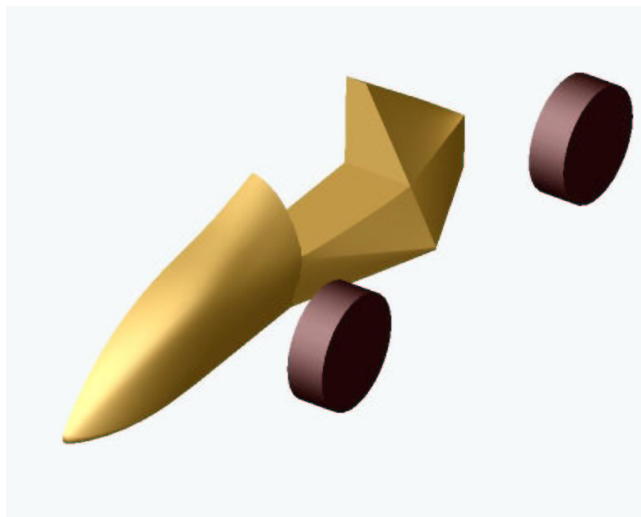


Figure 4.58: The defeatured CFD assembly model.

The fillet around the bottom edge of the nose was left as it was, because this is considered to be a major feature. If this were to be taken away, the results of the CFD would be substantially different from those if the fillet were left (see Figure 4.41). Consequently, the matching fillets around the bottom edges of the centre section and rear end were also left as-is.

The CFD defeature is also cut in half down the centreline, to exploit centreline symmetry. This halves the size of the mesh, and the CFD software can make allowances

for the fact that on the other side of the symmetry plane is supposed to be another half of the car. The outcome is the same, but the mesh is half as big (or twice as fine).

So was created the defeatured model for the car. Now that all solid models had been created, they had to be exported for the CFD analyses in a file transfer filetype.

4.7 Exporting The ACIS File

Once the full model had been created, the file was saved as an ACIS file (.sat). GAMBIT can read .sat files as real geometry, and can process the resulting geometry in order to mesh it.

There were other filetypes available, including Parasolid and Binary Parasolid (.x_t and .x_b), but the ACIS model worked well enough for our requirements.

4.8 Review Of Solid Modelling

The creation of the solid models of the parts of the car was very time-consuming, and was held up by the design of several other parts of the car. However, it did get done in time, and was very effective, using the single file to allow the shapes to be analysed in a CFD program (described later), and cut on a CNC milling machine (described later), as well as to be used in promotional material and advertising. Solid modelling is definitely an extremely powerful method of design.

In this chapter, we have seen the design of the chassis, nose cone and the side panel models and the creation of the CFD defeatured model, now we must see how this allows us to perform CFD analyses on such shapes.

Chapter 5

Methodology - Geometry Processing and Mesh Creation

5.1 Chapter Overview

After the geometry for the CFD analysis has been created, it must have a mesh applied to it. This breaks a single fluid zone (for example, the air around the car) down into many small pieces, allowing a computational analysis of the zone to be executed. As outlined previously, the software package used to apply this mesh is GAMBIT, from the Fluent Incorporated team.

GAMBIT is not simply a meshing tool. It also allows the creation of the geometry which is to be meshed. The operator does this in a different way from one who is using a solid modelling package.

In solid modelling software, such as SolidWorks, the operator creates geometry, as described in the last chapter, by creating features such as lofts and extrusions, then creating on them other features like fillets and shells. The software then recognises those features as such, that is, the computer deals with an “extrusion” and a “fillet”. This is because such software is “feature-based”, i.e., based upon features, not upon points and lines.

GAMBIT's geometry creation ability is much simpler than that of a solid modelling package. It deals with points, lines areas and volumes, and so cannot recognise a set of lines as a particular feature. This is not ideal for three dimensional modelling, or for modelling using complex curves, but for the creation of simple, rectangular-based models, it is perfect, as it does not take much time at all to create an acceptable model.

5.2 The 2-Dimensional Tests

Before work began on the full analysis of a complete defeatured model of the vehicle, two dimensional models of simpler shapes with known coefficients of drag were analysed. These were intended to ensure the correct choice of certain variables.

There are some variables and settings which must be set in FLUENT, which are not easily known before the analysis begins. For example, it is unclear whether using a segregated or a coupled solver, or implicit or explicit formulation would yield more accurate results. Also which viscous model, which sub-model of this, and what values for the relevant model constants will be used is also unclear.

A cube has a C_D of 1.05 (Figure 5.1 (Fox & McDonald 2003)). A simple two dimensional model of this, looking face-on to the prism, and defining a numerical depth of 1 to the model, would allow experimentation with the related inputs which must be set in FLUENT, until the correct values are found. The correct inputs will yield a calculated C_D figure of 1.05 for a model as outlined above, which corresponds to experimental data, proving that they are correct. These correct values may then be used in the analysis of the car, whose C_D is not known, with some certainty that they are correct, and therefore that the output of the final analysis is correct.

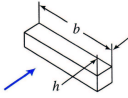
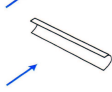
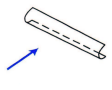
Object	Diagram	$C_D(Re \geq 10^3)$
Square prism		$b/h = \infty$ 2.05
		$b/h = 1$ 1.05
Disk		1.17
Ring		1.20 ^b
Hemisphere (open end facing flow)		1.42
Hemisphere (open end facing downstream)		0.38
C-section (open side facing flow)		2.30
C-section (open side facing downstream)		1.20

Figure 5.1: C_D figures for some simple shapes (Fox & McDonald 2003).

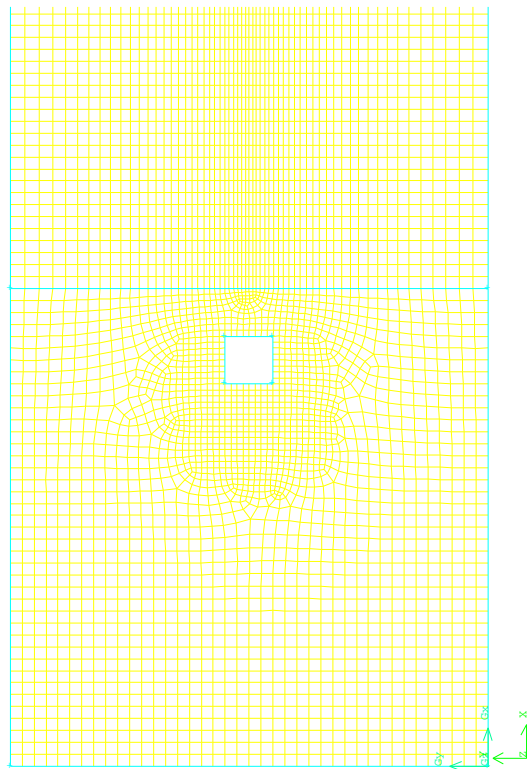


Figure 5.2: The mesh applied to the simple 2D square test model.

To this end, a simple square was created and meshed in GAMBIT, initially exploiting

centreline symmetry. The final mesh was quite small by current standards, and it was considered that doubling the mesh size would not make a significant increase in solving time, so the entire square was modelled. The decision not to exploit the symmetry of the model was made simply because the mesh is not large enough for this to make a significant difference in solving time, and because asymmetric wakes may be encountered (see Figure 5.3). The mesh is shown in Figure 5.2.

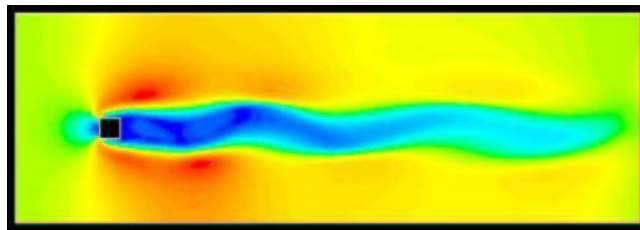


Figure 5.3: An asymmetric wake pattern.

The 2D model was created in GAMBIT, by defining vertices that define a $10 \times 10\text{m}$ square, a $10 \times 60\text{m}$ rectangle added onto the back (downstream of the flow) of that, and a $1 \times 1\text{m}$ square inside the first square. Edges were then constructed between these vertices, and areas defined by the edges. Three areas were defined, one for the small, square “test piece”, one for the larger square around that piece, and one for the downstream mesh zone. The area of the small square was subtracted from that of the larger square, using boolean operations, and meshes applied to the edges around all areas. The areas were then meshed using 16,721 two dimensional quadrilateral elements.

These two dimensional analyses served another purpose, by indicating appropriate dimensions for the brick which must be placed around the model.

The edge on the left-hand side of the 2D model was created as a velocity inlet, and the one on the right-hand side as a pressure outlet. The top and bottom edges were defined to be “walls”, as were the four edges comprising the small square in the middle. The areas left after the boolean operation, which were meshed, and which represent the airflow in the “duct”, were defined to be fluid areas.

At this stage, the model was exported as a .msh file.

This is how the 2D test models were created. Their testing procedure is explained in the next chapter. Before we see that, we will look at how the three dimensional models were created.

5.3 Importing The ACIS File

Initially, (after following GAMBIT's online tutorial), the solid models were exported from the solid modelling package and imported into GAMBIT in .igs format. This is how it is done in the tutorial. It would appear from limited personal experience that .igs is the most commonly used format for transferring three dimensional model data. However, .igs tends not to be accurate enough for some applications.

A prime example of this was discovered when an .igs model of the SAE vehicle had been imported into GAMBIT, and the geometry was being processed. Here, a symmetry face was being created along the y-z plane (vertically down the centreline) of the car, but a condition of creating faces in GAMBIT is that the points which define the edges which define the face must be collinear. In the model in question, two points were 1×10^{-5} mm and 1×10^{-6} mm out of the y-z plane, respectively. Consequently, GAMBIT could not create the symmetry plane. Any attempts to translate the points into the plane were fruitless, because the points had higher geometry (edges and faces) attached to them, so the condition that allowed translation of these points required equal translation of all related points, edges and surfaces. Therefore, the points were able to be translated into the y-z plane, but this resulted in the rest of the car model being 1×10^{-6} mm out of the plane!

Upon seeking advice from my supervisor, Mr. Chris Snook, I was advised that "ACIS" and "Parasolid" were both more accurate means of transferring the data.

So, the original model was exported from SolidWorks in ACIS format (.sat), as well as Parasolid and Binary Parasolid (.x_t and .x_b, respectively), as an alternative filetype.

Importing the .sat file (and earlier, the .igs file) was a simple matter of opening the "Import..." submenu, selecting ACIS (or IGES, if an .igs file is being imported), and

browsing to find the correct file.

5.4 Cleaning Up The Geometry

Once the data had been read into GAMBIT, there was a small amount of “cleaning” to be done, although in the case of the .igs file, this amount was somewhat larger. First, we will outline the procedure associated with the .igs file, merely as a comparison of the two file types. Figure 5.4 shows the results of importing an ACIS file. If the edges are coloured blue, that indicates that they are connected, and do not need cleaning up. However, if the are orange, then require some extra clean-up geometry processing.

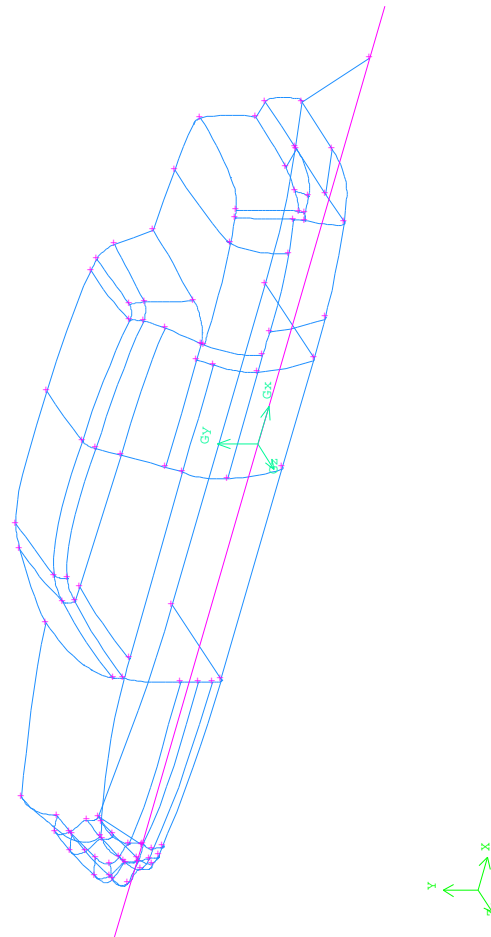


Figure 5.4: The ACIS file imported. The blue coloured lines indicate correct connectivity with adjacent areas.

5.4.1 IGES Files

The model in GAMBIT, having come from an .igs file, consisted of vertices, edges, faces and volumes, most of which *should* have connected or been a single entity, but weren't. Most of the edges were doubled up, creating two edges within microns of each other, but one of which defined one face, and the other of which defined a neighboring face. This geometry is impossible to mesh, as the gap between the edges defeats the purpose of the Finite Element Method (to have two elements sharing a node, providing one equation to link the two elements). It is sometimes possible in this situation to choose the "Connect Edges" option, which merges the two nearly collinear edges into one, and redefines one of the adjacent faces to follow the other edge. However, this is only applicable if the same pair of vertices define the two edges, and the edges are within a certain distance tolerance of each other (a set fraction of their lengths).

If this is not the case, then one of the edges must be deleted. This requires deletion of the attached face, which in turn requires the deletion of the attached volume, and any associated meshes. After the edge has been deleted, the end vertices should also be deleted, to avoid confusion, but these are often defining other similarly doubled-up edges.

So it continues, until all vertices, edges, faces and volumes associated with a doubled-up edge have been deleted. Then, the vertices which define a required edge are used to create this new edge. This edge is used to create a face to replace one that has been deleted, and so on, until the geometry had been reconstructed without doubling up any entities.

5.4.2 ACIS Files

The .sat file that was imported did not require *any* geometry clean-up. All edges remained connected to both faces in contact with them. However, as a result of the way the solid model had been assembled (it was assembled from three parts), there were some internal faces in the GAMBIT model that intruded inside it.

So, the three volumes had to be deleted, these face deleted, and two new faces reconstructed from the edges of the ole ones. The volumes did not have to be reconstructed, because there is no requirement for a volume inside the car, as this is not being meshed.

Once this was done, the model could be further processed to make it able to be meshed.

5.5 Adding The Duct

The model in the computer must have some boundaries. If it didn't, and the air around in went to infinite, the mesh size would also be infinite. This is clearly unacceptable, so a duct must be placed around the model, not unlike a wind tunnel.

To do this, a similar procedure to the 2D models was followed, but extrapolated to 3D. Eight vertices were created, to define a rectangular prism whose extents are $(0, -65, -30000)$ mm to $(14000, 14000, 10000)$ mm. The solid model was created in millimetres, so the duct must also be created in millimetres. This can be scaled down when imported to FLUENT.

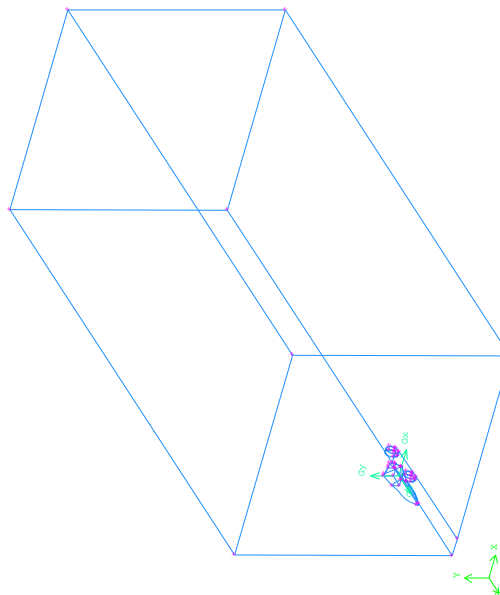


Figure 5.5: The wireframe of the CFD defeatured model. The extra area on the duct floor is used to make meshing the floor easier and faster to re-mesh.

Edges were created to join the vertices, and to define the faces around the car. Now, we had a wind tunnel wall, ceiling and floor (65mm, our specified ride height, below the bottom of the car). However, the wheels were present in this analysis, and they met the floor tangentially. If this were to be meshed as it was, this area would require some extremely highly skewed elements. So the bottom 65mm of the wheels was made square, the bottom coincident with the bottom of the duct (Figure 5.6). This was considered to be unlikely to make a difference to the outcome of the analysis, but to give the the mesh a much higher quality ratio.

Now, these areas had to be subtracted from the area of the duct floor. After this was done, and areas had been added to the ends of the duct, and a volume had been defined inside, edge meshes were applied to every edge in the model.

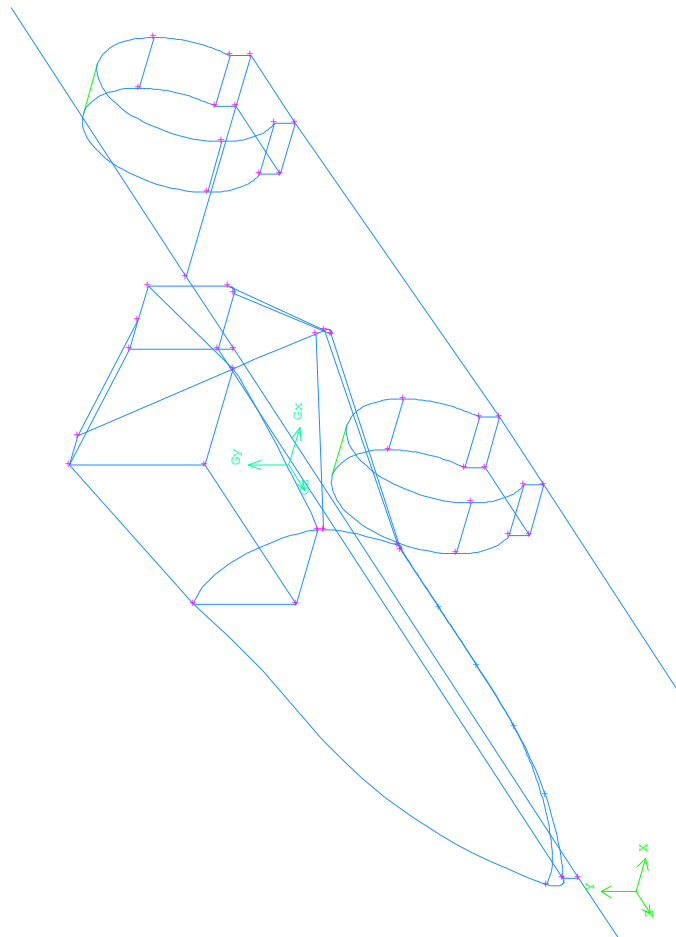


Figure 5.6: The wireframe of the geometrically-clean car. Note the square bottoms on the tyres.

5.6 Applying The Meshes

As in the 2D case, the mesh ratio tool was used to fine up the mesh around the car body, and coarsen it further away.

The meshing of the edges was tedious, as care had to be taken to fine up a mesh sufficiently to do what was required of it at one end, while also making sure that the first and last elements on an edge were about the same size as those on neighboring edges.

Once all the edge meshes had been applied, the faces could then be meshed. Initially, quadrilateral elements were used, but it is not possible to use this type of element with any mesh scheme (map, pave, etc.) on some of the face in the model. Also, when meshing the floor under the car, the mesh becomes overly complex in terms of gradient around the wheels, and sometimes, the program will simply not mesh the area. The largest problem was that, if all areas *could* be meshed with quad elements, FLUENT was unable on every attempt to mesh the volume with either of the element types available.

So the change to using triangular elements was made. It appears (although it was not anticipated by me) that it is *much* easier to mesh an area using triangular elements than it is using quadrilaterals. The computation time taken to apply the mesh in triangular elements was substantially smaller than that using quads. Then, upon applying a mesh to the volume, FLUENT succeeded on the first attempt. The triangular mesh as applied to the nose (omitting the rest of the car, for clarity), as well as the floor and symmetry plane, is shown in Figure 5.7.

Another problem found with quadrilateral elements was that in some cases (where manual meshing of certain edges had been omitted), an automatic mesh was applied to these edges. This automatic mesh used an interval size of 1mm, where the meshes that had been applied used interval counts that worked out to an interval size of approximately 30-50mm. This large difference in adjacent mesh size results in 2D mesh elements having aspect ratios and equi-angle skewness near 1. This does not occur with as serious consequences with triangular elements.

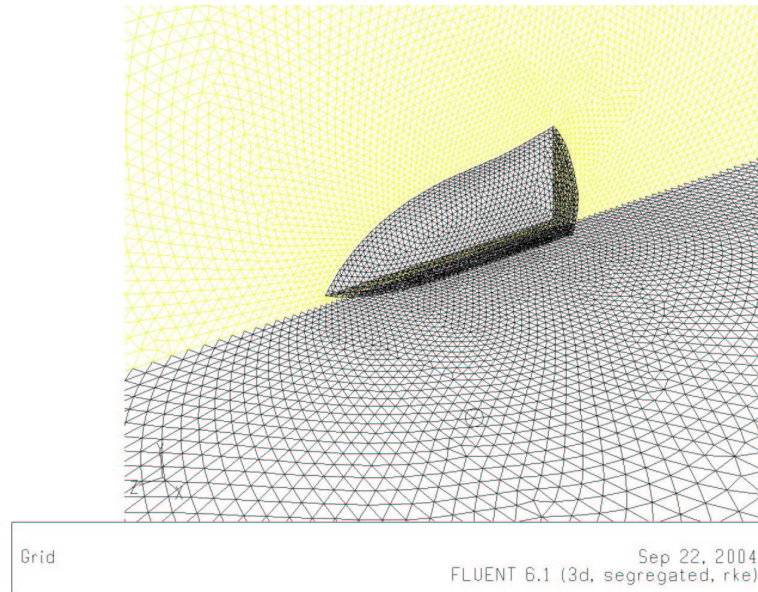


Figure 5.7: The triangular mesh as applied to the nose of the car.

5.7 Setting The Boundary Types

After the mesh had been applied to the volume of the model, the boundary types had to be specified.

Figure 5.5 shows the car body and the surrounding duct. The square face on the left-hand end was selected and set to “Velocity_inlet”, while the opposing face was set to be a “Pressure_outlet”. These would act as the intake and outlet for the analysis. The walls of the duct, except the one to which the car body is attached, were set to “Wall”, as were all of the faces defining the body of the car and its wheels, and the remaining wall was set to the boundary type, “Symmetry”. It is a symmetry plane, as we are making use of the symmetry of this model.

The volume bounded by all of these areas was defined as a fluid zone, named “air”.

5.8 Exporting The Mesh File

Once all of these boundary conditions have been set, the file is ready to be exported as a mesh file (.msh). This type of file contains all the geometrical information needed for FLUENT to apply whatever conditions it needs to, then to solve the analysis.

So in the File menu, Export - Mesh... was selected, which opened a window allowing the specification of the folder and filename, and the file was exported.

5.9 Review Of Geometry Processing And Mesh Creation

In this chapter, we have created two different test models. The two dimensional square test was drawn completely in GAMBIT, and the three dimensional model was created from a solid model.

Two of the different filetypes associated with file transfers were compared, and the ACIS filetype was found to be far superior to IGES.

Chapter 6

Methodology - CFD

6.1 Chapter Overview

As described earlier, a simple two dimensional model was experimented with, in an effort to find the most applicable values for such settings as the under-relaxation values, among others. The method for the two dimensional tests will be described in this chapter, and then the changes made from the 2D to the 3D case will be outlined. There were not many changes.

6.2 Importing The Mesh File

Once a mesh file has been produced in GAMBIT, it may be imported into FLUENT for the CFD analysis. This is done for a new analysis through the File menu, by choosing “Read” then “Case...”. This opens a browser window in which the .msh file is selected. The mesh for the two dimensional case is shown in Figure 6.1. The dimensions of the duct are $10 \times 70\text{m}$, and the square test piece is one metre square.

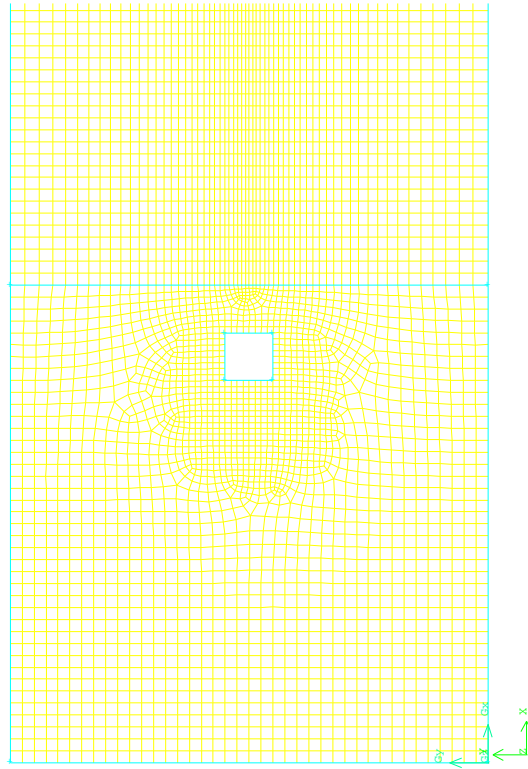


Figure 6.1: The mesh used for the square test.

Once an analysis has been run, FLUENT will save the .msh file along with the option settings that were used for the analysis, and the output data together in a .cas and a .dat file. If it is desired to continue with a previous analysis, rather than starting a new one, the .cas file may be opened at this stage by choosing File - Read - Case & Data. . . .

At this stage, FLUENT has the geometry, the mesh and the boundary types set, and now requires its solution-specific options to be set.

6.3 The Grid Menu

The Grid menu allows manipulation of the mesh(es), such as smoothing, merging, fusing, separating, moving and scaling. It also displays information about the given mesh(es), such as its size, memory usage and zones included. These particular models use only one mesh, which requires no modification, so the Grid menu is only used to

scale the mesh, and to print the file and grid information.

Since the final design was created in millimetres, FLUENT gives outputs and requires inputs which are scaled accordingly. Therefore, the geometry was scaled down by a factor of 1000, to make the entry of variables easier, and to reduce the risk of operator error. From the grid menu, Scale was selected, then “Grid was created in...” was set to “mm”. Pressing the “Scale” button then scaled the entire model, so that “ X_{MAX} ” read 14, not 14 000.

6.4 The Define Menu

The Define menu is used to set variables and settings with relation to such aspects as how the solver goes about solving the equations for each element (coupled or segregated; all at once or one at a time), whether to calculate heat transfer, what material properties to use, and whether the output shows non-steady characteristics such as periodic vortex shedding (Von Karman’s Vortex Street - for further reading, see (Hucho 1987) and (Gillespie 1992)). In the following sections, we will briefly discuss the settings set in this menu, ordered by menu and simplified, where possible.

6.4.1 Models

The mathematical models used in the solution of the equations assigned to each element of the mesh are set in this menu.

Solver...

The solver window allows the operator to set *how* the program solves the associated equations. The available fields here are:

- Solver - set to “Segregated” to begin with, and experimentation with this setting was to take place later. Whether a segregated or a coupled solver was better for

this application was not known at the time.

- Formulation - set to “Implicit”, as this is the only allowable choice with a segregated solver.
- Space - set to 2D to make FLUENT not include the z -terms or any axisymmetric action in its equations.
- Time - set to “Steady”, because non-steady characteristics (such as vortex shedding) are not being investigated.
- Velocity Formulation - set to “Absolute”, because without a moving mesh, the outcome is the same as “Relative”, so it is left as-is.

Axisymmetric or Axisymmetric Swirl Space were not used here, because there is no rotational symmetry. This is a two dimensional rectangular duct problem.

Multiphase...

The Multiphase window applies only to models with multiple meshes or sections of fluid, and therefore does not apply to these analyses. So the “Off” box is checked.

Viscous...

Here are set the models to determine the formulation of the viscous component of the flow: Turbulent formulation is justified, as the Reynolds number for the flow over this car is around:

$$\begin{aligned} Re &= \frac{\rho V D}{\mu} \\ &= \frac{1.225 \times 16 \times 1.5}{1.7894 \times 10^{-5}} \\ &= 1.643 \times 10^6 \end{aligned}$$

This is much larger than Re_{crit} ($= 2300$) for internal flow (remember that the test is being modelled in a duct), and the flow will therefore be turbulent. Therefore, neither

the inviscid nor the laminar models may be used. The choice is now which viscous solver will be used?

- The k-epsilon model was chosen, as this provides the easiest specification of turbulence in this case. It solves the flow for turbulent kinetic energy (k) and turbulence dissipation rate (ϵ)
- The specific k- ϵ model chosen was the Realisable model. A discussion on this can be found in the FLUENT on-line help file, by pressing the “Help” button at the bottom of the “Viscous...” window. (A.P. Gaylard, A.J. Baxendale, J.P. Howell 1999) used the RNG model to achieve turbulence convergence in their modelling of simple automotive shapes, however, the FLUENT help file discusses the relative merits of the Realisable model over the standard and the RNG models, especially in terms of the realisable model’s variability of C_μ .
- The model constants, $C_{2\epsilon}$, TKE (Turbulent Kinetic Energy) Prandtl Number and TDR (Turbulence Dissipation Rate) Prandtl number, default to 1.9, 1 and 1.2, respectively. These have been found experimentally to be accurate, and should not require changing. However, if the experimentation with the models does not yield results close enough to those anticipated, these model constants may be varied, and the results of this variation noted.
- The Near-Wall Treatment used was the Standard Wall Functions setting (for simplicity), and was to be varied later if the anticipated results were not forthcoming.
- No user defined functions were used in these analyses.

Energy...

The Energy equation adds the heat energy transport equations to the flow equations, for analyses involving heat flow. This is not selected for this model, as there is no heat flow analysis.

Radiation, Species, Discrete Phase, Solidification and Melting and Pollutants

None of the Radiation, Species, Discrete Phase, Solidification and Melting or Pollutants windows were required, as none of them apply to the analysis at hand. Therefore, all relevant boxes were unchecked, or set to “Off”, to disable all of these options.

6.4.2 Materials...

The “Materials...” panel allows us to set variables about the materials being analysed, of which there is only one here, which is air under atmospheric conditions (at sea-level). Therefore, upon opening this window, under “Name” will appear the word “air”, with no chemical formula, and its properties will be already set to density = constant at 1.225 kg/m^3 , and viscosity = constant at 1.7894×10^{-5} .

The density will remain constant, as the flow, being less than 0.3 times the speed of sound, can be treated as incompressible, (“... gas flows with $M < 0.3$ can be treated as incompressible; a value of $M = 0.3$ in air at standard conditions corresponds to a speed of approximately 100 m/s” (Fox & McDonald 2003), and this car is not expected to go faster than about 30m/s).

The viscosity will also remain constant due to the fact that the car will be driving in atmospheric conditions which may reasonably be expected to change between 0 and 40° C, over which range, the viscosity will vary between about 1.75 and 1.85×10^{-5} , a range which is negligible for our purposes.

6.4.3 Operating Conditions...

In the Operating Conditions panel are set the operating pressure (ambient absolute pressure), the reference location at which this is set, and whether gravity (the “gz” term in Bernoulli’s equation) is taken into account.

The operating pressure is set to the International Standard Atmosphere (ISA) value of

101325 Pa, and the reference pressure location set to the middle of the Inlet face (on the symmetry plane, for the 3D models), the coordinates of which, for the 2D model are $(x,y) = (0,5)$. Gravity is not taken into account here, as the change in height is negligible ($\rho gh = 1.225 \times 9.81 \times 5 = 60$ Pa, which is only 0.06% of an atmosphere).

This is the only place where pressure is absolute. Everywhere else in the program, and therefore, hereafter in this report, any pressure is defined as the gauge pressure.

6.4.4 Boundary Conditions...

The mathematical models (and therefore equations) used and their associated solver schemes, turbulence models and wall treatments are all merely different ways of processing the actual physical information of the model. The physical information is set here in the Boundary Conditions window. The .msh file carries enough information to set what *type* of boundary is defined by a given face, but its related numerical values have yet to be set.

The boundary conditions for the model carry all the information required by FLUENT to put into the equations and solver schemes and turbulence models mentioned earlier. These boundary conditions include the temperature, pressure and viscosity of the local air, and the roughness of the boundaries across which it flows. These settings are defined here.

Air

The zone which is the area created in the 2D GAMBIT mode (the volume around the 3D model of the car, in that analysis) was named “air”. This is the only zone that has a mesh applied to it. Highlighting “air” in the Zone list and pressing the “Set...” button opens a new window in which the zone’s boundary conditions are set. Here, the “Source Terms”, “Fixed Values” “Laminar Zone” and “Porous Zone” boxes are left unchecked, because the last three do not apply to this model, and the first is already fully defined (by setting the inlet area and the inlet speed to 16m/s). There is no general rotation here, and there are no moving meshes or moving reference frames, so the entire panel

is left as default.

Default-interior

The default-interior is a zone created by FLUENT upon importing the .msh file. There are no options to set regarding this zone.

Inlet

The velocity specification method for the inlet was set to “Magnitude, Normal to Boundary”. This constrains the incoming airflow to be coming straight into the duct, i.e., with a velocity vector of (1,0) at the inlet. From there, it must bend around the shape of the test piece.

The reference frame choice makes no difference to the calculation, as it preforms the calculation with respect to either the selected mesh, or to the global coordinate system origin. If the mesh is not moving, there is no difference.

Velocity magnitude was set to a constant 16m/s, as described earlier.

The turbulence specification method used was the “Intensity and Hydraulic Diameter” scheme. This allows the hydraulic diameter (definitely known from the model, = 10m) and the turbulence intensity (estimated using experience and engineering judgement) to fully define the turbulence already in the airflow at the inlet. My supervisor, Dr. Ruth Mossad said that a turbulence intensity of about 10% is usual for pipe and duct flows, but that this model is of a different nature, being a model of the car moving through previously stationary air. Therefore, a turbulence intensity of 5% was decided upon. This could always be changed later, in the experimentation phase, when we search for the correct variable values to give the correct C_D .

Outlet

The outlet panel is similar to the inlet panel, except that it is a pressure outlet, not a velocity outlet. So, the pressure at this face was defined as atmospheric ($0Pa_{(g)}$), the backflow turbulence specification method also set to 5% turbulence intensity, with a hydraulic diameter of 10m.

Square

The zone named “square” represents the physical surface of the test piece, and therefore will create a boundary layer. So, the wall motion field was set to “Stationary Wall”, the shear condition to “No Slip”, and roughness height to 0.001m (about the roughness height of the surface finish of fibreglass). The roughness constant was left at 0.5.

Walls

In a real duct, as in a wind tunnel, the walls would create a boundary layer. This is an undesirable outcome. So the “walls” zone in this 2D model were set to be a stationary wall, with specified shear, being zero. So the x-and y-components of shear stress were set to 0Pa, and the wall roughness height and constant were both set to zero. This provides a method for the CFD software to use a relatively small mesh, but not be affected by boundary layer formation.

The Rest Of The Define Menu

The Define menu also contains options named:

- Periodic Conditions...
- Grid Interfaces...

-
- Dynamic Mesh...

 - Mixing Planes...

 - Turbo Topology...

 - Injections...

 - Ray Tracing...

 - Custom Field Functions...

 - Profiles...

 - Units...

 - User Defined...

Of these, the only option which pertains to the analyses that we will be doing is Units... This window allows the user to view and alter the units in which values are measured and output. One could change the unit scheme to SI, imperial, or CGS, or change one quantity to a different unit system. These are defaulted to the SI system, and do not need to be changed.

6.5 The Solve Menu

6.5.1 Controls

Solution...

The solution controls panel shows the operator which equations will be solved in every iteration, and therefore, what outputs will be obtainable. The equations are set in the Define - Models... menu, and appear here under the “Equations” field. In this case, only the flow and turbulence equations are being solved, and so only these two should appear in the field.

It was claimed that the Under-Relaxation Factors do not affect the final result of the analysis, but they do affect the rapidity with which the solution converges. Through experiment (detailed later), it was found that they do in fact change the accuracy of the final result. However, in the following testing procedure, it is anticipated that the values for these factors will be found to give the best convergence, then other variables will be changed to find an accurate solution. There are seven factors which must be set, and in their default conditions are as set out in Table 6.1:

Table 6.1: Under-Relaxation Factor default values

Pressure	= 0.3
Density	= 1
Body Forces	= 1
Momentum	= 0.7
Turbulence Kinetic Energy	= 0.8
Turbulence Dissipation Rate	= 0.8
Turbulent Viscosity	= 1

These are the values which will be altered later, in an effort to speed up the convergence.

The Discretisation schemes used were left as default. Some experimentation was undertaken, but found to either slow or prevent convergence, or to increase the turbulence

in certain cells to a point where it had to be limited. This was deemed a net negative result, and so the following defaults were set.

- Pressure = Standard
- Pressure-Velocity Coupling = SIMPLE (as used by (A.P. Gaylard, A.J. Baxendale, J.P. Howell 1999))
- Momentum = First Order Upwind
- Turbulence Kinetic Energy = First Order Upwind
- Turbulence Dissipation Rate = First Order Upwind

6.5.2 Initialise...

Now that all relevant settings have been designated, an initial (but wrong) solution for the entire grid (or mesh) must be set.

In the initialisation of a model, the program goes through the entire mesh and assigns a value to each node or element, for each equation used. This value might be zero, or the rest value for each equation used. In this example, it may set every element, except for those on the inlet face, a pressure value of 101325 Pa, and a velocity of 0 m s^{-1} . These values are not the correct steady-state ones, but at least they are in existence.

When the iterations begin, the program forms its matrices, solves them, then from the result, assigns a new value to each element, overwriting the old one. The initial values are used to fill a column in the matrix equation, allowing the operation to proceed. Without them, the matrices would not be complete, and the operation would not be able to be executed. So with every iteration, the old (and inaccurate) values are overwritten with a new (and slightly more accurate) value. The initialisation is merely the first step in that process.

So in the “Initialise...” window, the “Compute From...” field is set to Inlet, to make the known values at the inlet face be the ones that drive the entire analysis. This was learned through trial and error, and the results of neglecting to designate a zone from

which to compute are shown in Figures 6.2 and 6.3. Here, the outlet was selected to compute from, which “bunched up” the turbulent wake behind the test piece. At this stage, it appeared that the use of centreline symmetry was *not* justified, as the wake was not symmetrical. However, when the analysis was made more correct, the wake became symmetrical, so centreline symmetry could have been exploited. The decision not to change the model to do this was taken, because the mesh was so small that the time saved in computation did not justify the time taken to modify the mesh.

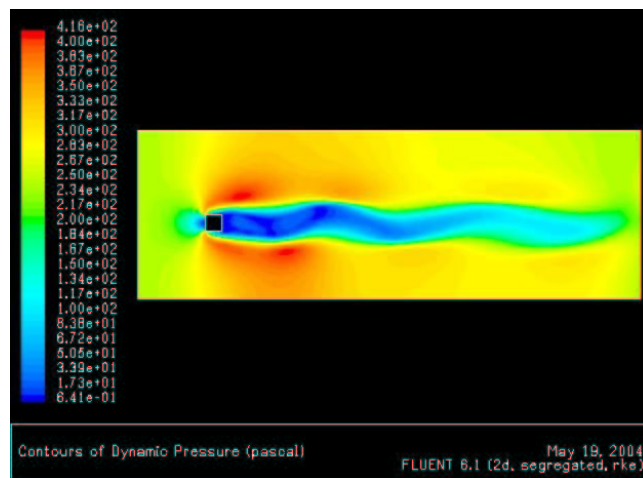


Figure 6.2: Dynamic Pressure contours on the square test, showing bunching resultant from incorrect designation of the “Compute from” field.

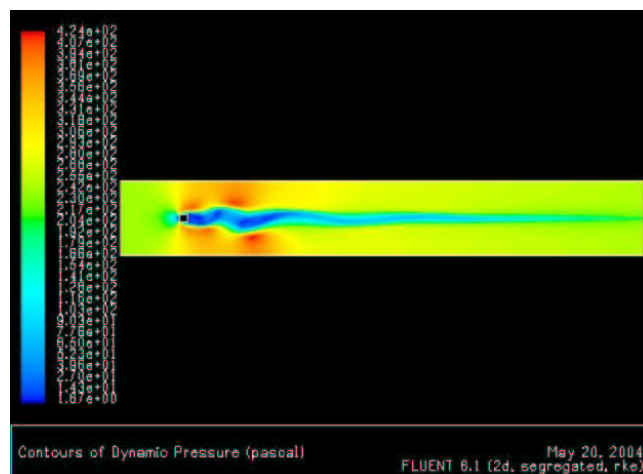


Figure 6.3: A similar effect to that shown in Figure 6.3, except using a lengthened duct.

Again, the Reference Frame choice makes absolutely no difference to the analysis, as

there is only one cell zone, and it is fixed in position with respect to the origin of the coordinate system.

Several Initial Values are set in their fields in this window when the Compute From field is set. These initial values are alterable, but are calculated from other settings that have been set previously. Changing them may cause conflict, se they were left as they were calculated.

The “Init” button is pressed to perform the initialisation.

6.5.3 Monitors...

During the analysis, certain outputs may be monitored to provide an indication of the progress of the analysis.

Residual...

The residuals from each iteration are effectively the nondimensional difference between the most recent result for a certain output and the result from the previous iteration (the overwriting of results for each node was described earlier). For example, the output value for turbulent kinetic energy on the 10th iteration may be called k_{10} . On the 11th iteration, the same output may be amended to a figure which is not defined by, but may be described by:

$$k_{11} = 1.024 k_{10}$$

Now the difference between these values,

$$|k_{10} - k_{11}| = 0.024 k_{10} = 2.4 \times 10^{-2} k_{10}$$

is the “residual”.

The convergence criteria are set (default = 0.001), such that when

$$|k_i - k_{i+1}| \leq 0.001 k_i$$

the solution is said to be converged.

That is, the result from the (i+1)th iteration is within 0.1% of the result from the previous iteration, and therefore, the increase in accuracy from doing another iteration is now insignificant compared to the time taken to do that iteration. The convergence criteria may be easily changed, such that the cutoff is tighter or looser than the default, depending on the time available and the accuracy requirement of the application.

The solution only “converges” when *all* monitored criteria (in our case, continuity, x-velocity, y-velocity, k, and ϵ) are below their preset limits.

So in this window, all boxes are checked (“Monitor” and “Check Convergence” boxes for each of the above criteria), the convergence criterion for each is left at 0.001, and the options to print and to plot the outputs are both selected.

Forces...

Forces acting on the bodies being analysed may also be monitored. C_D and C_L are both of interest to us in this application, and may be monitored here.

Unfortunately for this analysis, (A.P. Gaylard, A.J. Baxendale, J.P. Howell 1999) states that “...encouraging results for vehicle drag (coefficients to within 2% of experiment) and the effect of limited geometric modifications of drag (within 7% of full-scale experiment) were obtained. However these latter results should be viewed with some caution as the results for lift were considerably poorer.”

This applies to their analysis, however, some of their techniques are being used here, and this statement may be a reflection on CFD in general, not just their analysis. It is conceivable that this is the case, as the ability of CFD to predict flow separation over curved surfaces may be currently improving (A.P. Gaylard, A.J. Baxendale, J.P. Howell 1999), but still has some way to go before it could be trusted implicitly to give correct values. Prediction of drag forces and coefficients does not rely on flow separation over large-radius curves to as great an extent as that of lift, and is therefore inherently more accurate. This would mean that any lift values that may come from this analysis (on the USQ’s SAE car) may be misleading.

So the drag force on the square test piece is monitored. The options to print and to plot are selected again, and the wall zone, “square” is highlighted. This means that the program will analyse the drag force on *only* the walls of the test piece, and not on the walls of the duct.

The Force vector is set to run parallel to the x-axis (1,0), and the drop-down menu named “Coefficient” is set to “drag”.

This will now print the C_D at every iteration, and plot it on a set of axes.

The rest of the Define menu contains options to monitor other things such as pressure, temperature, turbulence, heat flux, etc. on set surfaces and in or through volumes, to play back animations after the solution has converged, and to execute user-defined commands at given stages in the calculation. These are not used in this analysis, because they are not needed here.

6.6 Reference Values

Before the iterations can begin, the reference values for calculating the forces monitored must be set. These values do not take part in the computation, and therefore do not affect the final outcome, but if forces are being monitored, these reference values must be taken into account to calculate their coefficients.

The reference values are set in the Report menu, by opening the Reference Values... window. Here, again, can be seen the “compute from” menu, were the inlet is selected. Then the fields are set as shown in Table 6.2.

The depth was set to 1, because from (Fox & McDonald 2003, Hucho 1987), a cube in a flow at $Re \geq 10^3$ has a C_D of 1.05, and an infinitely long square rod, normal to the flow, has a C_D of 2.05. These are the figures that we will try to obtain by changing some of the estimated and unsure values set previously.

Table 6.2: Under Relaxation values for the 2D tests.

Area	= 1	m ²
Density	= 1.225	kg/m ³
Depth	= 1	m
Enthalpy	= 0	J/kg
Length	= 1	m
Pressure	= 0	Pa
Temperature	= 288.16	K
Velocity	= 16	m/s
Viscosity	= 1.7894e-05	kg/m.s
Ratio Of Specific Heats	= 1.4	

6.7 Iterate...

The last thing to be done is to define the number of iterations the program will do on the mesh. If convergence is not achieved, the computation would go on indefinitely, so a maximum number of iterations is required. If convergence is achieved, the computation will stop when this happens.

From the Define menu, the “Iterate...” window is opened, and the number of iterations set to 100. This number depends on the time available and the size of the mesh, and is purely arbitrary.

The “Iterate” button is pressed to begin the analysis.

6.8 The Other menus

There are several other menus in FLUENT’s menu bar. These are: Adapt, Surface, Display, Plot, Report, and Parallel. The Display menu is used to show coloured contour diagrams, vector plots, path lines and to show the mesh on the model. The Report menu allows the operator to print reports concerning such information as the forces and fluxes acting on and passing through set areas. The rest of the menus in the menu bar were not used in this analysis.

The display menu was the most used of these. This menu contains options called

“Contours...” and “Vectors...”. These open windows which allow figures like Figure 6.4 to be displayed. This figure was created by selecting “Vectors...”, then:

- “Vectors of” = Velocity
- “Colour By” = Velocity... Velocity Magnitude
- “Surfaces” = default-interior

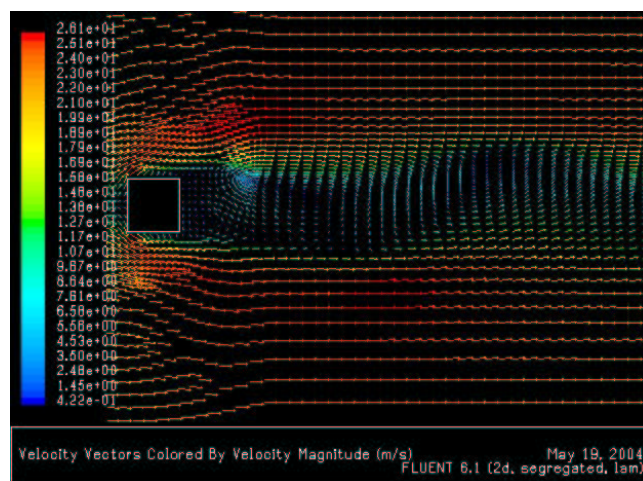


Figure 6.4: Velocity vectors, coloured by velocity magnitude, of the 2D test.

6.9 2D Experiments

6.9.1 Gaining Convergence

Now that the settings for the first 2 dimensional had been entered, the analysis was conducted. This analysis initially began to converge, but after about 75 iterations, began to diverge. The residuals (as described in the section on residuals) began to increase, meaning that the error was increasing, not decreasing. The convergence plot is shown in Figure 6.5.

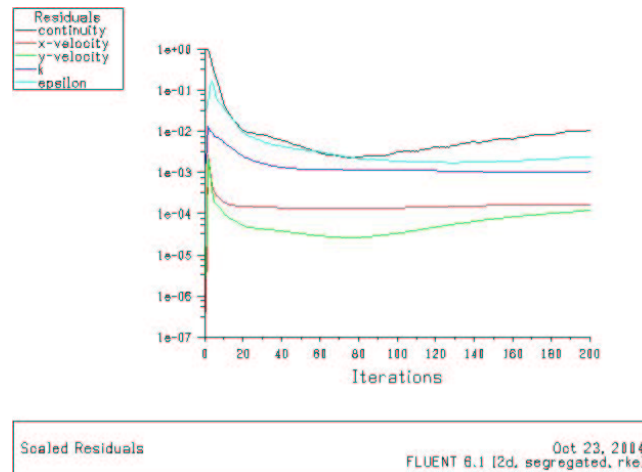


Figure 6.5: The convergence plot for the first 2D analysis.

After 200 iterations, the C_D figure was 1.5865. The anticipated figure was 1.05. So this is at least in the “ballpark”. Now, the aims of the following experimentation were first to gain convergence, then to get the C_D figure as close as possible to 1.05.

So, the settings previously set were changed, as shown in Table 6.3. Only one under relaxation factor was changed at a time, and when the set of changes had been completed with that factor, it was reset to its default. In Table 6.3, only the continuity residual was monitored. The condition for convergence is that *all* residuals are below their criterion on a given iteration, so all of the residuals may have been tabulated. However, the continuity residual is nearly always the last to drop below its limit. This was the case in all tests shown in the table, with the exception of the test using $P = 0.6$. In this test, the continuity residual did drop below its limit, but the TDR residual (ϵ) did not. So the continuity residual was considered to be an acceptable measure of how close, and how soon, the analysis had come to convergence.

From Table 6.3, it can be seen that:

- Changing the Density factor has no effect
- Changing the Pressure factor increases the time taken to converge as P is reduced, has a minimum at $P = 0.6$, then increases sharply again above this
- Changing the Body Force factor has no effect

Table 6.3: Under Relaxation values for the 2D tests.

Change	Min. Continuity	Final Continuity	C_D	Notes
NO CHANGE	3.8925×10^{-3}	6.5913×10^{-3}	1.5865	
$\rho = 0.9$	3.8925×10^{-3}	6.5913×10^{-3}	1.5865	
$\rho = 0.8$	3.8925×10^{-3}	6.5913×10^{-3}	1.5865	
$\rho = 0.7$	3.8925×10^{-3}	6.5913×10^{-3}	1.5865	
$\rho = 0.6$	3.8925×10^{-3}	6.5913×10^{-3}	1.5865	
P = 0.1	1.2646×10^{-2}	1.4414×10^{-2}	1.5865	
P = 0.2	7.5806×10^{-3}	1.2868×10^{-2}	1.5865	
P = 0.4	2.2472×10^{-3}	3.4855×10^{-3}	1.5865	
P = 0.5	1.3785×10^{-3}	2.2014×10^{-3}	1.5861	
P = 0.6	$8.5362 \times 10^{-4\dagger}$	1.2650×10^{-3}	1.5860	
P = 0.7				DFS
B/F = 0.8	3.8925×10^{-3}	6.5913×10^{-3}	1.5865	
B/F = 0.7	3.8925×10^{-3}	6.5913×10^{-3}	1.5865	
B/F = 0.9	3.8925×10^{-3}	6.5913×10^{-3}	1.5865	
$\tilde{P} = 0.9$				DFS
$\tilde{P} = 0.8$	4.1666×10^{-3}	1.3211×10^{-2}	1.5829	
$\tilde{P} = 0.6$	2.9487×10^{-3}	2.9641×10^{-3}	1.5947	
$\tilde{P} = 0.5$	2.2698×10^{-3}	4.0933×10^{-3}	1.5890	200 iterations
$\tilde{P} = 0.4$	1.6376×10^{-3}	3.0798×10^{-3}	1.5885	300 iterations
$\tilde{P} = 0.3$	9.9724×10^{-4}	9.9724×10^{-4}	1.6053	Converged @ 280 it.
$\tilde{P} = 0.2$	9.9919×10^{-4}	9.9919×10^{-4}	1.6723	Converged @ 227 it.
$\tilde{P} = 0.1$	9.9604×10^{-4}	9.9604×10^{-4}	1.7379	Converged @ 160 it.
$\tilde{P} = 0.01$	1.9661×10^{-4}	1.9661×10^{-4}	2.8247	Converged @ 43 it.
k = 0.7	5.2420×10^{-3}	7.4973×10^{-3}	1.5905	
k = 0.85	2.2006×10^{-3}	2.3517×10^{-3}	1.5944	
k = 0.9	2.4624×10^{-3}	2.6773×10^{-3}	1.5956	
k = 0.95	2.9289×10^{-3}	3.7809×10^{-3}	1.5872	
$\epsilon = 0.9$	3.4167×10^{-3}	5.5506×10^{-3}	1.5945	
$\epsilon = 0.8$	2.2795×10^{-3}	3.1198×10^{-3}	1.5944	
$\epsilon = 0.7$	5.4791×10^{-3}	6.4288×10^{-3}	1.5887	200 iterations
$\mu_T = 0.9$	4.5950×10^{-3}	5.3541×10^{-3}	1.5990	
$\mu_T = 0.8$	6.3447×10^{-3}	9.3516×10^{-3}	1.6222	
$\mu_T = 0.7$	1.6482×10^{-2}	1.6512×10^{-1}	1.6898	

† Did not converge because $\epsilon_{min} = 2.131 \times 10^{-3}$

DFS = Diverges From the Start

Under Relaxation Factor nomenclature :

$$\left\{ \begin{array}{l} \rho \Rightarrow \text{Density} \\ P \Rightarrow \text{Pressure} \\ B/F \Rightarrow \text{Body Forces} \\ \tilde{P} \Rightarrow \text{Momentum} \\ k \Rightarrow \text{Turbulence Kinetic Energy} \\ \epsilon \Rightarrow \text{Turbulence Dissipation Rate} \\ \mu_T \Rightarrow \text{Turbulent Viscosity} \end{array} \right.$$

- Decreasing the Momentum factor increases the speed with which the analysis converges, at the expense of accuracy¹. So it is believed that a trade-off between low solution time and higher accuracy will determine the final value of the under-relaxation factor.
- Changing the TKE factor produces a minimum at $k = 0.85$
- Changing the TDR factor produces a minimum at $\epsilon = 0.8$
- Changing the μ_T factor reduces the probability of gaining convergence at any value other than 1

From this, it was anticipated that combining the best performing Under-Relaxation factors, (i.e., setting $P = 0.6$, $k = 0.85$, $\epsilon = 0.8$, and $\tilde{P} = 0.01$) should produce the fastest possible convergence. This would appear to be impractical, as $\tilde{P} = 0.01$ gives a very inaccurate answer, and a more accurate answer can be gained from a higher value, at the expense of computing time. This was considered to be an acceptable trade-off, because the simulation did not take long at all to run 100 iterations.

So a test was run, using the following values:

$$\begin{aligned}
 P &= 0.6 \\
 \rho &= 1 \\
 B/F &= 1 \\
 \tilde{P} &= 0.1 \\
 k &= 0.85 \\
 \epsilon &= 0.8 \\
 \mu_T &= 1
 \end{aligned}$$

The results of this test are shown in Figure 6.6. This test converged *very* quickly, after 46 iterations, but gave a C_D figure of 2.3234. As can be seen from Figure 6.6, the residuals were very unsteady, and this was mirrored in the screenprint, which notified that turbulent viscosity was limited (to a ratio of 1×10^5) in a large number of

¹It was claimed earlier that changing the under-relaxation factors does not affect the final solution of the analysis. This was found here to be incorrect. Some explanations for this have been hypothesised, but this is outside the scope of this project.

elements. This indicates that the flow had jumped to being very turbulent, and was most likely producing incorrect results, which is true. The anticipated C_D , as stated previously, was 1.05.

So the momentum factor was altered a number of times. When it was set to $\tilde{P} = 0.4$, the result was promising. Figure 6.7 shows the residual plot. This test yielded a C_D figure of 1.6678 after 86 iterations. This was closer to the anticipated value.

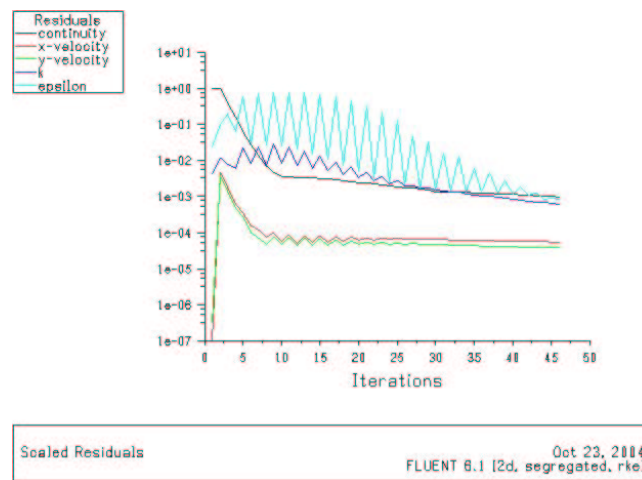


Figure 6.6: Residual plot for square test, using a combination of the fastest-converging under-relaxation factors.

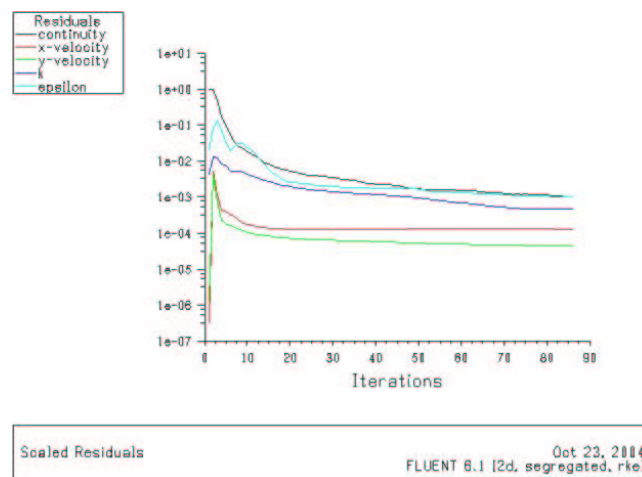


Figure 6.7: Residual plot for square test, using the same under-relaxation factors as Figure 6.6, except $\tilde{P} = 0.4$.

Next, the TKE (k) under relaxation factor was altered. When this factor was set to

0.82, the trial resulted in a C_D of 1.6190 after 159 iterations. This residual plot is shown in Figure 6.8

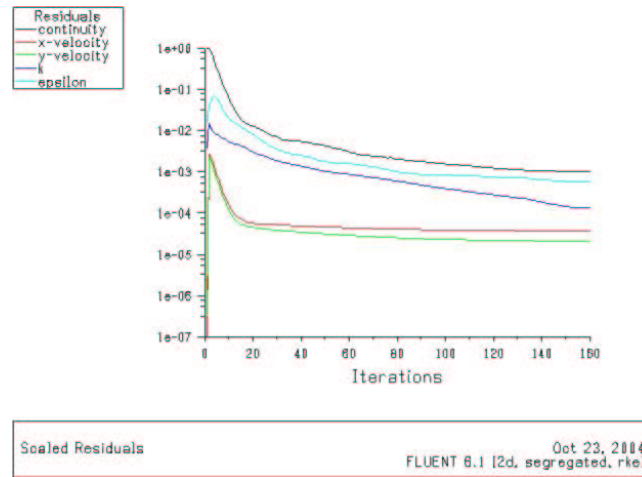


Figure 6.8: Residual plot for square test, using final under-relaxation factors.

6.9.2 Gaining Accuracy

Now that a suitable combination of under-relaxation factors had been found to provide adequate accuracy, in an acceptable solve time, other factors had to be altered to find the correct result ($C_D = 1.05$).

During the course of many experiments, the discretisation methods and model constants were altered, as well as changing the $k-\epsilon$ model itself to the RNG model. However, while some of these changes on their own made a slight improvement to the result of the analysis, when combined with any other changes, they generally tended to create divergence and turbulence limiting. The RNG $k-\epsilon$ model was found to be no more accurate than the Realisable model, but substantially slower. Using a coupled solver created *very* bad convergence (see the plot in Figure 6.9). The discretisation settings were adjusted, but each change showed a distinct reduction in convergence performance. So, the discretisation was left set at:

- Pressure - Standard
- Pressure-Velocity Coupling - SIMPLE (as used by (A.P. Gaylard, A.J. Baxendale,

J.P. Howell 1999))

- Momentum - First Order Upwind
- Turbulence Kinetic Energy - First Order Upwind
- Turbulence Dissipation Rate - First Order Upwind

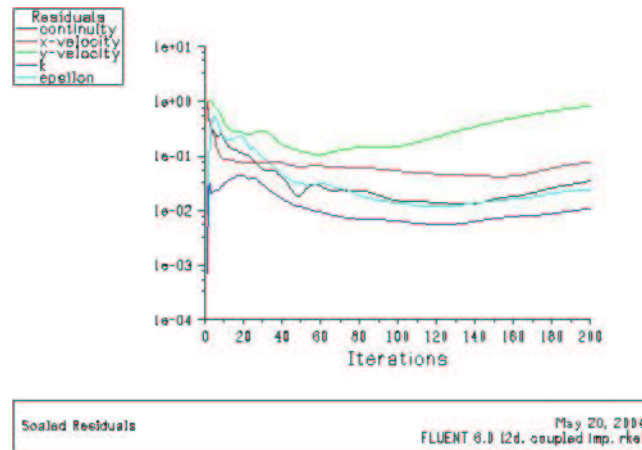


Figure 6.9: Deconvergence resulting from the use of a coupled implicit solver scheme.

During this experimentation, the under-relaxation values were adjusted in an effort to make a promising combination of other settings converge. During this phase, a new combination of under-relaxation values was found, which provided a fairly close result to the expected one.

The combination of all standard discretisation settings, the abovementioned operating and boundary conditions (with roughness height set to 0.001m on the zone, “square”), along with the following under-relaxation factors, produced an acceptable result.

$$P = 0.3$$

$$\rho = 1$$

$$B/F = 1$$

$$\tilde{P} = 0.35$$

$$k = 0.8$$

$$\epsilon = 0.85$$

$$\mu_T = 1$$

This combination produced a C_D of 1.0402 in 179 iterations. The residual plot is shown in Figure 6.10.

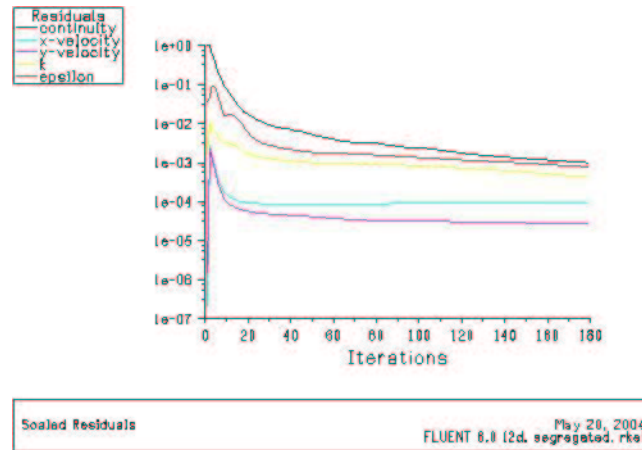


Figure 6.10: The final convergence plot for the 2D model.

So here, we have the settings that produce an accurate result in the case of a two dimensional square test piece of known C_D .

Now, this may be applied to the 3D case.

6.10 The 3D models

GAMBIT has an online tutorial database, which includes a tutorial about meshing a sedan car. The tutorial includes an .igs file of the port side of an American sedan, and in the tutorial, this is “cleaned up” and meshed. After following this tutorial, it was easy enough to apply all the relevant conditions to the mesh to create a three dimensional test of another shape of (approximately) known C_D . Not knowing exactly what make of car the .igs file was modelled on, there was no way of knowing its *exact* C_D , but this shape of car invariably has a C_D value between 0.36 and 0.4. So this was the anticipated value in the following test.

A .msh file was created in GAMBIT in exactly the same manner as that for the SAE car. This was imported from GAMBIT into the the 3D version of FLUENT. The same relevant settings were placed as with the most recent 2D case, and the simulation run.

This returned a C_D figure that was slightly higher than expected, at 0.4531, after 83 iterations. Some further adjustment of the under relaxation values was undertaken, and it was found that adjusting the Momentum under-relaxation factor to 0.1, as well as adjusting the roughness height of the surface of the sedan to 0.04m (which would go some way to accounting for joins in bodywork, radio aerials, window seals, wing mirrors, etc.) produced a C_D of 0.4146 after 129 iterations. Again, this is slightly higher than expected, however, no combination of variables could be found to reduce this any further, and the expected value was derived from general knowledge. So a value near this range is acceptable for the purposes of this analysis.

A contour plot of static pressure over the surface of the sedan is shown in Figure 6.11, and upon comparison to Figure 6.12, it would appear that the pressure distribution is correct.

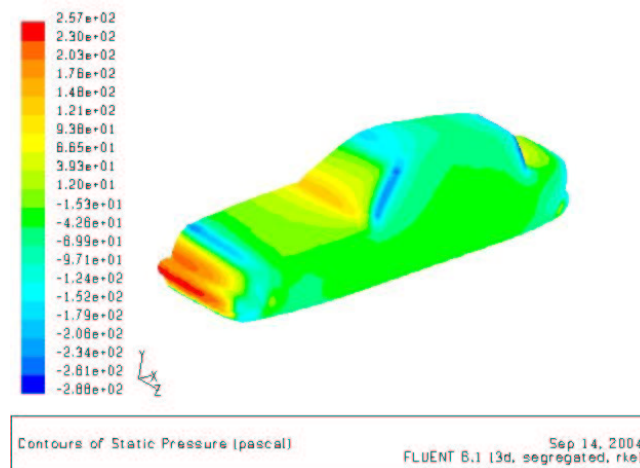


Figure 6.11: Static pressure contours over the body of the sedan model.

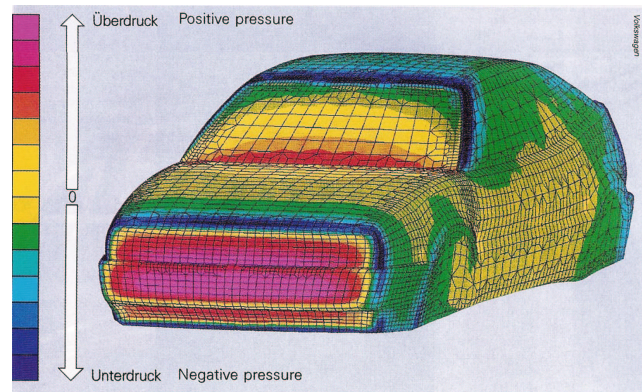


Figure 6.12: Static pressure contours from a professional CFD analysis (Edgar 2000).

The C_D was close to the anticipated result, and the pressure distribution over the surface of the car is exactly what was expected, now, it was time to place the CFD defeatured model of the SAE car into FLUENT.

Little modification of the settings had to be made for the SAE car model. There was another zone created, called “wheels”, which had to be specified in the Boundary Conditions panel. The wheels were specified as stationary walls, with a non-slip condition, a roughness height of 0.01m, and a roughness constant of 0.5. This is a fair, but not good, approximation of the behaviour of the wheels, because their rotation changes the way the airflow interacts with them. According to (Hucho 1987), the rotation of the wheels *increases* the lift coefficient (i.e., produces positive lift), and *decreases* the drag coefficient.

A summary of all the settings that were specified for this analysis is shown in Tables 6.4, 6.5 and 6.6.

Table 6.7 shows the known C_D values of some cars, as measured by the car companies.

Table 6.4: Summary of variable Define menu settings for the analysis of the SAE car in FLUENT.

Submenu	Panel	Settings
Models	Solver	Solver = segregated Time = steady
	Viscous	Model = k- ϵ k- ϵ model = Realisable Near-wall treatment = standard wall functions Model constants = (default) UDFs = none
Operating Cond ⁿ s	Pressure = 101325Pa	Ref. Pressure location = (0,7,6)
	No gravity	
Boundary Cond ⁿ s	Air	Default (all off)
	Bodywork	stationary wall, no slip, roughness height = 0.001m, roughness constant = 0.5
	Duct Floor	stationary wall, specified shear = (0,0,0), no roughness
	Inlet	$v = 16\text{m/s}$, Turbulence Intensity = 5%, $D_H = 14\text{m}$, Turbulence Specification Method = "Turbulence Intensity and Hydraulic Diameter"
	Outlet	$\rho_g = 0\text{Pa}$, Turbulence Spec ⁿ Method = T.I. = 5% and $D_H = 14\text{m}$, Backflow Direction Spec ⁿ Method = "Normal to Boundary"
Wheels	stationary wall, no slip, roughness height = 0.01m, roughness constant = 0.5	

Table 6.5: Summary of variable Solve menu settings for the analysis of the SAE car in FLUENT.

Panel	Field	Settings
Controls - Solution	Under-Relaxation Factors	$P = 0.3$ $\rho = 1$ $B/F = 1$ $\tilde{P} = 0.1$ $k = 0.8$ $\epsilon = 0.85$ $\mu_T = 1$
	Discretisation	Pressure = Standard P-V Coupling = SIMPLE Momentum = 1 ST Order Upwind TKE = 1 ST Order Upwind TDR = 1 ST Order Upwind

Table 6.6: Summary of reference values for the analysis of the SAE car in FLUENT.

A	= 0.47m ²
ρ	= 1.225kgm ⁻³
Length	= 3.2m
Pressure(gauge)	= 0Pa
Temperature	= 288.16K
Velocity	= 16ms ¹
Viscosity	= 1.7894 × 10 ⁻⁵ kgm ⁻¹ s ⁻¹

Table 6.7: A listing of some known C_D figures (Edgar 2000).

Name	C_D
Parachute	1.4
Porsche 356B	0.40
Porsche 944	0.35
VN Commodore	0.36
VR Commodore	0.34
Mitsubishi Magna	0.28
1970s Italian record-breaking car	0.26

Taking these into account, the anticipated C_D figure for the SAE car is estimated at around 0.45. As there has been no literature found regarding this particular subject, this is derived from general intuition, and a simple extrapolation, considering the information in Table 6.7.

Upon using the settings from Tables 6.4, 6.5 and 6.6 on the CFD defeature of the SAE car in a duct, the results of the first analysis were a C_D of 0.34 after 134 iterations. This would seem to be too low for an vehicle of the shape of the F-SAE car. However, with no was of knowing an *exact* C_D , we have no way of knowing when to stop adjusting the above variables if we were to begin doing that again.

It was decided to take 0.34 as a preliminary C_D , then test the actual car when it gets built.

Unfortunately, there is no other option for the team. A different C_D figure will be obtained if the Under-Relaxation factors are experimented with again, but there is no way on knowing the accuracy of our intuitive estimate. Additionally, there is no reason to expect that the Under-Relaxation values and the other settings used in the sedan test would be any different from those used for the SAE car. It may be a reasonable assumption that our predicted value of C_D was incorrect.

The results of the SAE car's analysis are reviewed in Chapter 8.

6.11 Review of CFD

The CFD used in this project comprised some high-quality packages. All software was easy enough to use, and was able to do the job required of it.

The surprising lesson learned here, is that while CFD analysis is such an advanced and powerful tool, unless the operator has access to all the knowledge he or she requires, CFD will remain for a long time, merely a checking tool, or a tool by which to investigate the impact of a small change on a system whose properties are already known accurately.

In this chapter, we have seen the method that was used to take the mesh file from GAMBIT, apply all relevant conditions, then run analyses on this mesh.

Next, we will see how the construction of the bodywork was executed.

Chapter 7

Methodology - Construction

7.1 Chapter Overview

USQ was entered in the 2004 Formula-SAE-A competition, and therefore, the bodywork *had* to be taken beyond the design stage, to the completion of its construction.

The bodywork must protect the driver from flying objects (see Appendix B, rule 3.1.1), and provide ample area for sponsorship logos, as well as the compulsory stickers required by the competition rules. A full copy of these rules may be found at (*Formula SAE-A Rules Webpage* 2004). A cost report for the manufacture of these parts (at a production volume of five per day) is presented in Appendix D.

After the decision to use fibreglass had been made (that process is described later), a local fibre-composite design and manufacturing company called Buchanan Advanced Composites (BAC), based in Production Court near the Toowoomba Airport, generously offered to help the USQ Motorsport team in the construction of the bodywork.

BAC is a relatively small, local company, but has an international clientele, due to the superior quality of the products that are constructed there. BAC's Managing Director, Norm Watt, offered to sponsor USQ Motorsport, by donating the fibreglass mat, resin, materials for the plug(s), and some floor space. With some much appreciated input and guidance from BAC employees, in particular Anil Puttaswamy, BAC's CNC expert,

members of the USQ Motorsport team went to BAC to work on the construction of a male core (plug) over which the bodywork would be laid up, and on the actual lay-up of the fibreglass.

The original method decided upon for the construction of the plug was to have it cut from polystyrene foam on a three-axis milling machine.

However, this machine appears to be the bottleneck of BAC's operations, and in an effort to save machining time, at the expense of actual labour time, the decision was made to use this machine to cut seven cross-sections out of 16mm MDF sheet, and use scrap blocks of polyurethane foam to fill the gaps between them in the construction of a male core, then sand the foam to shape.

A problem was encountered before these sections were cut, because the solid model was designed such that the bulge over the bulkhead is larger than the sections behind it. If the core was to be constructed, then the fibreglass laid up over it, the core would not be able to be extracted in one piece. It would have to be destroyed in order to be extracted. So the decision was made to cut the cross-sections in two halves, making a separate plug for each side of the nose. This would allow the fibreglass to be laid up in two separate parts. It was proposed that only one or two layers be laid up in this way, allowed to cure, then the plugs extracted, the two fibreglass halves of the nose connected and the rest of the fibreglass laid up over the top (and on the inside) of this.

The cockpit side panels were to be cut from polystyrene foam on the milling machine, as per the original plan for the nose. The decision to use the two different methods of construction was aimed at reducing machining time, and at providing the opportunity to compare and contrast the two methods.

Another consideration regarding the two different methods of manufacture is that they require two different types of resin. The milling machine cuts shapes from polystyrene foam, and fibreglass is laid up on this using epoxy resin.

The other method uses polyurethane foam. Fibreglass is laid up over polyurethane using polyester resin, because it is cheaper than epoxy resin. If polyester resin is used to lay up over polystyrene, it will melt the foam, so epoxy resin *must* be used on

polystyrene foam. After curing, this does not pose a problem, as the two resins may be joined after they have cured, providing the surfaces are roughed up enough.

7.1.1 BAC's Milling Machine

BAC has an Advanced Robot Technology (ART) 3150, 3hp, 3-axis CNC milling machine, which can be used to cut a three dimensional model of any complex shape, provided the shape does not undercut itself. When used to cut polystyrene foam, the cutting tool fitted is a $\frac{3}{4}$ " (19.1mm), two blade ball cutter, turning at 18000 rpm, and moving at a maximum tool speed of 10 metres per minute. Maximum cutting depth is 250mm.

This machine takes input from a computer in the form of a toolpath (derived via software from a .dxf or a .prt or .sldprt file), and cuts along this toolpath to an accuracy of within a millimetre. First, it makes a rough cut, to cut away all unwanted material not near the surface of the finished product, and to form the general shape of the finished product (Figure 7.1), then the machine makes a second pass over the surface of the part, cutting a smoother surface. This provides the surface finish shown in Figure 7.2.

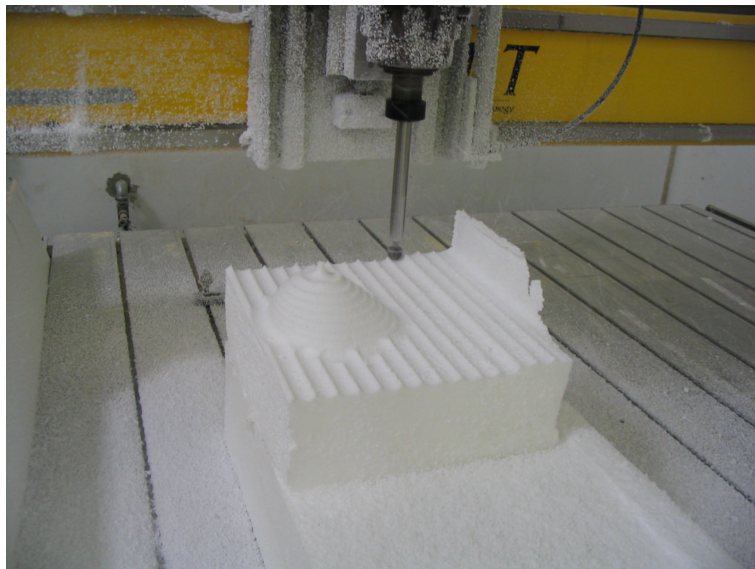


Figure 7.1: BAC's milling machine executing its rough-cut.

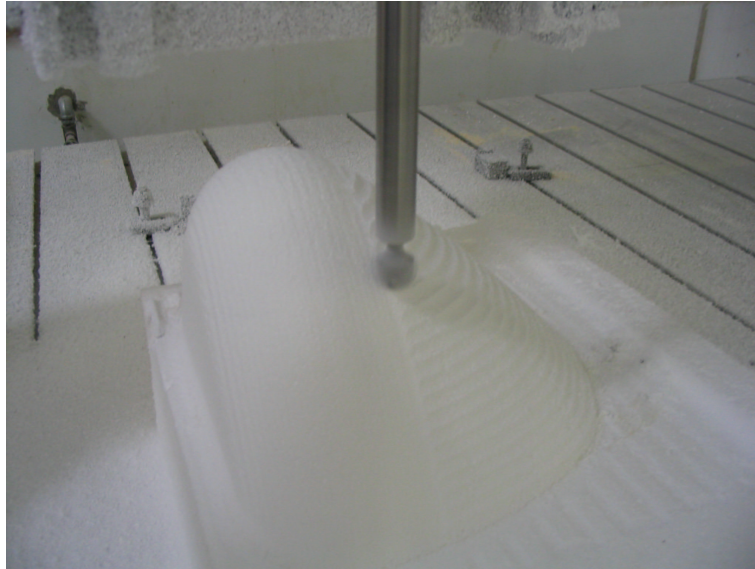


Figure 7.2: The surface finish after the smooth cut (to the left of the cutter) is very different from that after the rough cut (to the right).

7.2 Materials, and Thickness and Fastening

But how did we arrive at the decision to use fibreglass in the first place? After all, the material from which the bodywork was to be constructed had to be decided before any companies were approached to investigate possible sponsorship. Only three materials were seriously considered: aluminium, fibreglass or carbon fibre. Sheet steel could possibly be used, but the construction technique is exactly the same as that of aluminium sheet, and aluminium, as well as being lighter, is easier to panelbeat into shape.

So the positive and negative aspects of these three materials were weighed up in 7.1.

Table 7.1: Summary of properties of Aluminium, Fibreglass and Carbon Fibre (densities averaged from (*Matweb Website Properties Search 2004*))

Material	Positive Properties	Negative Properties
Aluminium	Light (2.7 kg/m^3), cheap (price), able to be reshaped	Highly resonant, requires rivets (weak points), requires panelbeating
Fibreglass	light, easy to shape, aesthetically attractive	expensive, impossible to reshape
Carbon Fibre	extraordinarily light (1.8 kg/m^3), extremely strong and rigid	<i>very</i> expensive, impossible to reshape

Upon weighing up the abilities and requirements of each material, the two fibre composites were chosen as the best material to use in this application. Fibreglass and Carbon Fibre are both much easier to shape than aluminium, and will resonate much less. They also do not need to be riveted, and therefore, do not need the many attachment points that aluminium does.

The only downsides to the use of a fibre composite over aluminium are the cost and the fact that fibre composite materials cannot easily be reshaped after their construction. Aluminium may easily be beaten to a new shape, where Fibreglass or Carbon Fibre cannot. However, this is offset slightly by the fact that the fibre composites may be cut, and patches shaped over the cut section.

Now, which fibre composite material will be used? Carbon Fibre is known to be much lighter, more rigid, stronger, and aesthetically attractive than Fibreglass. If parts of the bodywork were to be left unpainted, it would be good to have Carbon Fibre woven cloth showing, merely from a spectator's point of view. However, the added rigidity is not required this year, and the lower weight, while being of great advantage, was deemed not worth the extra cost. The decrease in weight would have been very small, anyway. The entire final solid model, shelled to a thickness of 2.5mm, has a calculated

volume of $3.41132 \times 10^{-3} \text{ m}^3$. At (average) densities for aluminium, Fibreglass and Carbon Fibre of 2700, 2400, and 1800 kg/m³, respectively (*Matweb Website Properties Search* 2004), the weight of the same part, made from the three different materials, are as follows:

$$\begin{aligned}m_{Aluminium} &= \rho_{Al} V \\ &= 2700 \times 3.411 \times 10^{-3}) \\ &= 9.21 \text{ kg}\end{aligned}$$

$$\begin{aligned}m_{Fibreglass} &= \rho_{glass} V \\ &= 2400 \times 3.411 \times 10^{-3} \\ &= 8.19 \text{ kg}\end{aligned}$$

$$\begin{aligned}m_{Carbon Fibre} &= \rho_{CF} V \\ &= 1800 \times 3.411 \times 10^{-3} \\ &= 6.14 \text{ kg}\end{aligned}$$

The weight increase of using Fibreglass over Carbon Fibre was deemed worth the cost saving.

Now that we have decided to use fibreglass, what type of mat (chopped strand or woven cloth), and what thickness will be used? Mr. David Guscott, from Skelta Sportscars gave the advice that for an application such as this, six layers of chopped strand mat, coming to a thickness of approximately 2mm, would be more than enough to meet our strength needs. Having no other way to predict the required thickness for this unique shape, expert opinion will be relied upon for this aspect of the design. Once the body has been constructed, simple physical tests will be conducted to determine the suitability of this thickness. If greater rigidity is required, more layers can be added later. The ability to do this is another advantage that fibre composite materials have over sheet metals.

The next question to be answered is how is a fibre composite body attached to the chassis of a car like ours? Before long, a member of the USQ Motorsport team, Mr. Chris Hannifan, who has years of experience in the professional drag racing scene,

informed me that “Dzues fasteners” are most commonly used in that industry.

A Dzues fastener is a small device using a bracket attached to the chassis, a thick wire behind that, and a 12mm diameter screw. The bodywork panel (with a matching 12mm diameter hole) is placed over the bracket, the screw inserted through the panel and the bracket, engages the wire, is given a quarter-turn, and locks the panel in place. The simplicity of the device is well-suited to racing applications, as to take a panel off, the screw is given a quarter-turn, extracted from the hole, and the panel is free to be lifted off. By Mr. Hannifan’s judgement, it was decided to design initially for two fasteners on the nose, and one on each side panel. Twelve fasteners were ordered, as it was considered that four in total may be too few. It may be found that each side panel requires two or even three fasteners, while the nose requires four. It is impossible for the team to know the exact requirement until the car is constructed and run. Even then, some spares might come in handy.

The proposed method of attaching the nose using only two fasteners is as follows:

- A spike is attached to the underside of the rear end of the fibreglass, pointing backwards, protruding backwards to a few millimetres in front of the front hoop
- This engages a hole in a bracket welded to the hoop, locating the bodywork in the x-and y-directions (where the z-direction lies along the length of the car)
- Dzues fasteners, located in the bottom front corner of the side of the chassis (about 50mm behind the bulkhead, and 50mm above the floor of the car) are used to locate the bodywork in the z-direction, as well as in rotation about all axes.

So the bodywork material for the USQ’s F-SAE-A racer was decided upon; we would use fibreglass, fixing it to the chassis with Dzues fasteners. Then, as described earlier, BAC was approached, and they offered a large amount of support.

7.3 Construction Of The Nose

The method described at the beginning of this chapter, involving two separate plugs constructed from MDF cross-sections and polyurethane foam was the final design used for the construction of the nose.

The MDF cross-sections were cut on BAC's CNC milling machine. From the SolidWorks model, cross-section drawings were created (.SLDDRW file type), taking the sections level with the front roll hoop, the kneebox, and the bulkhead, with additional sections at 150mm forward of the front hoop, and 210, 420 and 630mm forward of the bulkhead (Figure 7.3). These were then converted to .dxf format, collated into one file, and this file then sent to the milling machine for cutting.

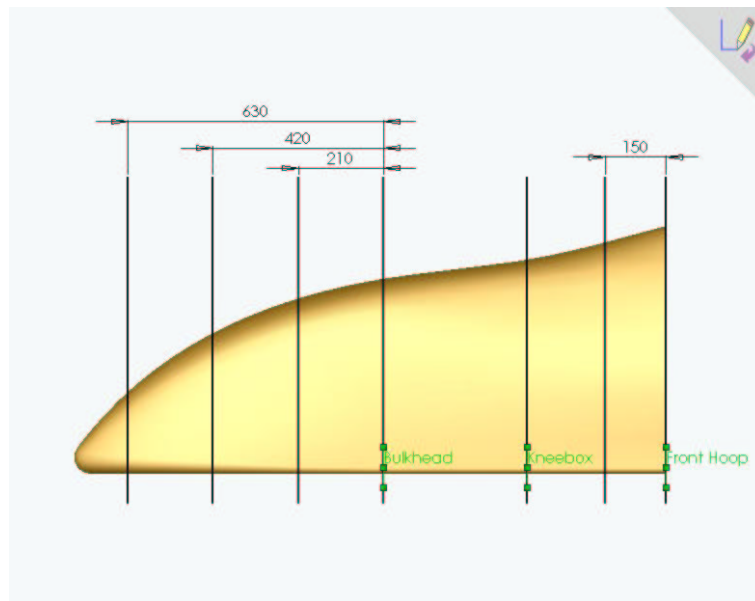


Figure 7.3: The locations of the MDF cross-sections, with respect to the front hoop and the bulkhead.

The foam blocks were marked out (Figure 7.4) and cut (Figure 7.5) by the author and another USQ Motorsport team member, Brad Moody. Brad has some experience in fibreglassing, and his advice was very helpful in this area.

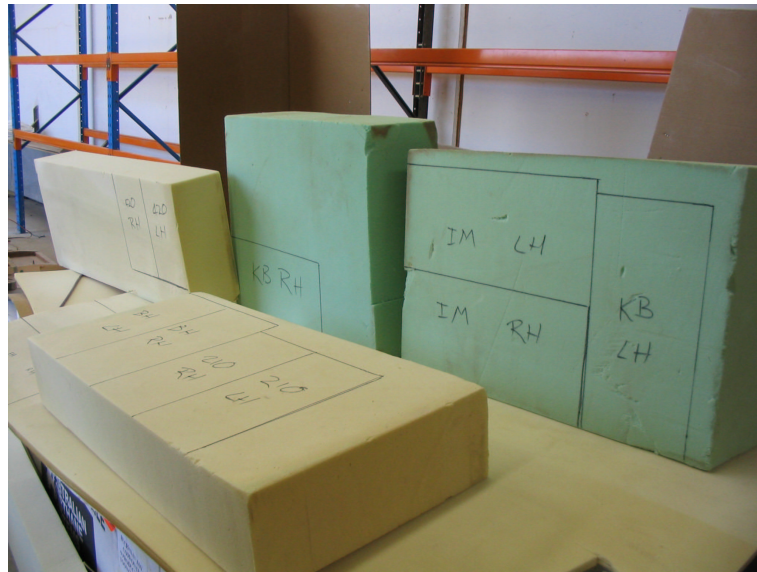


Figure 7.4: The foam blocks marked out, ready to cut.



Figure 7.5: Brad Moody cutting the foam blocks on a bandsaw.

The attachment of the foam to the sections was achieved by using resin in the same manner as a glue. The resin was painted on, the two pieces mated together, then left to cure with a weight on top of them.

The first attempt at this (without any previous experience), nearly failed. Too much was attempted at one time, and the “assembly” contained three layers of foam, MDF

two sections, and four layers of wet resin (Figure 7.6). These layers of resin tend to “float” around while the curing takes place, resulting in misalignment of the cross sections with respect to each other when the resin does cure. (The alignment of the cross sections was gained using the straight edges of the foam blocks. This was not entirely accurate, and the error was reduced using a straight edge to align the right-angled corners of the sections in the x- and y-directions).



Figure 7.6: The near-failure. Four layers of wet resin allow floating of the parts before it cures.

After this initial learning experience, only one layer of wet resin was allowed in each part that was to be glued. From here on, one MDF section was attached to one foam block, allowed to cure, then two of these parts were attached, until the entire cores were constructed (Figure 7.7).



Figure 7.7: Each section was mated to a foam block and the resin allowed to cure before continuing.

It may also be noted that the first attempt involved the use of too much resin. It is preferable not to allow the resin to leak out the sides of the face being glued, as this provides a problem when sanding; the resin is much harder than the foam, and therefore, the sanding procedure will result in some resin protruding from the required surface, and the neighboring foam being sanded to below the required level.

Another lesson learned from this first attempt at bonding the parts together, was that one has only a limited time from when the resin is mixed, and when it sets.

When resin is poured, it remains as a liquid or suspension for a long time. As it is, it does not set. It is made to set, or cure, chemically, using a hardening agent. This is the same method used to cure the resin used to lay up the fibreglass mat, and that used to mix “bog” (explained later). After being mixed with the hardening agent, the resin or bog does not appear to do much. However, a chemical reaction is building gradually. In the last few minutes before it hardens (the time taken for the whole process depends on the ratio of resin to hardener), the mixture heats up and begins to steam. If the person who is using the resin or bog takes too long to do the job, the mixture will set suddenly, before it has been applied.

The next day, some USQ Motorsport members returned and attached mating pairs of these cross-section/foam pieces together, and the following day, the rest were attached, to form the final plug.

It was found that some of the foam blocks were not as large as was required. This left some step-like depressions in the top and sides of the plug. This was fixed by adding a smaller block to fill the gap. This is not a perfect way to fix the problem, as this leaves a film of cured resin in the middle of the foam, where sanding will later take place. These extra blocks can be seen in Figure 7.8.



Figure 7.8: The blocks added to fill the gaps left by foam blocks that were too small.

While this was happening, Anil Puttaswamy had begun the cutting of the front 130mm of the nose cone on the milling machine. The volume in front of the foremost MDF

section would be very hard to shape by hand, so a small nose tip, 130mm front-to-back, was cut from polystyrene foam (Figure 7.9). This was a small operation, and the foam was available. The process took only about half an hour.



Figure 7.9: 130mm of nose cone being cut on the CNC machine.

After the resin had set, and the plugs were merely a pile of square foam blocks, the excess foam was cut away with a hand saw. This allows the quick, easy removal of excess material, bringing us closer to the final shape as quickly as possible. Figure 7.10 shows the rough shape of the plugs, after trimming with the hand saw, but before sanding. Vivienne French (pictured) and Les Rayner were most willing to help with all parts of the process, and their assistance was invaluable.



Figure 7.10: Vivienne French uses a handsaw to cut away unwanted material before sanding begins.

Once the rough shape was obtained, the rest of the excess foam was removed and the curvature of the bodywork shaped using sandpaper. 40 grit paper was used to begin with, attached to sanding boards. This removes the foam very quickly, compared to finer sandpaper. The sanding boards were used on an angle to the axes of the plugs, orienting them and the strokes at about 45° to the longitudinal axis. This technique, given to us by BAC employee, Bruce Dascombe, makes it easier to sand the curves to the right shape. If the board and the stroke are aligned with the longitudinal axis of the car, this will result in flat patches where material below the desired surface has been accidentally removed.

Figure 7.11 shows the difference between the rough cut and the sanded foam. Here also can be seen a small wedge placed between the third foam block from the top, and the MDF section below it. This was placed there, along with another on the hidden corner, to realign the foremost MDF section. Upon placing the two plugs side by side, it was found that the smallest cross-section was out of alignment on that plug by -18mm in the x-direction, and -13mm in the y-direction (i.e., 18mm inwards and 13mm downwards). Sanding a small amount off this block of foam, then inserting these wedges returned the foremost cross-section to its correct position and height.



Figure 7.11: Comparison of rough-cut and sanded foam.

The shape of the nose was effectively “sculpted” from the foam, then what depressions there were had to be filled in, or “bogged up”. Bog is merely a filler material, made from resin, using a fine powder as a bulking agent. This remains as a paste for days, until the hardening agent is mixed with it.

The bog paste is applied to fill the gaps left in the plug, allowed to set to a hard enough state to sand, then sanded to match with the surrounding foam. The bogging is shown in Figure 7.12. The problems associated with a hard material being sanded in close proximity to polyurethane foam can be seen in Figures 7.13, 7.14, and 7.15, where the surrounding foam has been sanded below the required level. This will have to be re-bogged later. Some areas still require bogging, and are seen in Figures 7.16 and 7.17.



Figure 7.12: The partially bogged nose plugs side by side.



Figure 7.13: Close-up of a patch of bog, showing the eroded foam on each side.



Figure 7.14: Eroded foam adjacent to the bog around the section 150mm forward of the front hoop.

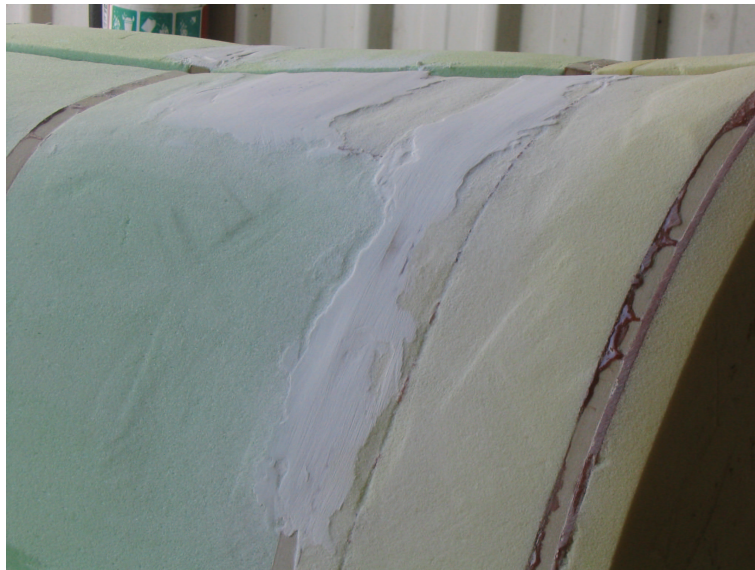


Figure 7.15: The light angle shows up eroded foam very well.

Unfortunately, this is the stage at which the construction of the bodywork is at the time of writing. However, work will progress, as the competition is going ahead in December, and the car will need bodywork for that event.

In the next few weeks, it is anticipated that the two plug halves will be bogged fully,

sanded, and waxed, at which time, the lay-up of fibreglass can commence. Two layers of fibreglass will be laid on these plugs, and allowed to set. These two layers will be extracted from the plugs, placed together, and three more layers of fibreglass mat laid up over the top of these, and one underneath, to bond the two halves together. This lay-up will involve preparing the plug surface with a layer of wet resin, over which the fibreglass mat is laid. Then, more resin is applied to the top of the mat, and rolled in, to fill all of the space between the fibres. This is allowed to cure, then the surface finished with more resin and paint.



Figure 7.16: Care must be taken to avoid removing good material with the handsaw.



Figure 7.17: A typical place that has yet to be bogged.

7.4 Construction Of The Centre Section

It was anticipated that plugs for the centre section (or cockpit sides) would be cut on the milling machine at BAC. These parts were much smaller than the nose cone, and would take much less time to cut, so being less of a disruption to BAC's production. The two models were constructed in SolidWorks, then placed together as an assembly, in order that they could be cut as one part (see Figure 7.18). This was intended to halve the set-up time for the operation.

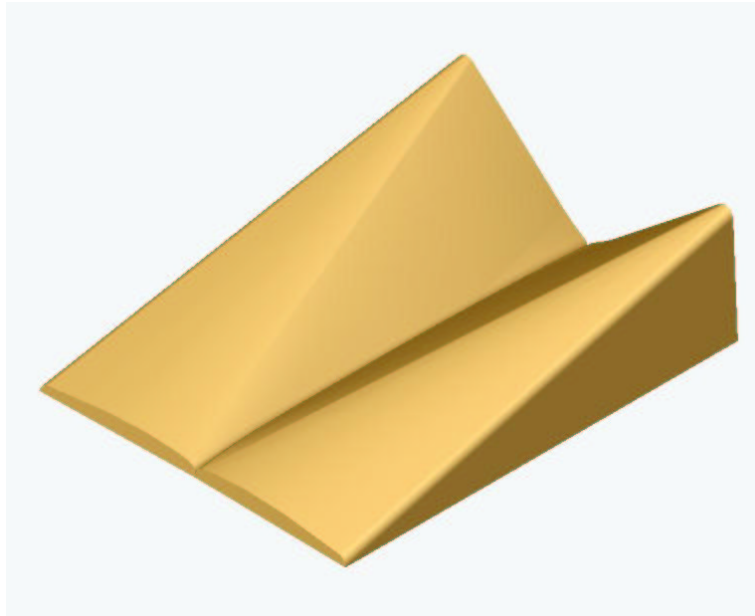


Figure 7.18: The assembly of the two side panel to form one part that may be machined in one run, thereby halving set-up time.

From there, the plugs would be bogged, sanded and waxed, and fibreglass laid up over the top, in the same manner as the nose cone.

Unfortunately, as previously described, the design of the side panels depends upon some other factors which have not yet been fully designed. The original plan was that when a seat was obtained, another chassis member would be added, extending from the front hoop, around the back of the seat, and back to the front hoop, thereby defining the cockpit rim. The shape of the cockpit rim defined the shape of the side bodywork panels, so this part was waiting first for a seat, then for the chassis member. The seat was not forthcoming in time for this project, and at the time of writing, BAC's milling machine was fully booked for nearly two months. This definitely precludes the planned construction of the side panels.

However, the side panels are a definite requirement by the F-SAE-A rules, and so they *must* be made.

The problem may be overcome, however, as the panels will be essentially two triangles and a rectangle all joined together. They will comprise a flat rectangular section

extending forward of the front hoop, between the top and bottom wishbones, a flat triangular section to cover the area from the diagonal side impact chassis member down, and another triangular section to cover from that member up to the upper side intrusion member. The fact that these pieces do not contain a complex curve, like the nose, is of great advantage, as this means that they can be bent from flat sheet. Sheet aluminium would be easily formable in this manner. A hole may also be drilled in sheet aluminium to allow the use of Dzus fasteners to attach the panels to the chassis.

Aluminium is an acceptable material for these panels, while it was no for the nose, because the requirements of the panel have changed. It was not used for the nose due to its complex curvature and its large area. These panels have neither, and to mould fibreglass over a shape like this would require the same amount of work as with a much more complex shape, while aluminium over a complex shape would need panelbeating, but with this shape, it does not.

This is planned to be constructed in the next month after writing.

7.5 Review of Construction

The construction of the bodywork for the USQ's F-SAE-A car has been a learning experience for all involved from the USQ Motorsport team. Only after the design had been finalised, can the construction begin, and therefore, urgency should be placed on the design of the part early in its design phase, allowing more time for its construction.

Some of the small hints and pointers that I have learned during the construction of this bodywork include:

- Avoid shapes which prevent extraction of the core after lay-up - design in a taper
- Where possible, avoid (inexperienced) manual labour - it takes far longer than using CNC machinery, and is less accurate
- Allow more time than anticipated for the creation of any required solid models
- Impress the urgency of other parts of the design, eg. chassis - sort out all details relevant to *your* part of the design as soon as possible

But the greatest lesson I have learned here is that if one intends to undertake a project, any time or anywhere, which involves designing then constructing (i.e., yourself, not getting it professionally built) a large part, such as automotive bodywork, *allocate at least half the time available to the construction*. At the conception of this project, the construction phase was given about one fifth, or less, of the time available, in the belief that the design would take most of the time, and the bodywork could all be built and assembled relatively quickly. This has turned out not to be the case.

However, although the construction is taking longer than expected, it is moving along steadily, and should be completed in time for the competition.

Chapter 8

Results

8.1 Chapter Overview

This project has looked at the design, analysis and manufacture of the different parts of the bodywork for the USQ's Formula SAE racer.

The modelling process was a long and tedious one, involving several redesigns due to a variety of reasons.

The CFD simulations were run according to the processes outlined earlier, in Chapter 6. The two dimensional cases were used merely to find the variables that had to be set, then these were applied to the three dimensional case of the SAE car. This is the case that will be discussed in this chapter.

The construction of the cores (to this stage) has been a learning experience for everyone involved.

8.2 Solid Models

The solid models produced are shown in Figures 8.1, 8.2, 8.3 and 8.4. These models are the results of inputs from several members of the team. The chassis model was modelled off the physical chassis, which had already been designed by Chris Baker. The shape of the nose was wildly influenced by the chassis, the suspension the steering and the radiator placement. The design of the side panels was to have been dependent on the choice of seat, but this was not timely enough, so it then reverted to being defined by the upper side intrusion member.

Several other systems in the car were able to be collated into one assembly, creating that shown in Figure 8.4. This assembly was used for marketing and promotion.

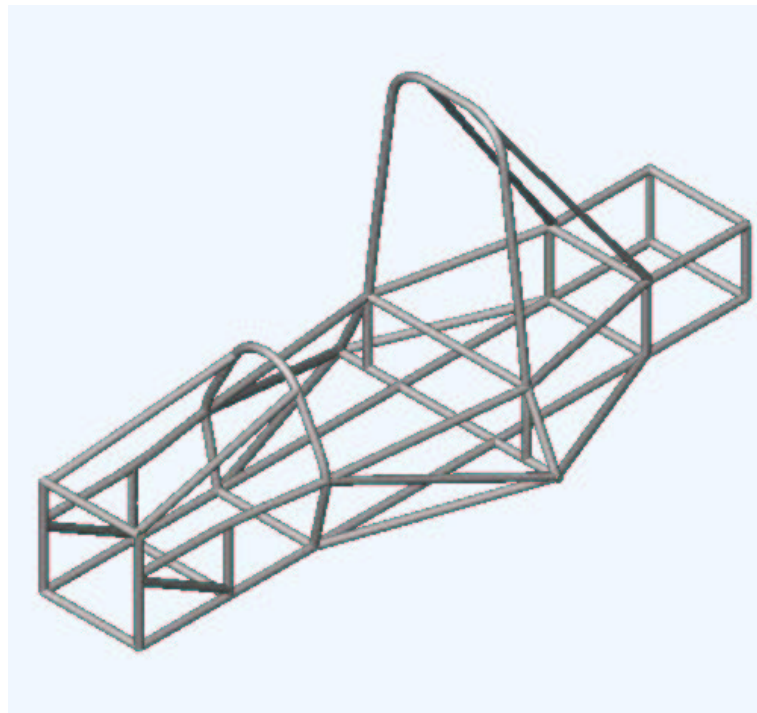


Figure 8.1: The SolidWorks chassis model.

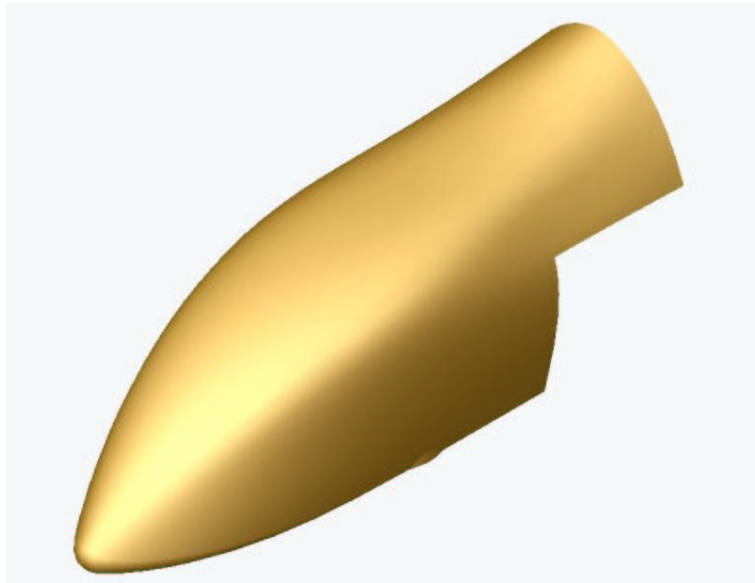


Figure 8.2: The final nose design.

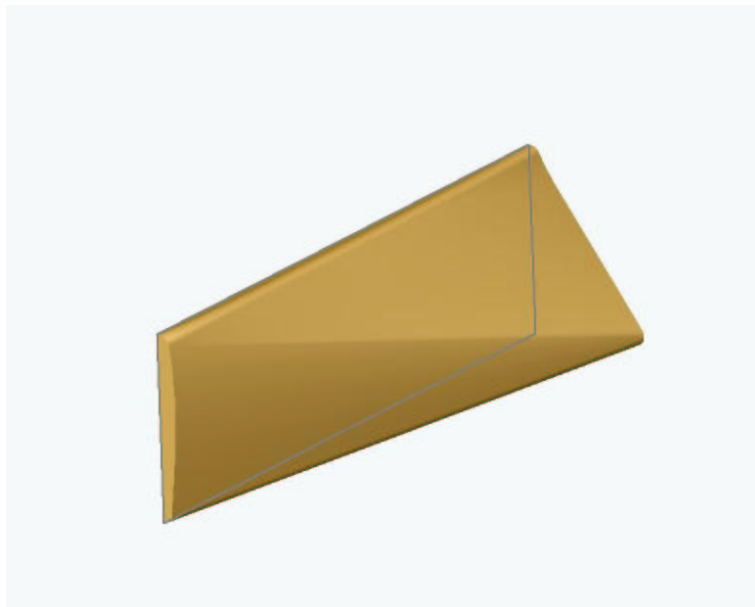


Figure 8.3: The port side panel.

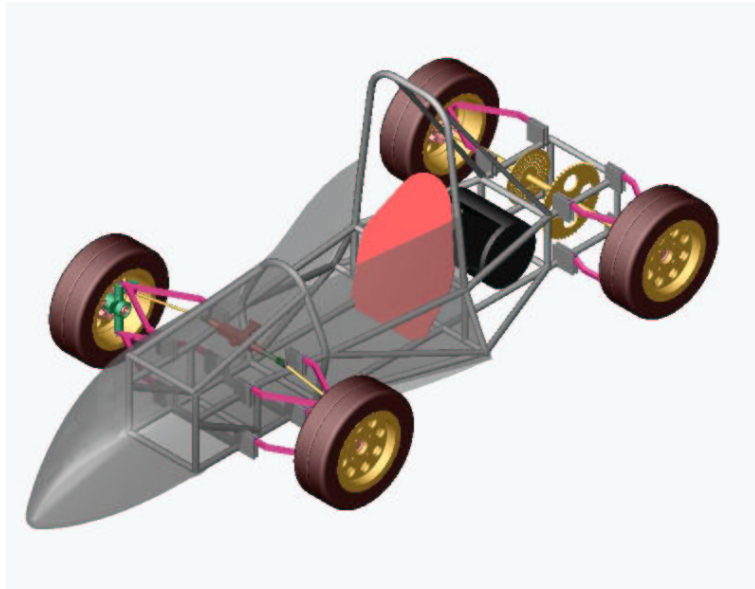


Figure 8.4: A full assembly model, including steering, suspension and drivetrain components.

The results of the modelling section of this project show just how effective good modelling can be. With a solid model of each major part of the car, I was able to import it into a CFD analysis, as well as being able to shape a physical core in order to construct the bodywork, and the members of USQ Motorsport's sponsorship team were able to use the models to invite sponsorship for the car.

8.3 The CFD Results

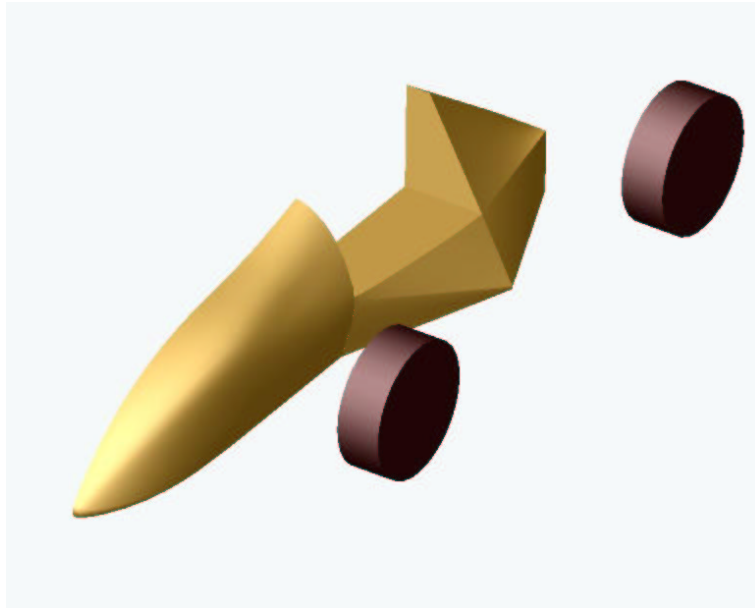


Figure 8.5: The CFD defeature in its correct colours.

Using the CFD defeature (Figure 8.5) in the analyses, the following results were obtained.

8.3.1 Contour Plots

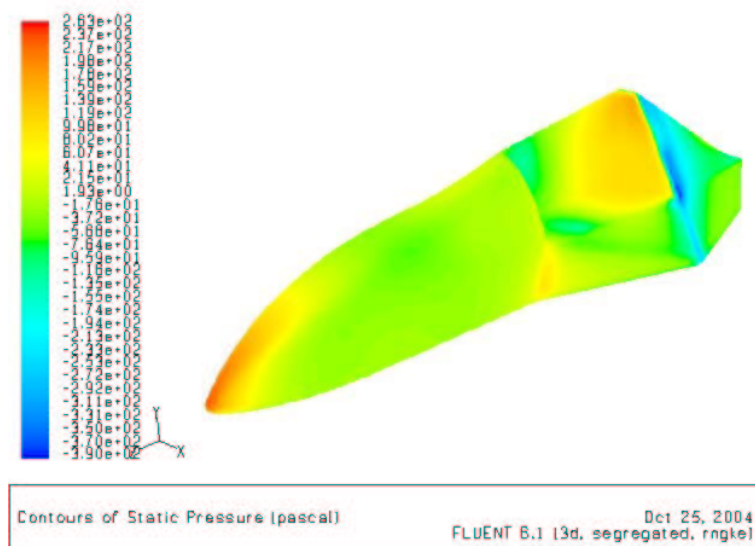


Figure 8.6: Static pressure contours.

Figure 8.6 shows contours of static pressure, with a maximum of about $260Pa_{(g)}$. The contours are smooth and in the expected position, which would indicate qualitatively that the solution should be close to correct. The contour gradients in the region around the front hoop, below the level of the upper side impact member indicate that there is some recirculation in that zone. This would most likely be due to the principle illustrated in Figure 8.12. This is one area that I would like to see improved in the future. It is possibly the worst part of the nose design, aerodynamically.

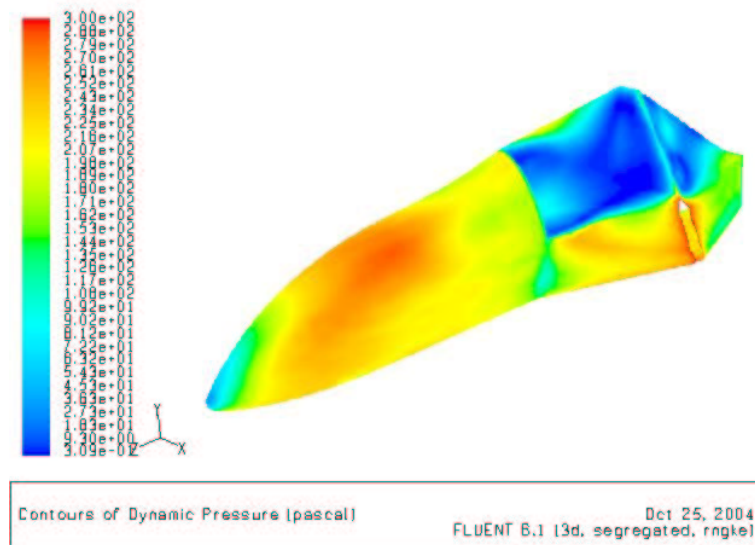


Figure 8.7: Dynamic pressure contours.

Figure 8.7 shows contours of dynamic pressure over the car. Here, the dynamic pressure indirectly represents the airspeed near the surface. It may be seen that the large red area over the top corner of the bulkhead is associated with a relatively high pressure gradient up and downstream from this. High adverse pressure gradients (where the static pressure goes from a low value to a higher value, like the area downstream from the bulkhead bulge) promote backflow and turbulence, and should therefore be avoided wherever possible.

A similar area is noticed along the crest of the diagonal side impact member, and the area of recirculation in front of this is also prominent in this figure.

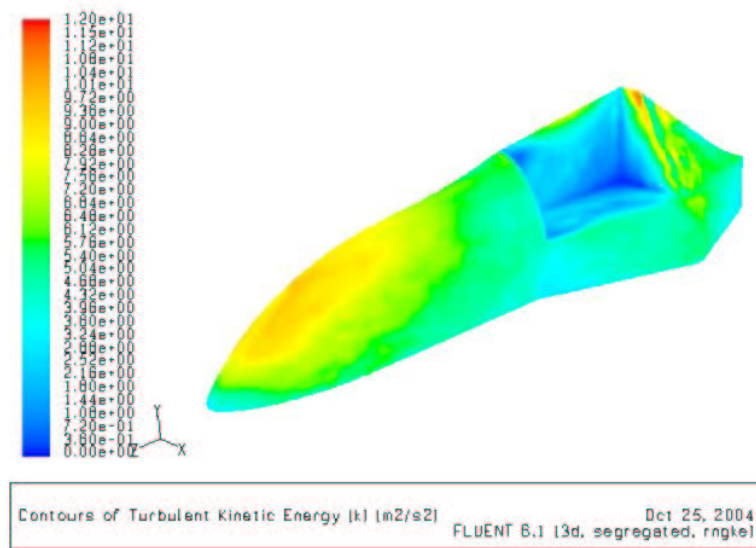


Figure 8.8: Turbulent Kinetic Energy (TKE, or k).

Figure 8.8 displays contours of TKE. While this plot is not exactly what was anticipated, it does show that the greatest turbulence occurs in the vicinity of an area of the bodywork that has the greatest convexity. It was expected that the greatest k values would be found in the area immediately aft of the bulkhead bulge.

This plot does contain something interesting, though: a spine of lower k values up the centreline of the car, extending in to the centre of the high- k patch. This could only be as a result of the symmetry plane. There is no other mechanism in the model or its settings that could produce this.

This gives rise to the hypothesis that exploiting centreline symmetry while modelling fluid flow may not be as accurate as originally thought. This may be the topic for further research.

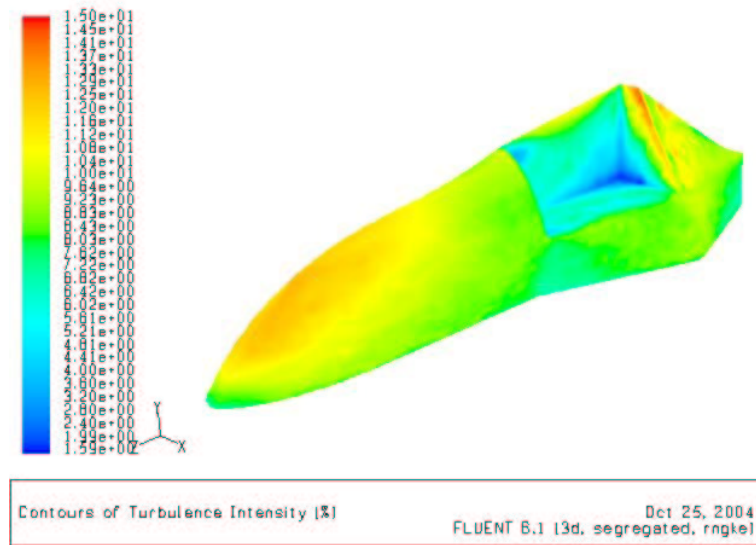


Figure 8.9: Turbulence intensity (%).

The turbulence intensity plot shows much the same as the TKE plot, except that the symmetry plane effects produce a narrower spine up the centreline of the car. This may well be resultant mere from different colour scaling when the plot was drawn.

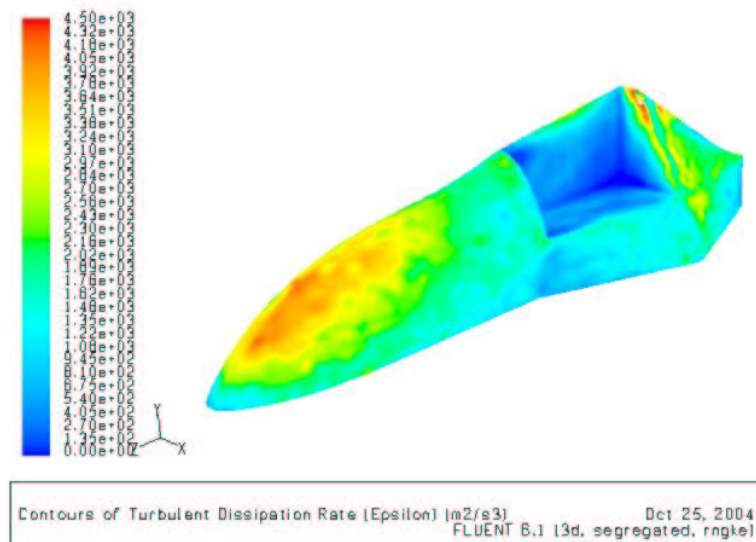


Figure 8.10: Turbulence dissipation rate, ϵ .

The TDR plot shows again the symmetry plane effects, as well as that TDR seems to match turbulence intensity. This makes sense, as the faster the eddy currents move, the greater the shear stress between fluid particles, thereby increasing energy dissipation.

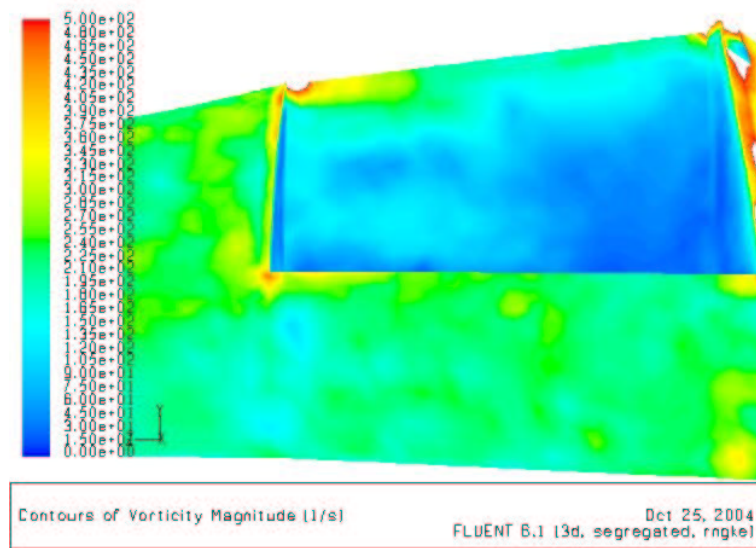


Figure 8.11: Vorticity magnitude.

The plot in Figure 8.11 shows no great trend in vorticity magnitude, except a slightly lower magnitude in the recirculation zone at the bottom of the front hoop and along the side, below the diagonal side impact member, after which there is a slight increase. However, these changes are even smaller than the local variations which produce the mottled effect, making these trends negligible. The interesting part is right at the bottom front corner of the cockpit opening. Here, vorticity (and therefore, energy bleeding) undergoes a marked increase. Right is the corner, a small vortex is being produced. This is another area that may easily be fixed by rounding this corner, and smoothing the transition from nose to side panel.

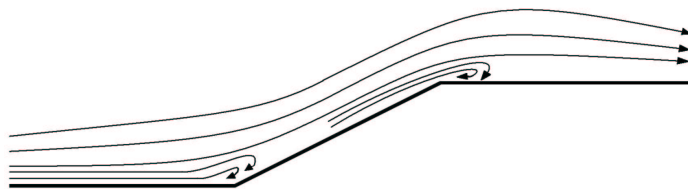


Figure 8.12: Recirculation occurring due to a change in geometry.

8.3.2 Vector Diagrams

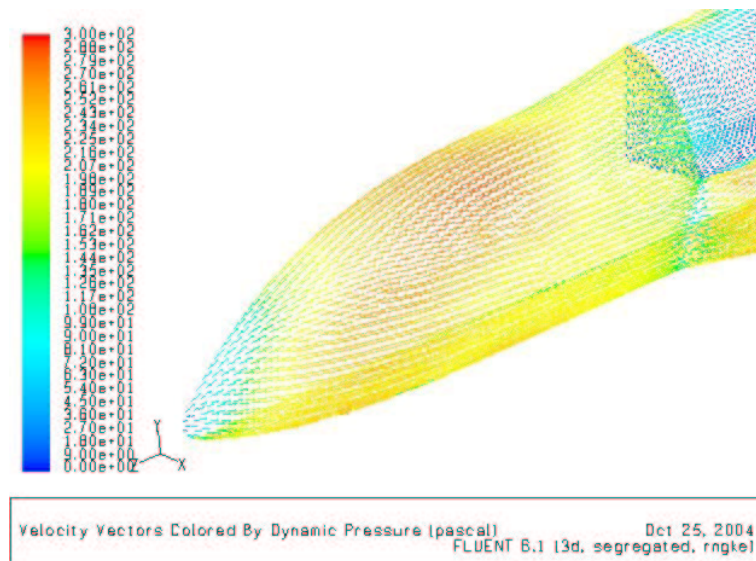


Figure 8.13: Velocity vectors over the nose.

The velocity vectors over the nose appear very streamlined. However, the steady formulation in the solver produces a time-averaged result, so turbulent flow is occurring, and at any given instant, a snapshot of the velocity vectors would show them pointing in random directions. So this plot does not say that the flow is nicely laminar over the whole surface, but it does show where, on average, the airflow is moving.

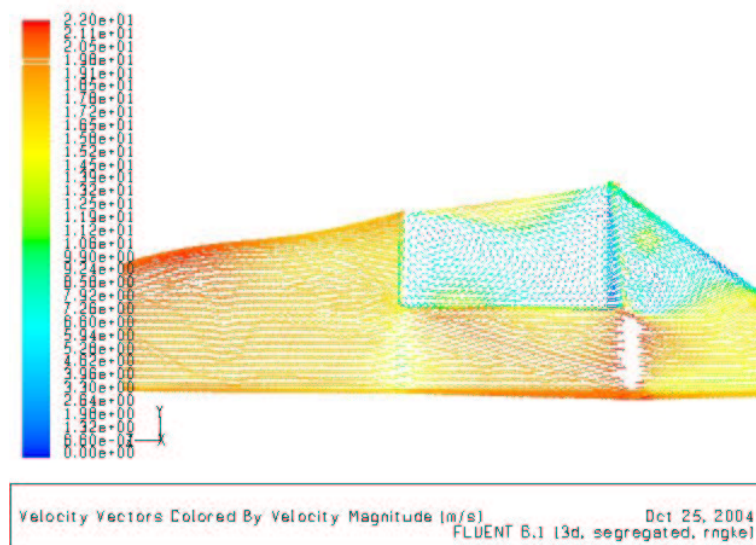


Figure 8.14: Velocity vectors over the side of the car.

The velocity vectors in Figure 8.14 show the time-averaged airflow to be flowing in a curvilinear path over the diagonal side impact member. This action is an undesirable outcome, as it leads to form drag.

The colouring of the vectors on the symmetry plane indicates that the wake of the nose cone is retracting into the cockpit, allowing freestream air to impact the driver's head. This can be very distracting for a driver of a car such as this. It was hoped that the airflow would spit up over the driver's head, but the car just will not go fast enough for this.

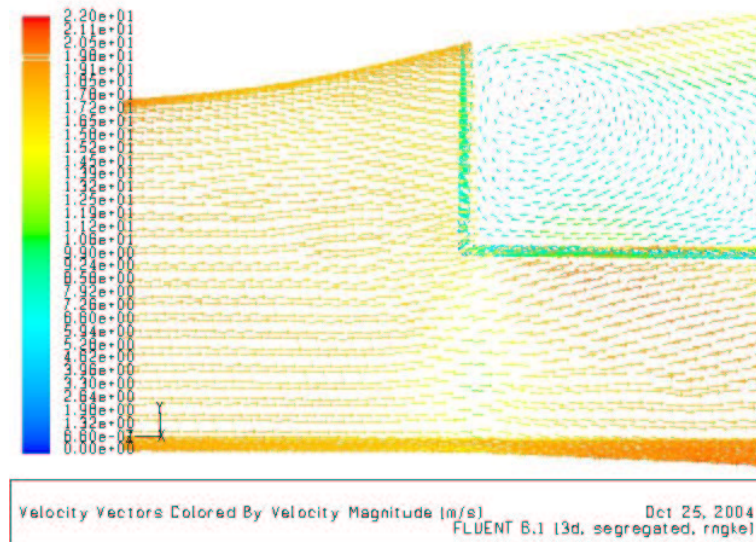


Figure 8.15: Close up on the cockpit rim from Figure 8.14.

Figure 8.15 shows the airflow near the cockpit rim spilling into the cockpit. This is because the rim is slightly side-on to the flow. This will produce vorticity around here, and should be fixed in the future. A more rounded cockpit corner (described earlier), and an upper side impact member that is parallel to the flow would reduce this substantially.

8.3.3 Turbulence

The turbulence shown in Figure 8.9 appears to increase by a factor of about three over the nose cone of the car. It was specified at 5% at the inlet, and over the nose, the

colour contours correspond to a value of about 13 to 15%. This is most likely due to the roughness height on the surface being 0.001m, or one millimetre. If the fibreglass were moulded in a female mould, instead of a male plug, the surface finish would be much smoother. If this could be done, it would solve many turbulence problems.

8.3.4 Coefficient of Drag

The coefficient of drag obtained from the analysis was only 0.34, which is a substantial amount less the anticipated value. This may be due to incorrect simulation, or to an incorrect derivation of the anticipated value. In this case, the latter is more likely, as the combinations of variables, factors and other settings was tried and proven on the 3D sedan model. The likelihood of these having to be changed from the sedan to the SAE car is small.

8.4 Chapter Summary

In the Results chapter, we have seen the contour plots and vector diagrams showing where the flow is going, and what it is doing there, however, we have also seen that there is still some doubt about the accuracy of the calculated C_D figure. This has reinforced the idea that CFD is *NOT* a faultless design tool. It must always be used to back up other results (from a wind tunnel, for example), or to predict the effect of a single, very small change to something whose characteristics are already known.

Chapter 9

Conclusions And Further Work

During the course of this project, we have seen the design process through which the shape of the F-SAE car came, then the CFD analysis, which has proved itself to be not quite as infallible as was first thought. We have also seen the beginnings of the construction of the bodywork, and this will be continuing very quickly in the month after this report is written.

This is the main piece of further work that *has* to be done. If the bodywork does not get constructed, the car will not run in the 2004 F-SAE-A competition.

There are some other pieces of further work that should be done at some time in the future. To obtain a more accurate C_D figure, a speed run on a test track, using an altered gear ratio, would be a very useful activity. If the power at the wheels is known (may be obtained from a dynamometer run), the equation,

$$C_D = \frac{\text{Power at wheels}}{0.6 \times \text{FrontalArea} \times \text{Velocity}^3}$$

This C_D figure would be able to be used to guide any further CFD analyses on this subject.

Some other forms of testing and flow visualisation may be used in the future. Wool-tuft testing (Figure 9.1) is an effective means of visualising turbulent or laminar near-

boundary layer flow.



Figure 9.1: Wool-tuft testing a VR Commodore (Edgar 2000).

Smoke testing (Figure 9.2) is another method of flow visualisation, but this shows where the flow is separating from a body, and reattaching to it.



Figure 9.2: Smoke testing the wake behind an R32 Skyline (Edgar 2000).

These and many more tests would be very interesting to do in the future, but for now, all concentration will be on the construction of the bodywork.

References

- A.J. Baker, W.P. Noronha, J.B. Woods (1989), 'Finite Element CFD Methods for Vehicle Internal Flow Simulation', *Automotive Simulation - The second European Cars and Trucks Simulation Symposium - Proceedings* .
- Anderson, J. D. (1995), *Computational Fluid Dynamics - The Basics With Applications*, McGraw-Hill Inc., Singapore.
- A.P. Gaylard, A.J. Baxendale, J.P. Howell (1999), 'The Use of CFD to Predict the Aerodynamic Characteristics of Simple Automotive Shapes', *Car Technology Yearbook, 1999* .
- Edgar, J. (2000), *21st Century Performance*, Clockwork Media, Sydney.
- F1 Racing* (March 2003).
- FLUENT/UNS And RAMPANT 4.2* (n.d.), Vol. 4, FLUENT Incorporated, chapter 22.
- Formula SAE-A Rules Webpage* (2004), The Society Of Automotive Engineers.
<http://www.sae-a.com.au/fsae/rules.htm>
current Oct 2004.
- Fox, R. W. & McDonald, A. T. (2003), *Introduction to Fluid Mechanics*, fifth edn, John Wiley and Sons, Inc., New York, New York.
- Gillespie, T. D. (1992), *Fundamentals Of Vehicle Dynamics*, Society of Automotive Engineers, Warrendale, Pasadena.
- Hucho, W.-H. (1987), *Aerodynamics Of Road Vehicles*, english edn, Butterworths, Cambridge, England.

- Katsuro Fujitani, Ryutaro Himeno, Michitoshi Takagi (1989), 'Unsteady 3D Calculation of Flow around a Car and its Visualisation', *Automotive Simulation* .
- Matweb Website Properties Search* (2004), Matweb.
<http://www.matweb.com/GetProperty.asp>
current Oct 2004.
- Smith, C. (1978), *Tune To Win*, Aero Publishers, Inc.
- Snook, C. (2003a), *Computational Mechanics In Design - Study Book 1*, USQ Publication.
- Snook, C. (2003b), *Computational Mechanics In Design - Study Book 2*, USQ Publication.
- Wilders, P. (2002), *Parallel Computational Fluid Dynamics - Proceedings of the Parallel CFD 2001 Conference*, Elsevier.

Appendix A

Project Specification

University of Southern Queensland
Faculty of Engineering and Surveying

ENG 4111 / 4112 – Research Project Project Specification

- FOR: **Ken Nelder**
- TOPIC: Aerodynamic package for USQ's Formula SAE Racer
- SUPERVISORS: Mr. Chris Snook
Dr. Ruth Mossad
- PROJECT AIM: To design and develop an aerodynamically “clean” external shape for the USQ's Formula SAE Racer.
- PROGRAMME: Issue A, 22nd March, 2004
1. Research automotive, especially racing aerodynamics, and become familiar with the relevant rules and regulations of F-SAE.
 2. Review the available software tools for CFD analysis, compare and contrast their capabilities, and use the most appropriate software packages to develop and analyse a simple 2D model of the basic car shape.
 3. Model the proposed body shape, looking in particular at the airflow over the shape, and the magnitude of its drag.
 4. Analyse these results, combined with the specifications of the spaceframe design, to develop and analyse a simple model that includes the external shape of the USQ's Formula-SAE Racer.
 5. Develop and document techniques for analysing the SAE car with different body geometry.



As time/resources permit(s):

6. Develop more than one basic shape (possibly three shapes) to test in step 4 above.
7. Construct and evaluate a full-size model, from suitable materials, possibly plywood, fibreglass, or timber and fabric.
8. Develop CFD/wind tunnel testing techniques to aid further work on the USQ F-SAE Racer.

AGREED:

 (student)



 (Supervisors)

Dated: 20/7/04

Appendix B

F-SAE Rules Extracts

B.1 Introduction to this Appendix

This appendix contains the relevant rules and regulations for the bodywork of a Formula SAE-A car. (*Formula SAE-A Rules Webpage* 2004).

For the full rules, see <http://www.sae-a.com.au/fsae/rules.htm>.

3.1.1 - Body and Styling

The vehicle must be open-wheeled and open-cockpit (a formula style body). To protect the driver, there shall be no openings through the bodywork into the driver compartment from the front of the vehicle back to the roll bar main hoop or firewall other than that required for the cockpit opening. Minimal openings around the front suspension components are allowed.

3.2.1 - Ground Clearance

Ground Clearance must be sufficient to prevent any portion of the car (other than tires) from touching the ground during track events.

3.2.3 - Suspension

The car must be equipped with a fully operational suspension system with shock absorbers, front and rear, with usable wheel travel of at least 50.8 mm (2 inches), 25.4 mm (1 inch) jounce and 25.4 mm (1 inch) rebound, with driver seated. The judges reserve the right to disqualify cars which do not represent a serious attempt at an operational suspension system or which demonstrate unsafe handling.

3.3.7 - Frontal Impact Protection Others

People shall not be endangered by contact with sharp edges on the forward facing bodywork or other protruding components. All forward facing edges on the bodywork that could impact people, e.g. the nose shall have forward facing radii of at least 38 mm (1.5 inches). This minimum radius shall extend to at least 45 degrees relative to the forward direction, along the top, sides and bottom of all affected edges.

3.4.3 - Driver Visibility**3.4.3.1 - General Requirement**

The driver shall have adequate visibility to the front and sides of the car. With the driver seated in a normal driving position he/she shall have a minimum field of vision of 200 degrees (a minimum 100 degrees to either side of the driver). The required visibility may be obtained by the driver turning his/her head and/or the use of mirrors.

3.4.4 - Head Protection**3.4.4.2 - Roll Bar Padding**

Any portion of the roll bar, roll bar bracing or frame which might be contacted by the drivers helmet shall be covered by a nonresilient, energy-absorbing material such as Ethafoam or Ensolite or other similar material, to a minimum thickness of 12 mm (0.5 inch). Pipe insulation material is unacceptable for this application.

3.4.5 - Floor Closeout

All vehicles must have a floor closeout made of one or more panels, which separate the driver from the pavement. If multiple panels are used, gaps between panels are not to exceed 3 mm (1/8 inch). The closeout must extend from the foot area to the firewall and must protect the legs and torso from track debris.

3.4.7 - Driver Egress

All drivers must be able to exit to the side of the vehicle in no more than 5 seconds. Egress time begins with the driver in the fully seated position, hands in driving position on the connected steering wheel, wearing the required driver safety equipment. Egress time will stop when the driver has both feet on the pavement.

3.4.10 - Fire Protection**3.4.10.1 - Firewall**

A firewall must separate the driver compartment from all components of the fuel supply, the engine oil and the liquid cooling systems. It must protect the neck of the tallest driver. It shall extend sufficiently far upwards and/or rearwards such that any point less than 100 mm (4 inches) above the bottom of the helmet of the tallest driver shall not be in direct line of sight with any part of the fuel system, the cooling system or the engine oil system. The firewall must be a non-permeable surface made from a fire resistant material. Pass-throughs for wiring, cables, etc. are allowable if grommets are used to seal the pass-throughs. Also, multiple panels may be used to form the firewall but must be sealed at the joints to meet the intent of driver protection.

3.6.1 - Car Number

Each car will receive a number at the time of its entry in the competition. This number must be displayed in 15.24 cm (6 inches), or larger, characters in three (3) locations; the front and both sides of the vehicle. The numbers must be composed of white numerals on a black background, black numerals on a white background, or high-contrast equivalents. The use of metallic, fluorescent or other reflective colors will not be approved.

3.6.2 - School Name

Each car must clearly display the school name (or initials - if unique and generally recognized) in 5.08 cm (2 inches), or larger, characters on both sides of the vehicle. The characters must be placed on a high-contrast background in an easily visible location.

3.6.3 - SAE Logo

The SAE logo must be displayed on the front and/or both sides of the vehicle in a prominent location. SAE logo stickers will be provided to the teams on site.

3.7 - GENERAL**3.7.1 - Wing Locations**

The wing or wings must be located in plan view within a quadrilateral defined by the outside of the tires on the sides, by a transverse line 460 mm (18 inches) in front of the fronts of the front tires, and by a transverse line between the rear of the rear tires.

3.7.1.1 - Driver Egress

Requirements Egress from the vehicle within the time set in section 3.4.7 - “Driver’s Egress,” shall not require any movement of the wing or wings or their mountings. The wing or wings must be mounted in such positions, and sturdily enough, that any accident is unlikely to deform the wings or their mountings in such a way to block the drivers egress.

3.7.1.2 - Wing Edges - Minimum Radii

All wings: leading edges shall have a minimum radius 12.7 mm (0.5 inch) unless a wing projects in front of the front tires, in which case it must have a minimum radius of 19 mm (0.75 inch). Wing leading edges must be as blunt or blunter than the required radii for an arc of plus or minus 45 degrees centered on a plane parallel to the ground or similar reference plane for all incidence angles which lie within the range of adjustment of the wing or wing element. If leading edge slats or slots are used, both the fronts of the slats or slots and of the main body of the wings must meet the minimum radius rules.

3.7.1.3 - Other Edge Radii Limitations

All wing edges, end plates and wing accessories must have minimum edge radii of at least 3 mm (1/8 inch) i.e., this would mean at least a 6 mm (1/4 inch) thick edge.

3.7.1.4 - Wing Edge Safety

No small radius edges may be included anywhere on the wings in such a way that would violate the safety intent of these rules (i.e. vortex generators with thin edges, sharp square corners on end plates, etc.).

3.7.1.5 - Ground Effect Devices - Prohibited

No power device may be used to move or remove air from under the vehicle except fans designed exclusively for cooling. No power ground effects are allowed.

Appendix C

Solid Modelling

C.1 Introduction to this Appendix

This appendix documents the design process of the nose cone of the car, and shows all cross-section sketches of each different nose design. Comparison of the sections shows the evolution of the shape throughout the design process.

This appendix is intended to contain sufficient information to reconstruct the nose cone.

C.2 Chassis



Figure C.1: The planes defined in Table 4.2.

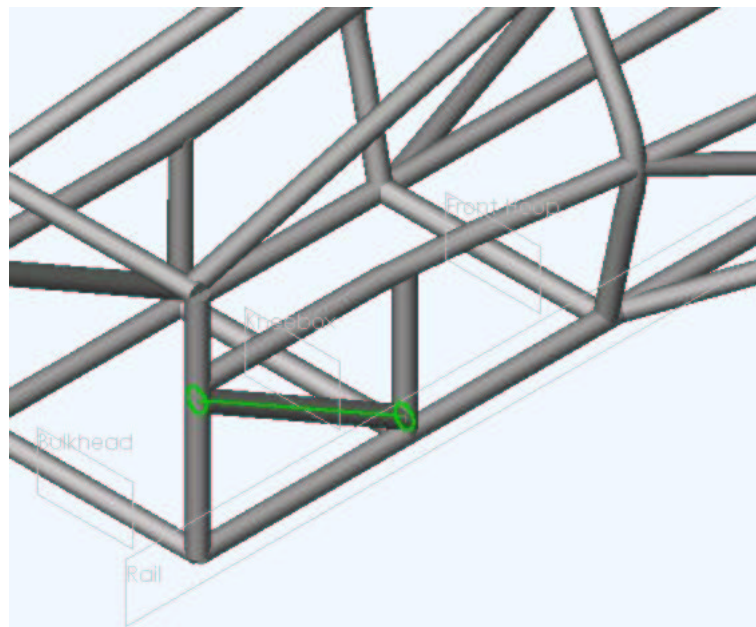


Figure C.2: The two elliptical end section sketches and the centreline for the port front diagonal member. Note also the reference planes, “Bulkhead”, “Kneebox”, “Front Hoop” and “Rail”.

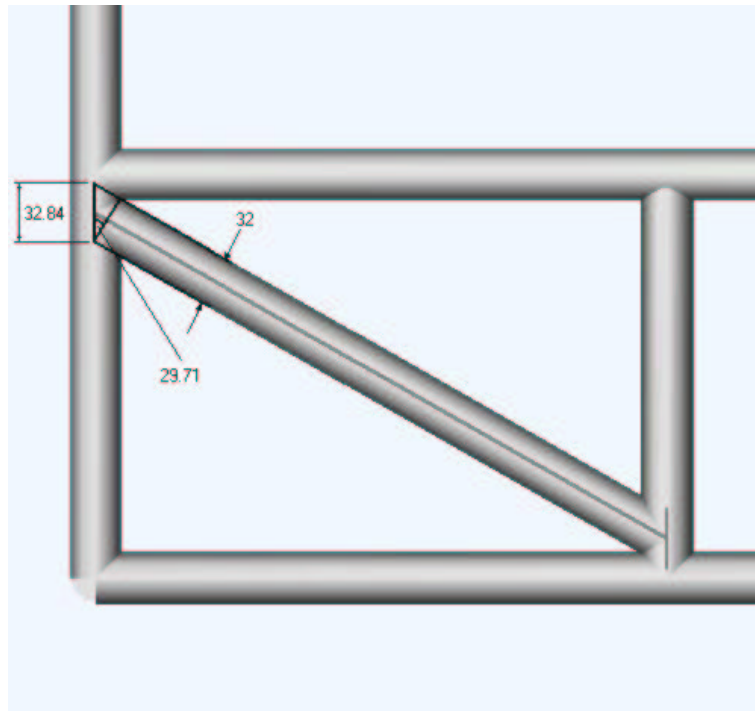


Figure C.3: Trigonometric calculation of the ellipse height for lofting the front diagonal chassis member.

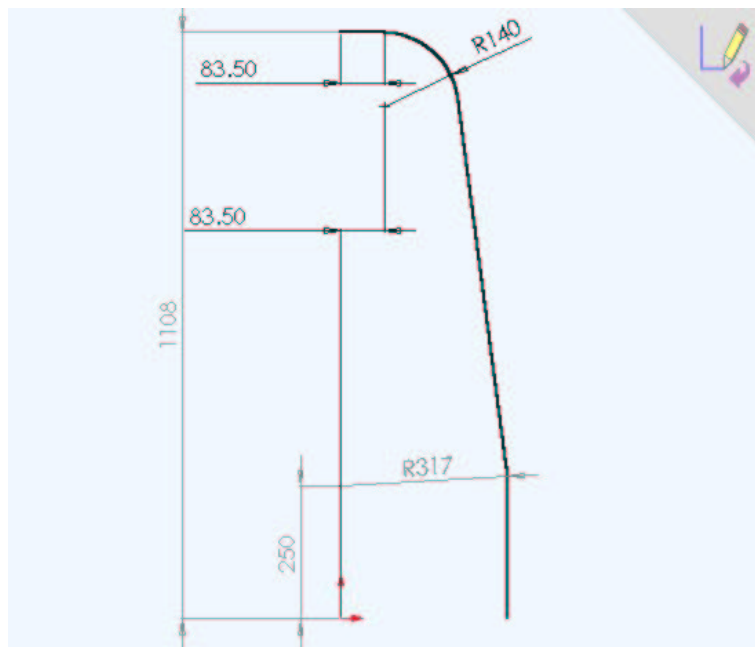


Figure C.4: Centreline sketch for the port side of the main roll hoop.

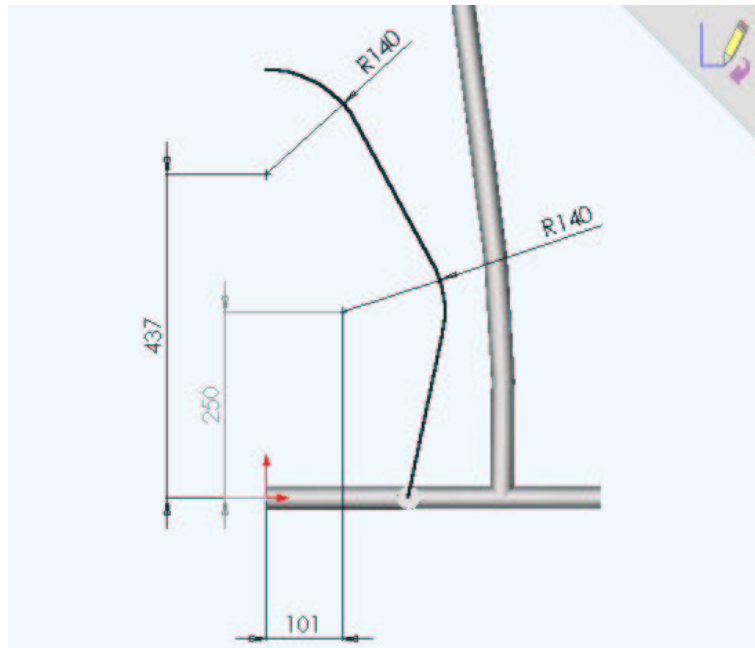


Figure C.5: Centreline sketch for the port side of the front roll hoop.

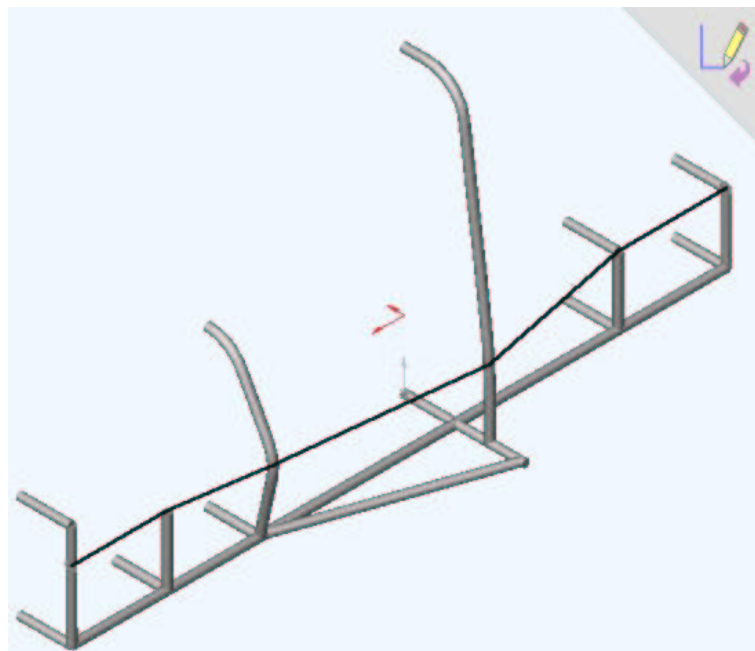


Figure C.6: Centreline sketch for the port upper side impact member.

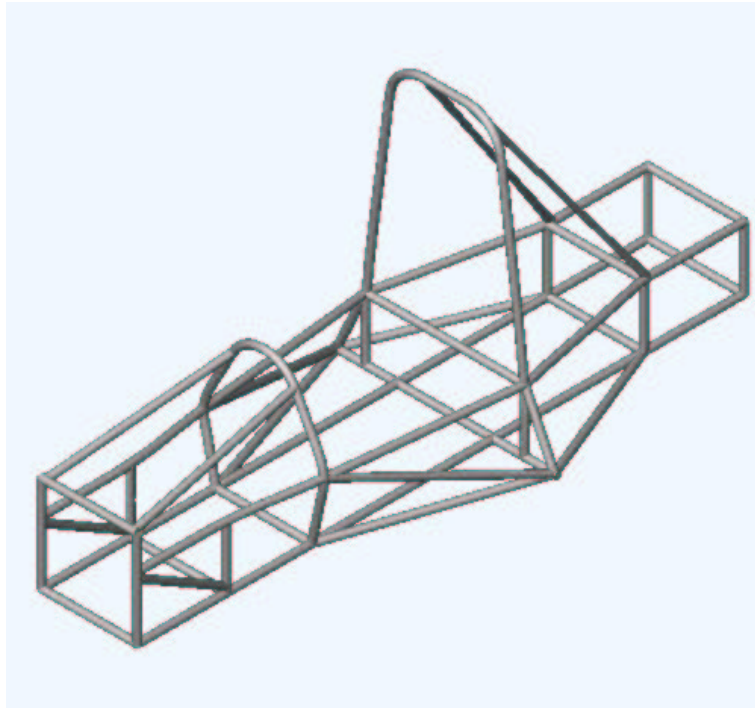


Figure C.7: The completed SolidWorks chassis model.

C.3 Nose

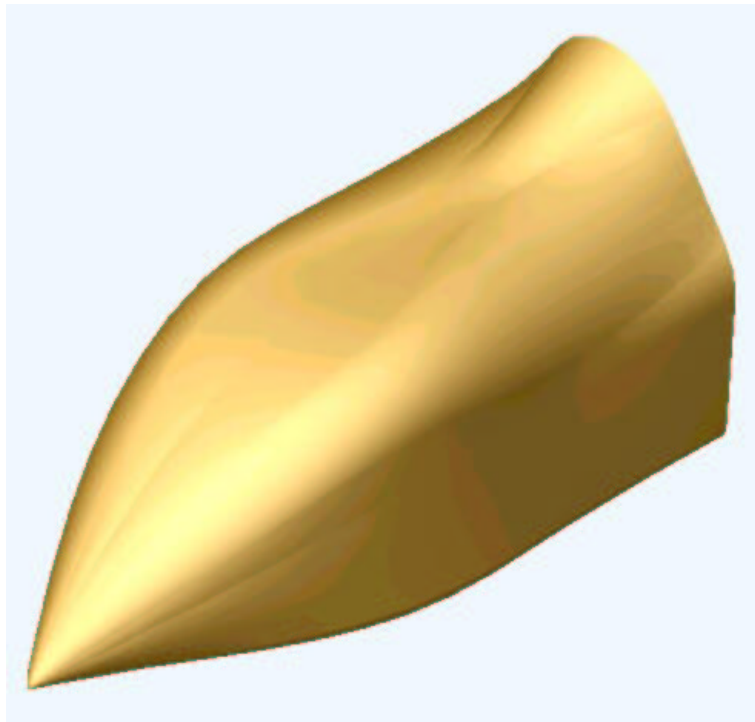


Figure C.8: The first nose model.

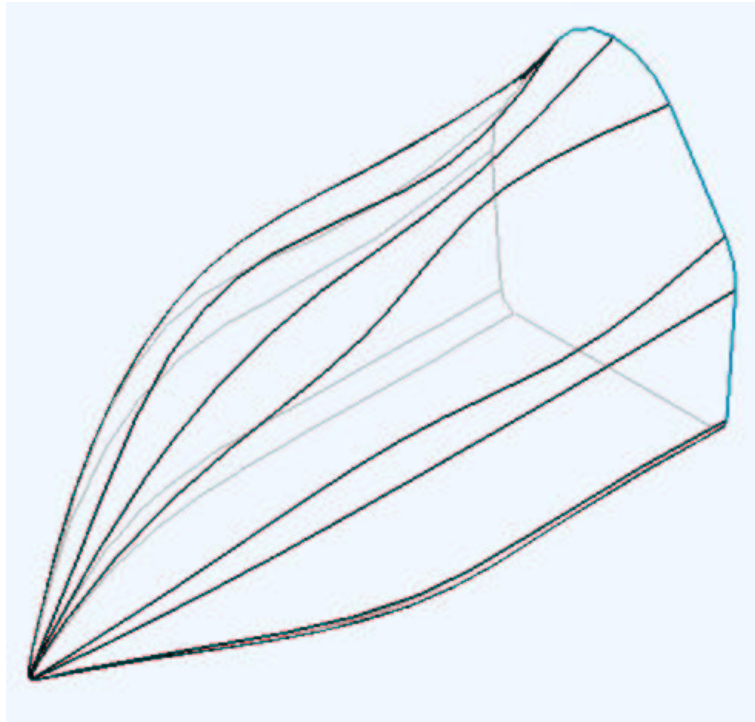


Figure C.9: The first nose model in wireframe, showing the many face edges, which will not be parallel to the airflow.

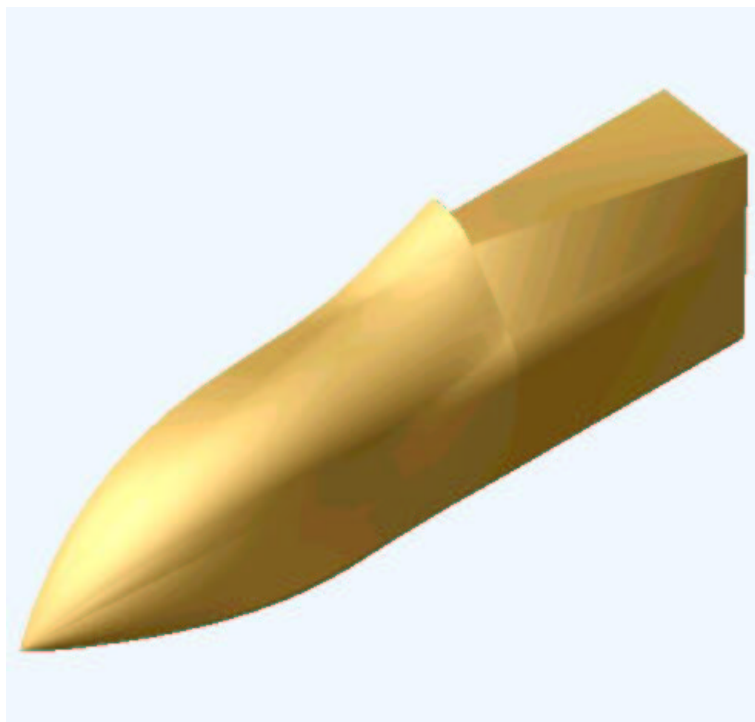


Figure C.10: The second nose model. Note the bulges over the bulkhead have been reduced.



Figure C.11: The second nose model in front view. Note the curvature of the face edges.

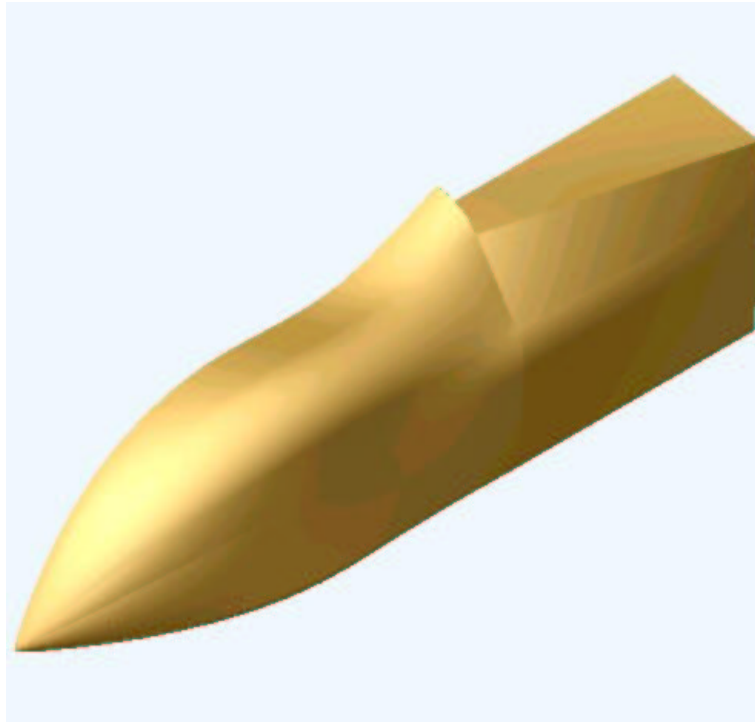


Figure C.12: The redesign of the second nose model. Note the slight streamlining of the face edges.



Figure C.13: The second model redesign, front view, showing the straighter edges.

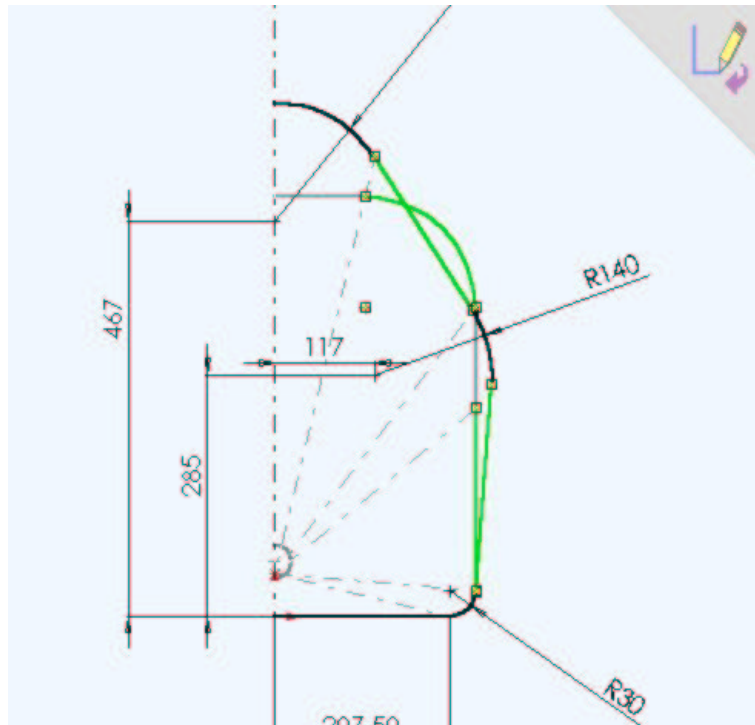


Figure C.14: The bulkhead sketch of the second model. Note the radiating construction lines defining the path for the face edges.

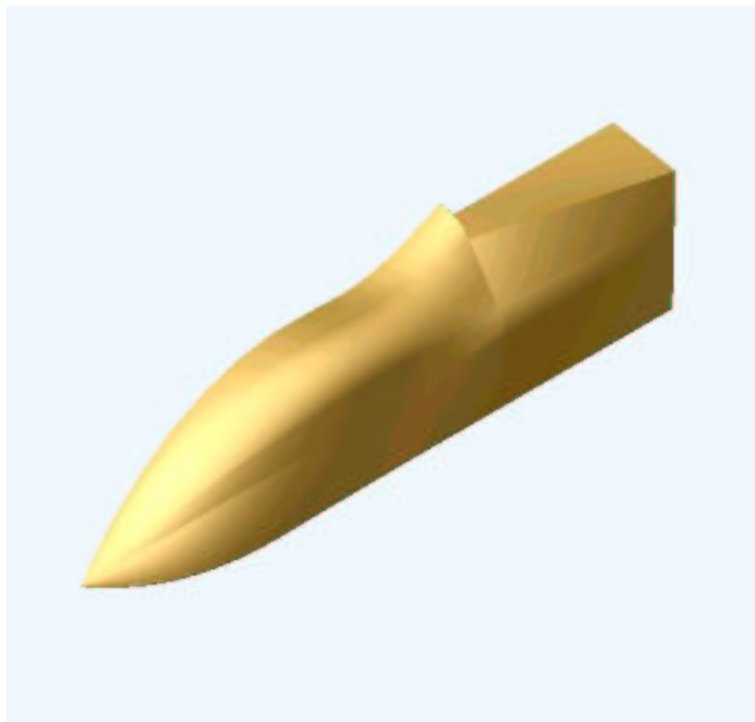


Figure C.15: The third model.

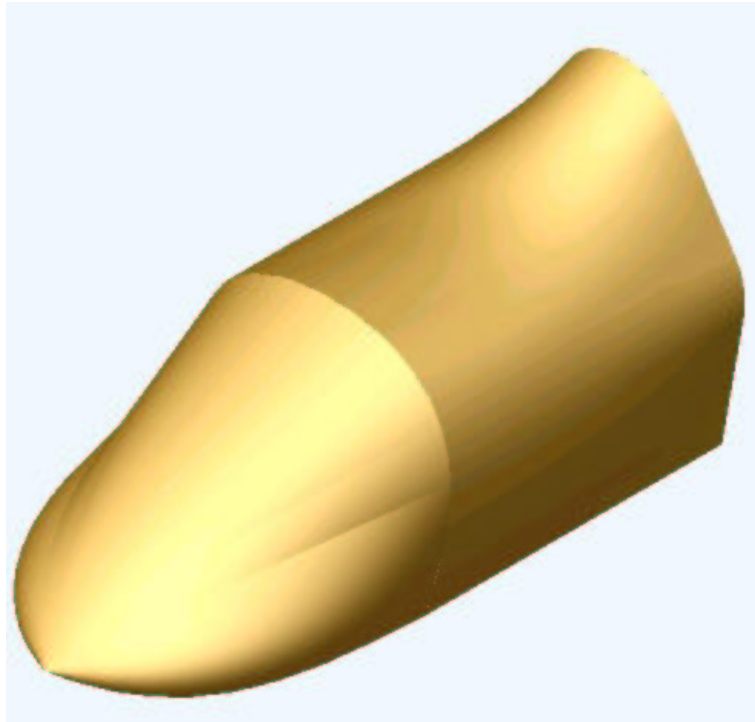


Figure C.16: The fourth model, showing the one-piece top surface, and the “duck-bill” nose”

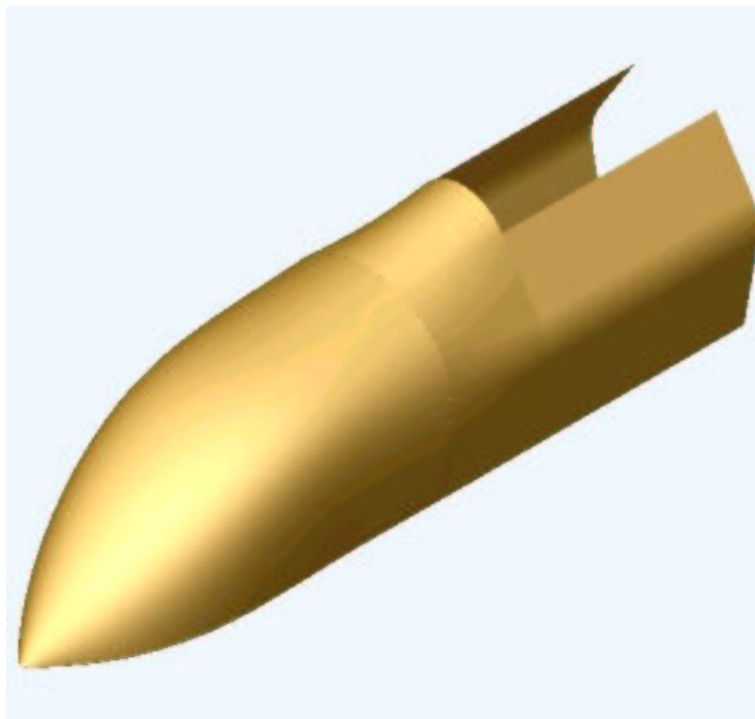


Figure C.17: The fifth nose model. Note the one-piece top surface.

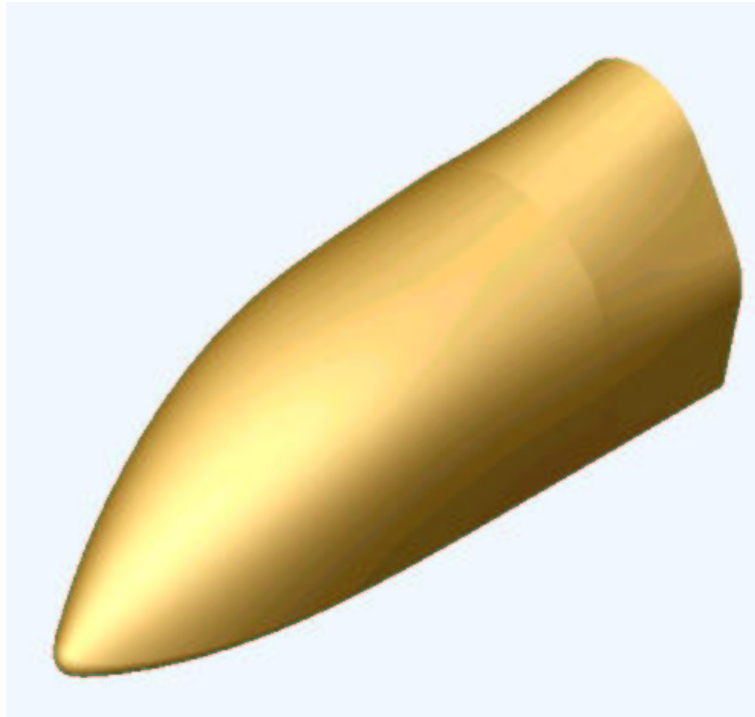


Figure C.18: The sixth nose model. Here, the fillet has been added around the nose point.

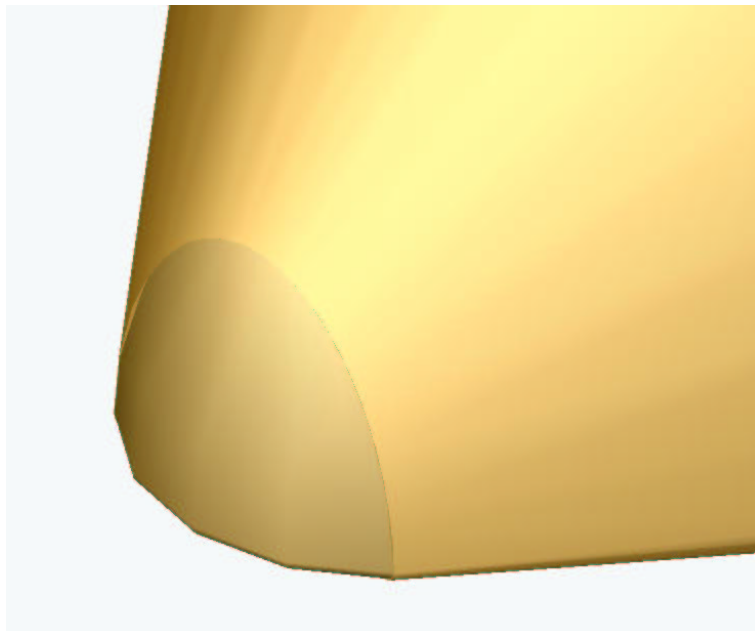


Figure C.19: The sixth model, using an extruded cut and a revolved solid to round off the nose point.

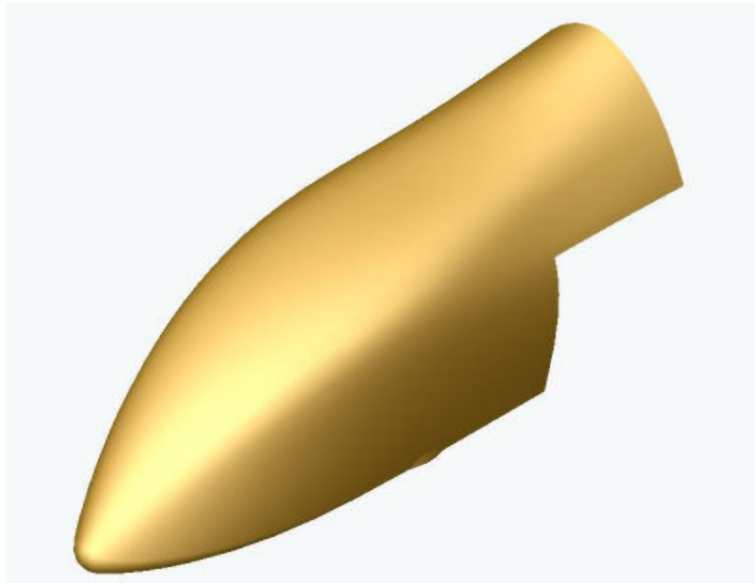


Figure C.20: The final model, showing the one-piece design, variable-radius fillet, and suspension cutouts.

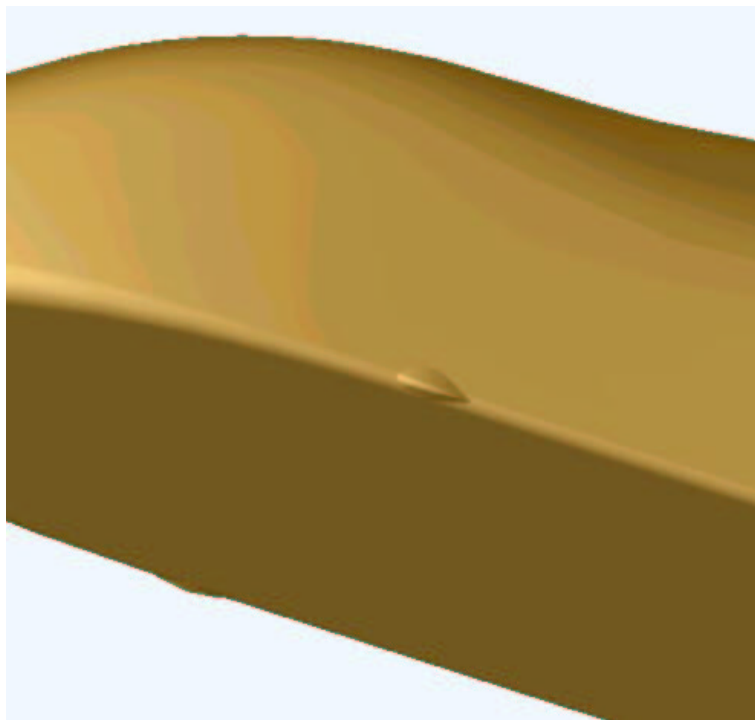


Figure C.21: The blisters designed to clear the attachment of the crush zone to the chassis.

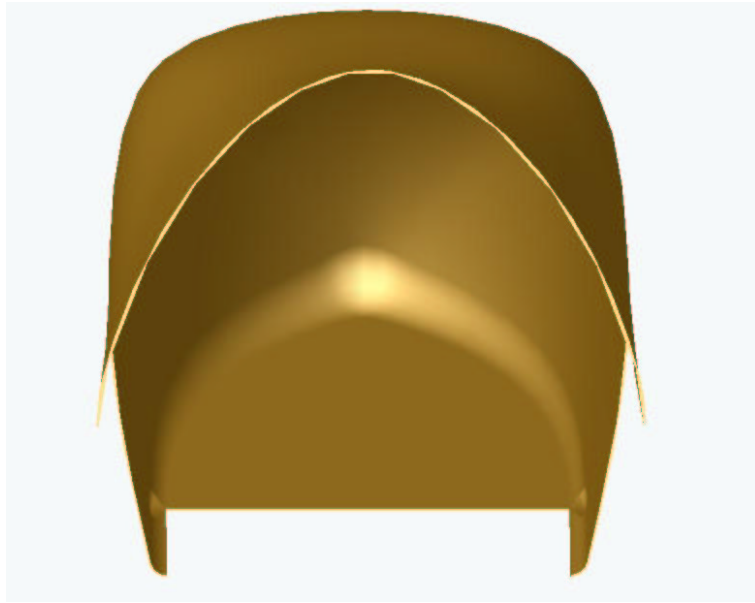


Figure C.22: Looking inside the final shelled model.

C.4 Nose Model Cross-Sections

C.4.1 Nose 1

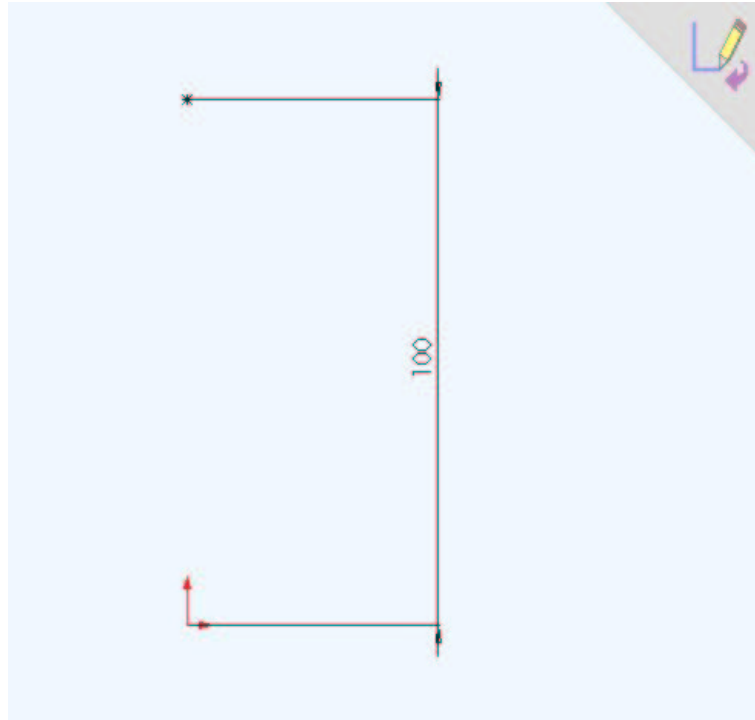


Figure C.23: First nose model “nose point” cross section.

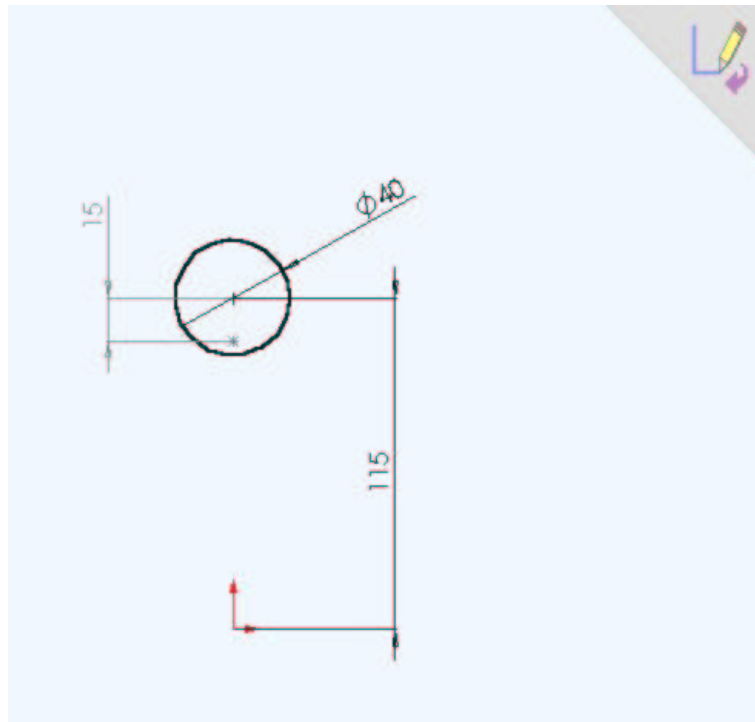


Figure C.24: First nose model “nose shaper” cross section.

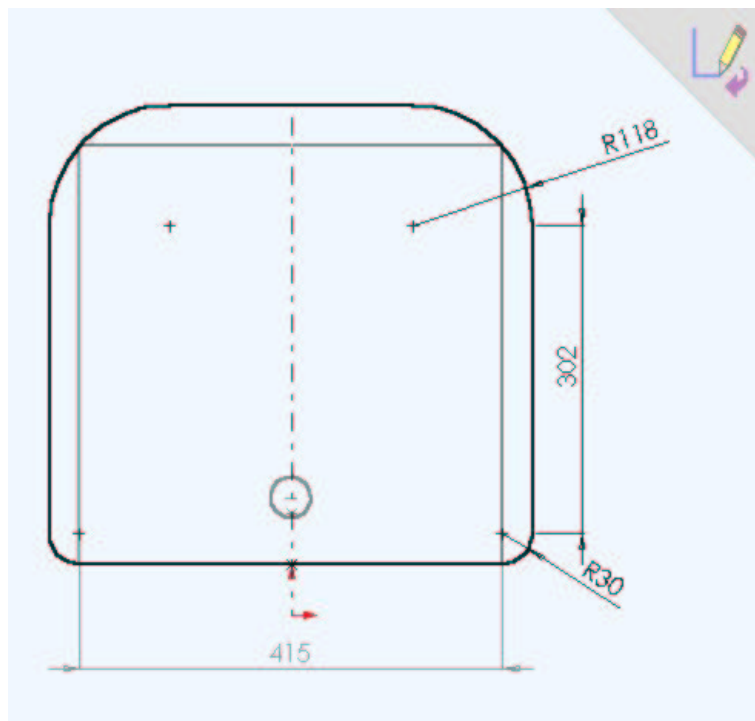


Figure C.25: First nose model “bulkhead” cross section.

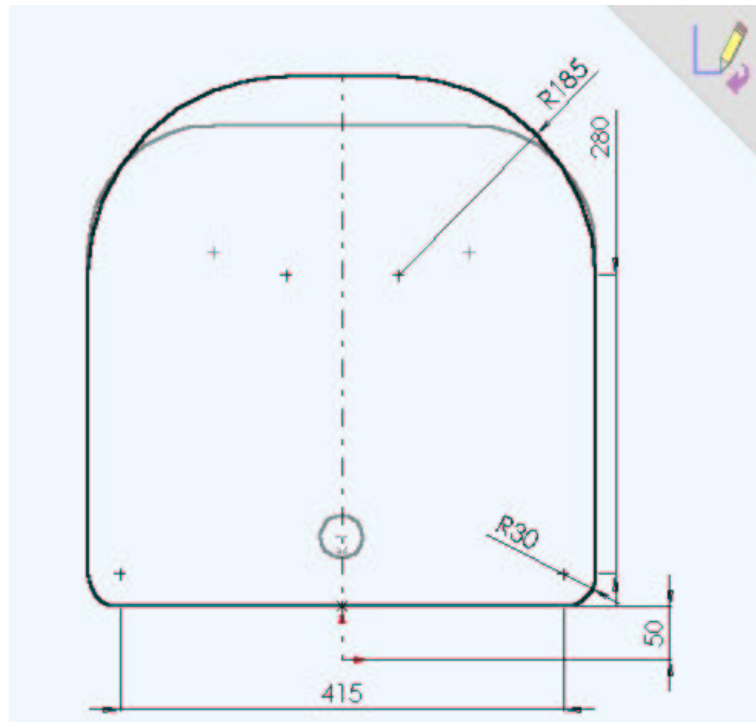


Figure C.26: First nose model "kneebox" cross section.

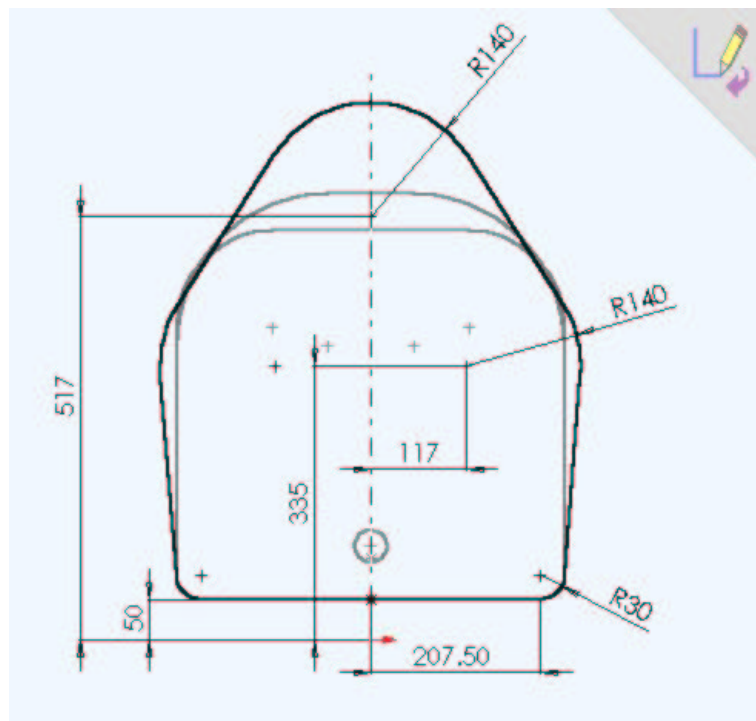


Figure C.27: First nose model "front hoop" cross section.

C.4.2 Nose 2

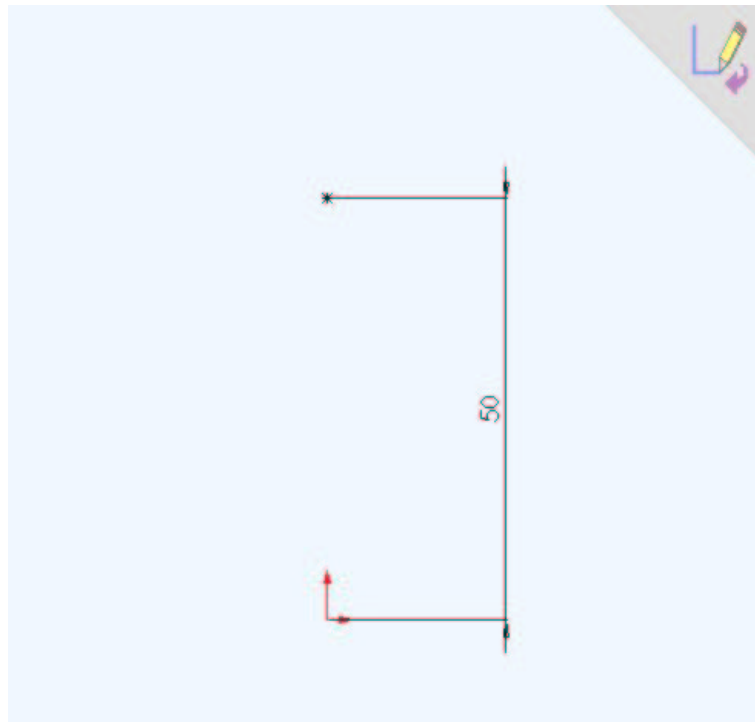


Figure C.28: Second nose model “nose point” cross section.

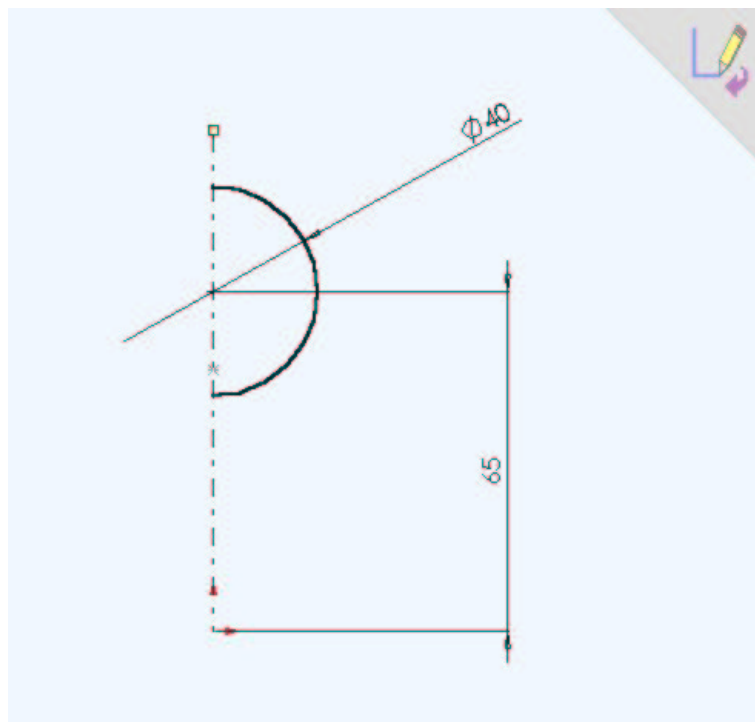


Figure C.29: Second nose model “nose shaper” cross section.

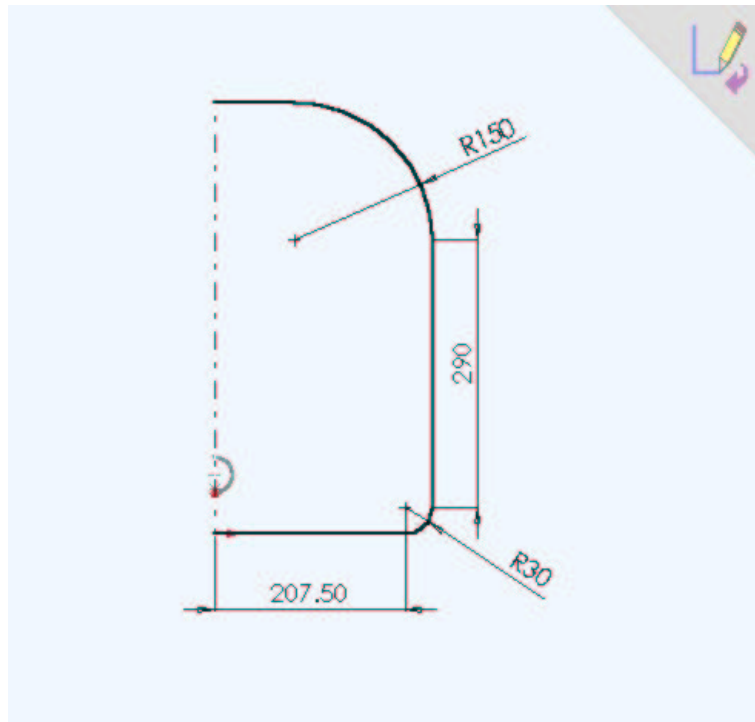


Figure C.30: Second nose model “bulkhead” cross section.

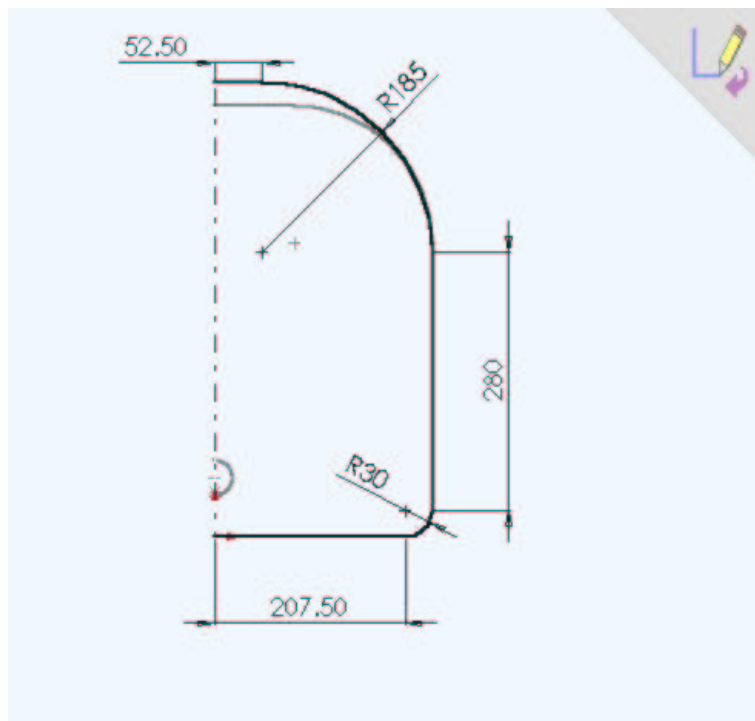


Figure C.31: Second nose model “kneebox” cross section.

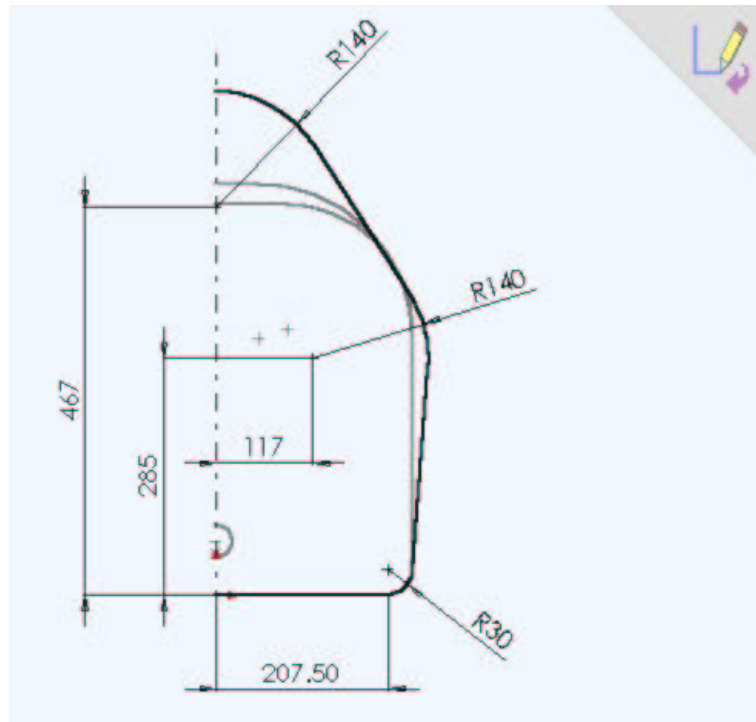


Figure C.32: Second nose model “front hoop” cross section.

C.4.3 Nose 2 - redesign

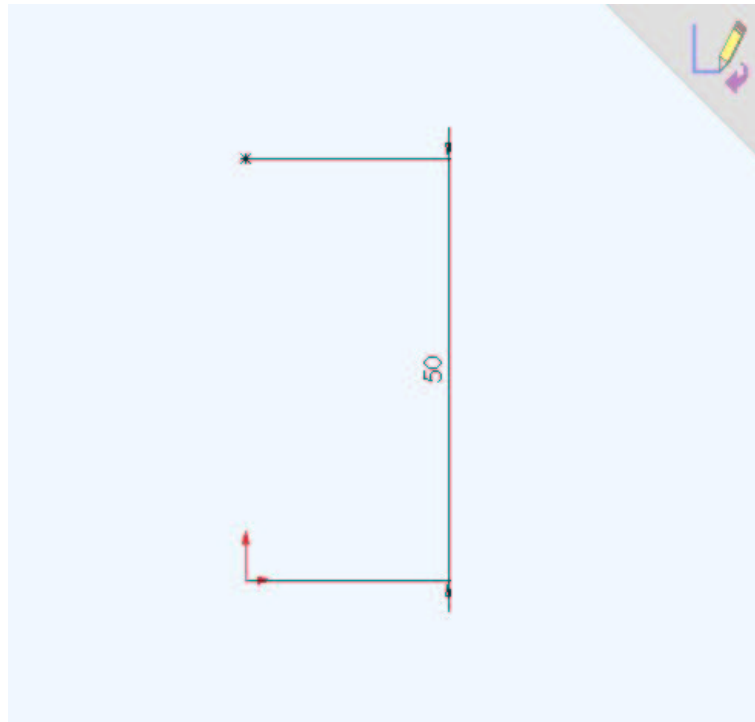


Figure C.33: Second nose model redesign “nose point” cross section.

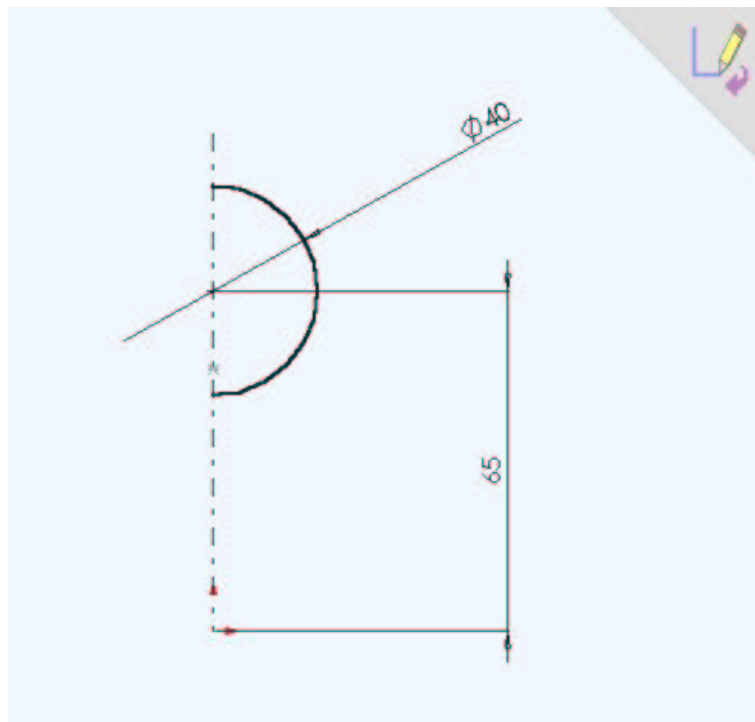


Figure C.34: Second nose model redesign “nose shaper” cross section.

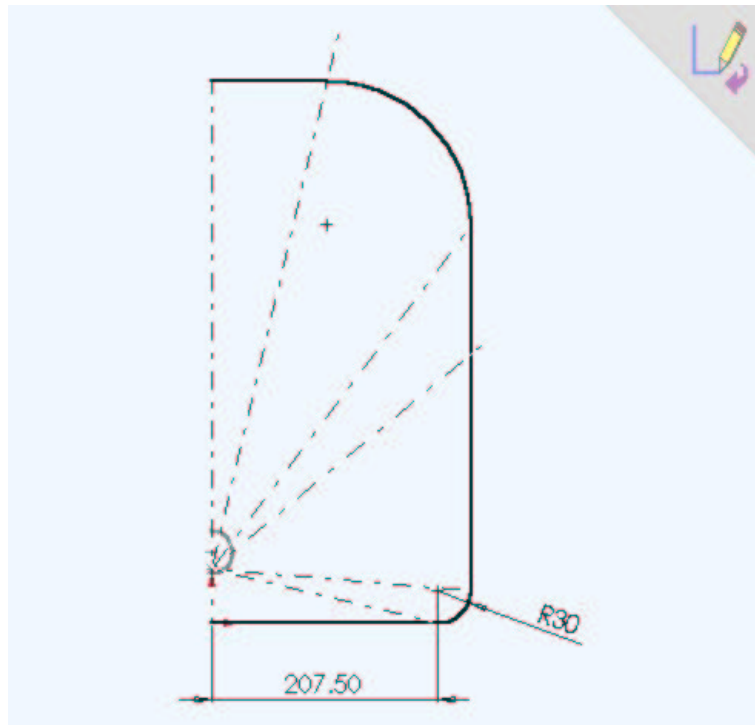


Figure C.35: Second nose model redesign “bulkhead” cross section.

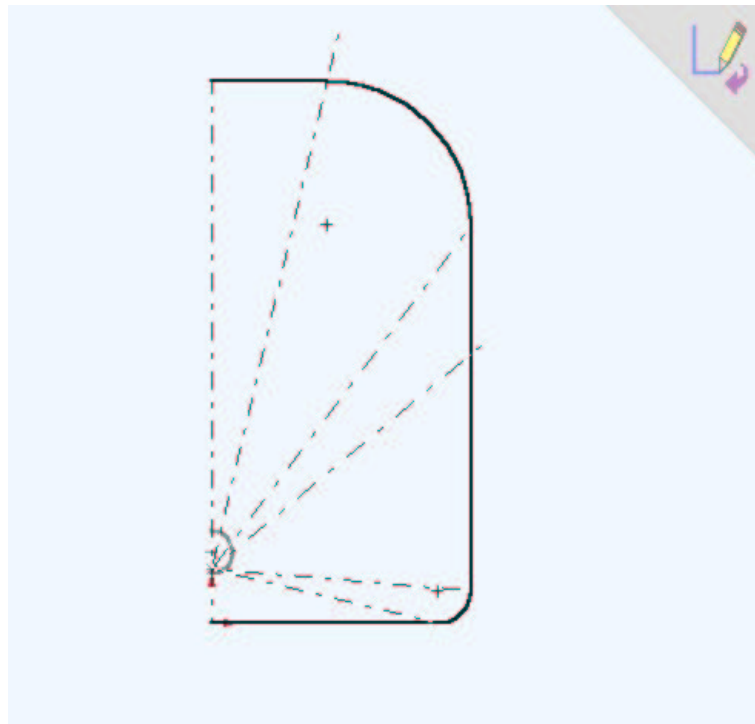


Figure C.36: Second nose model redesign “kneebox” cross section.

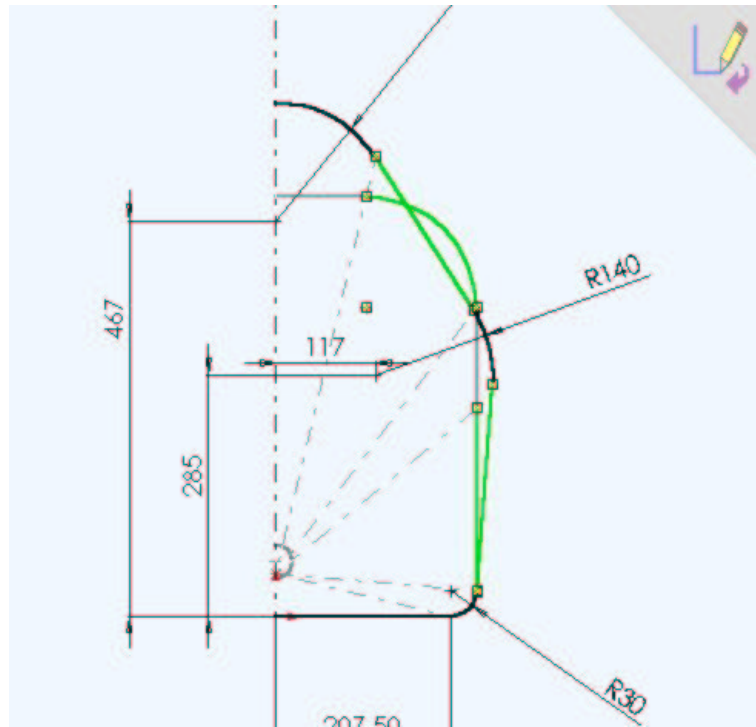


Figure C.37: Second nose model redesign “front hoop” cross section.

C.4.4 Nose 3

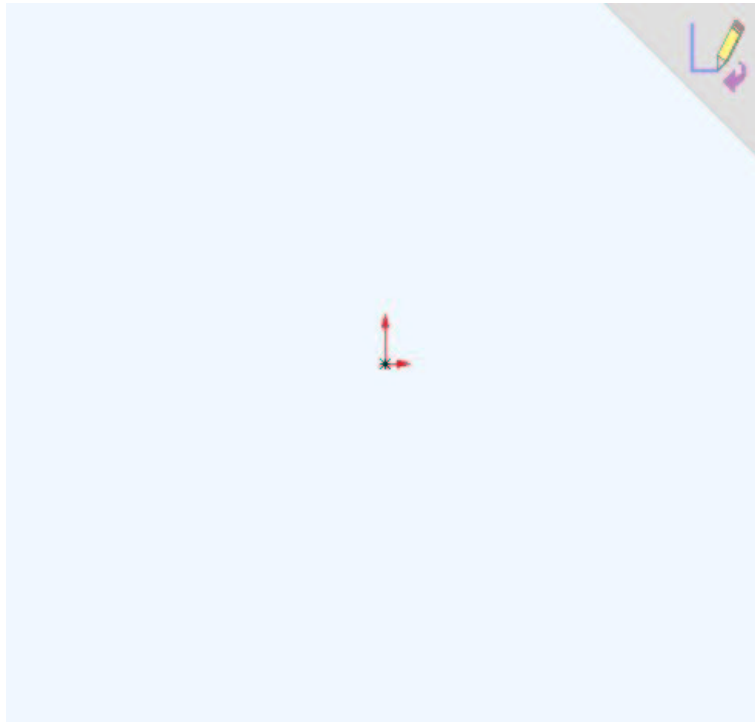


Figure C.38: Third nose model “nose point” cross section.

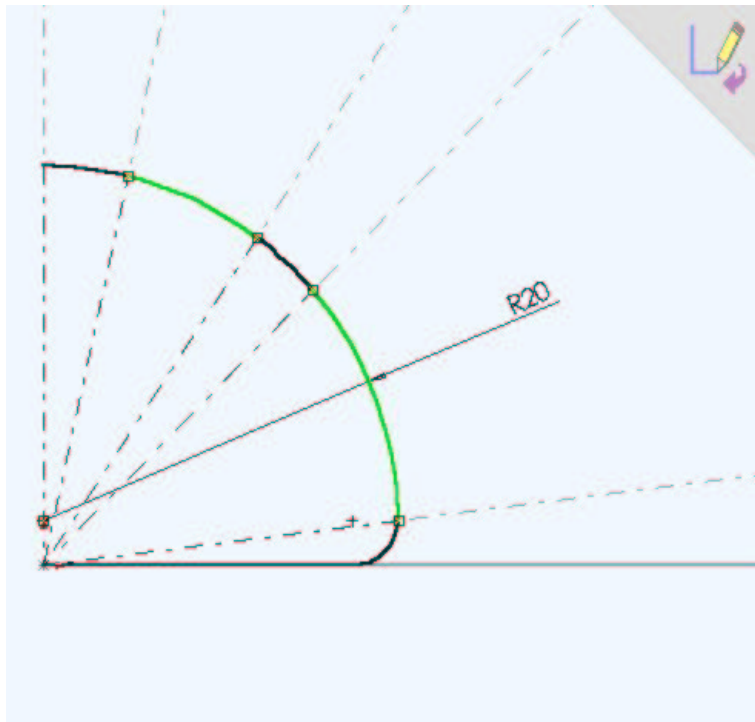


Figure C.39: Third nose model “nose shaper” cross section.

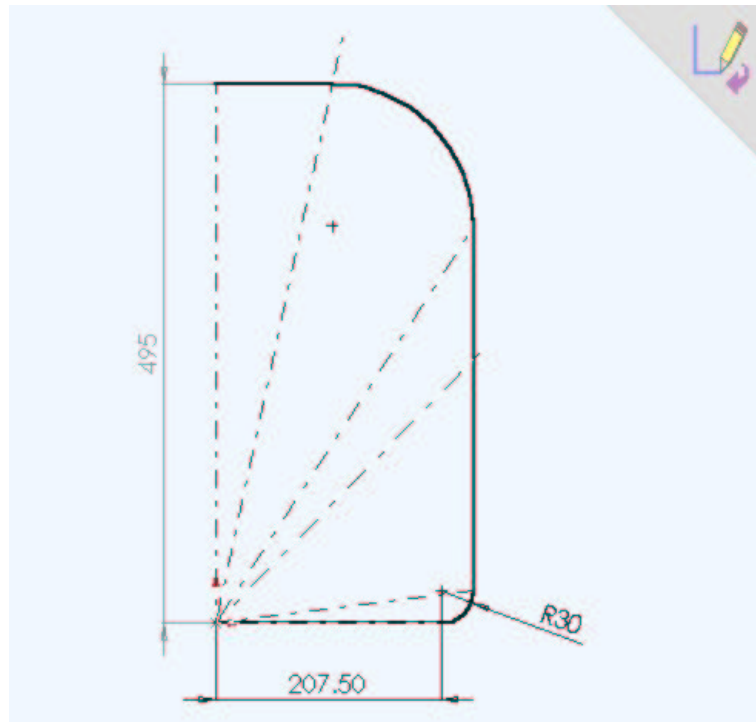


Figure C.40: Third nose model “bulkhead” cross section.

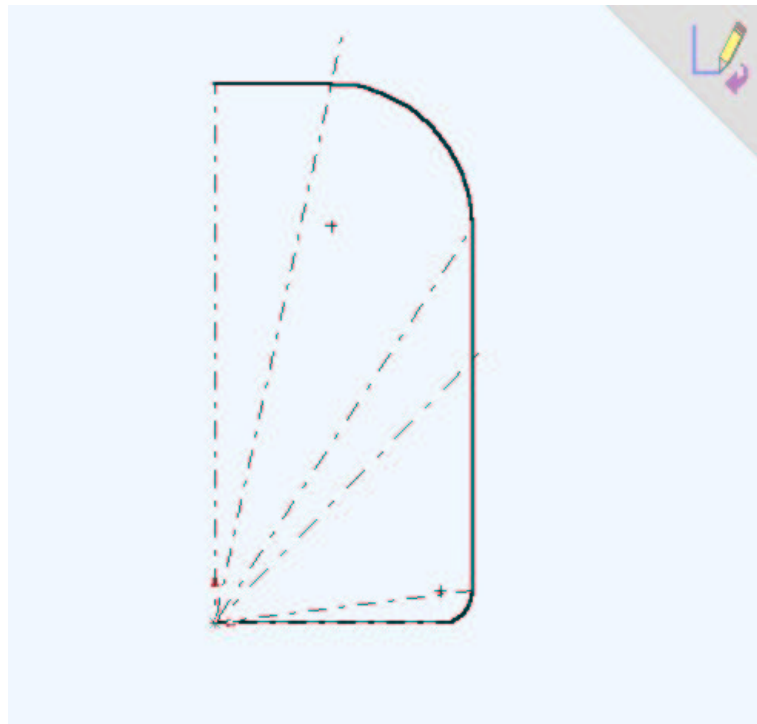


Figure C.41: Third nose model “kneebox” cross section.

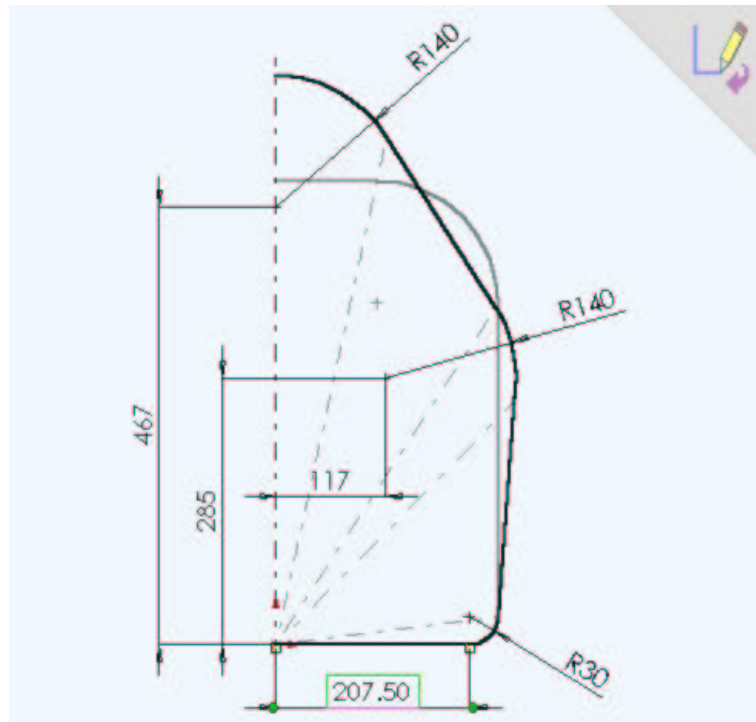


Figure C.42: Third nose model “front hoop” cross section.

C.4.5 Nose 4

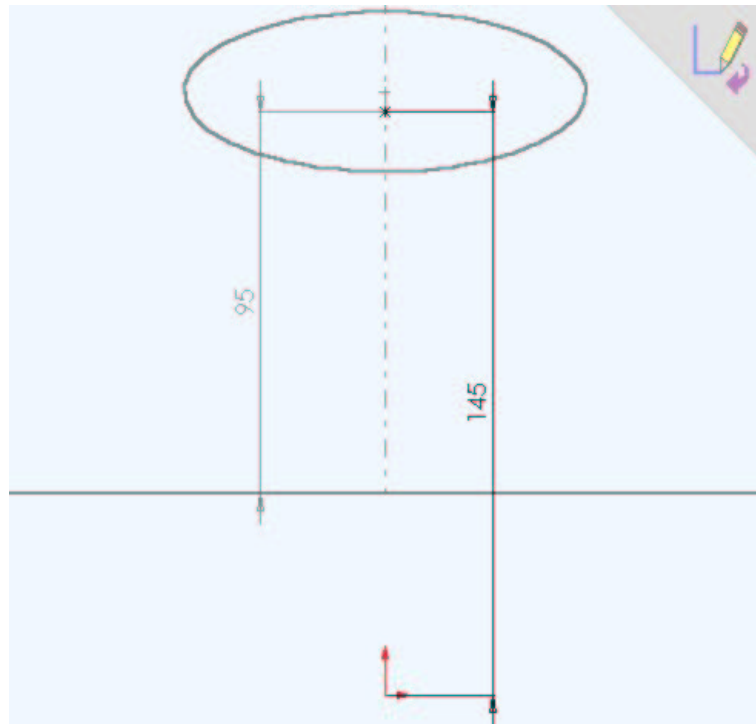


Figure C.43: Fourth nose model “nose point” cross section.

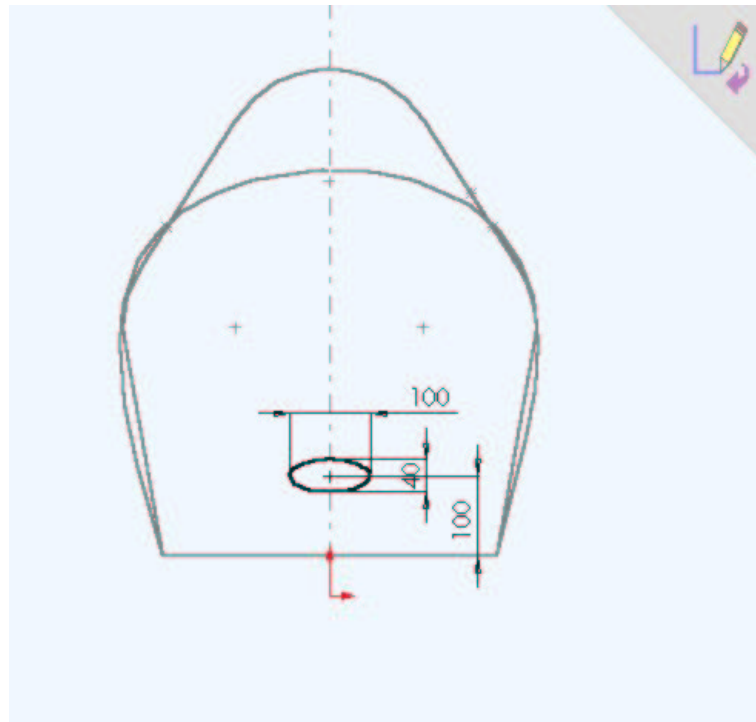


Figure C.44: Fourth nose model “nose shaper” cross section.

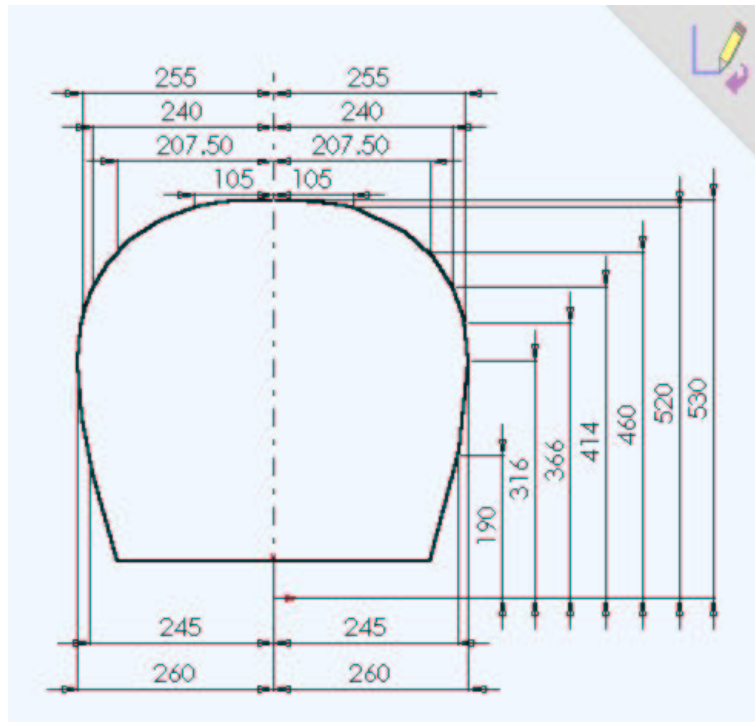


Figure C.45: Fourth nose model “bulkhead” cross section.

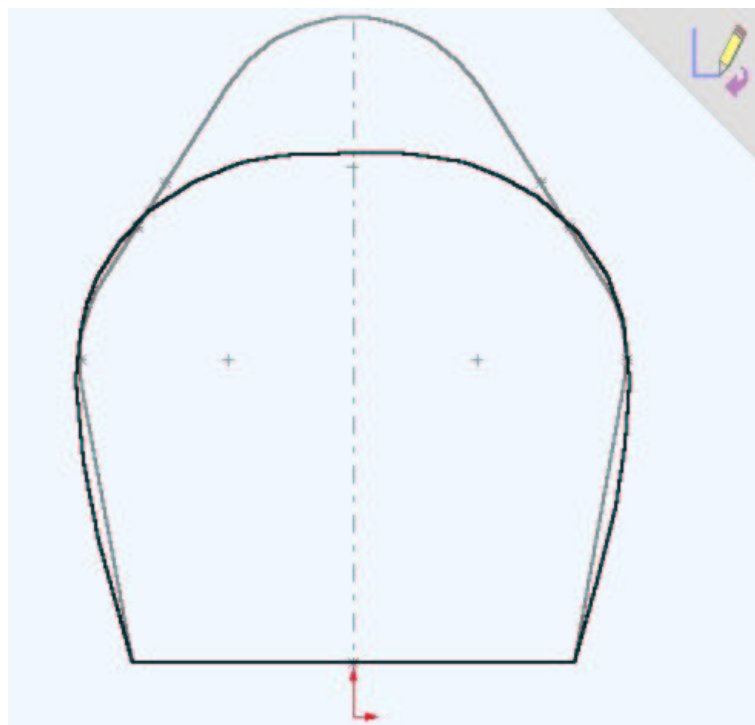


Figure C.46: Fourth nose model “kneebox” cross section.

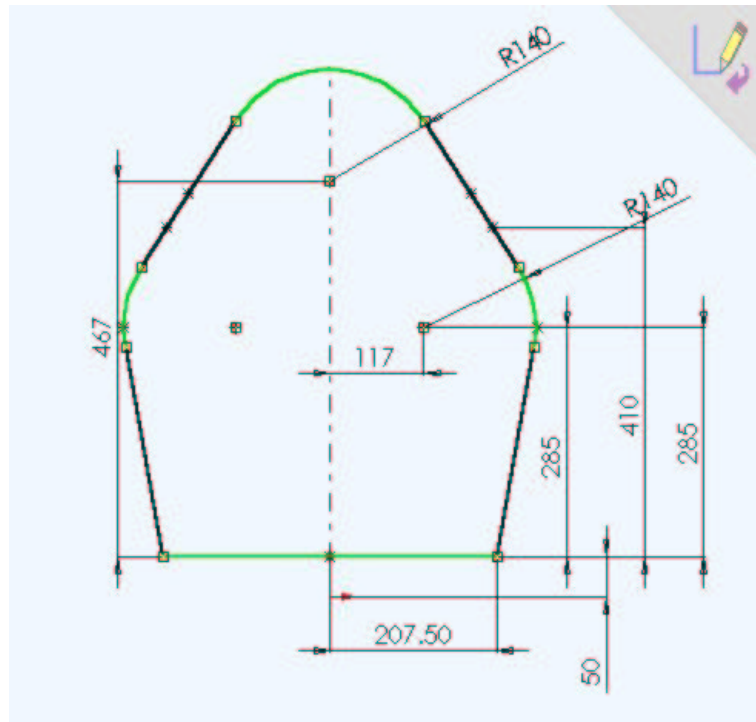


Figure C.47: Fourth nose model "front hoop" cross section.

C.4.6 Nose 5

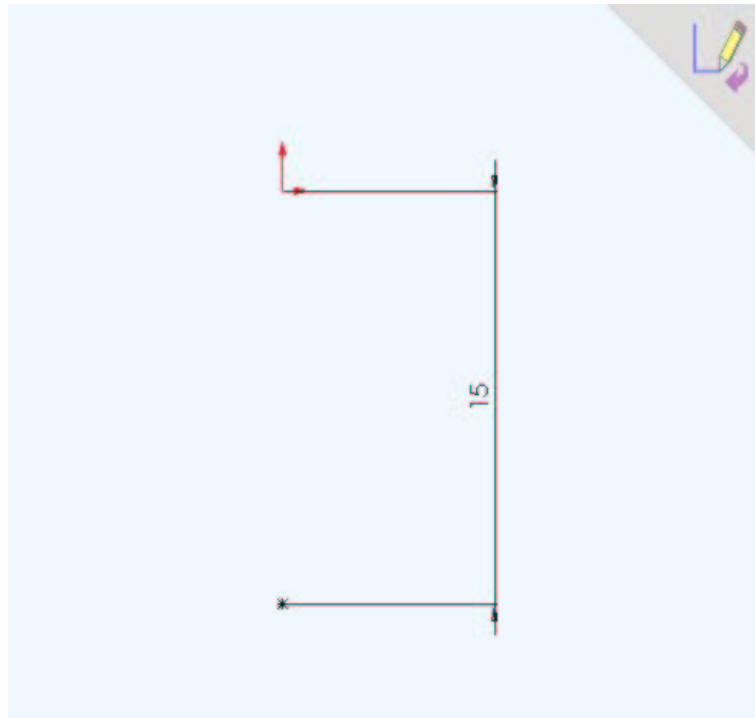


Figure C.48: Fifth nose model “nose point” cross section.

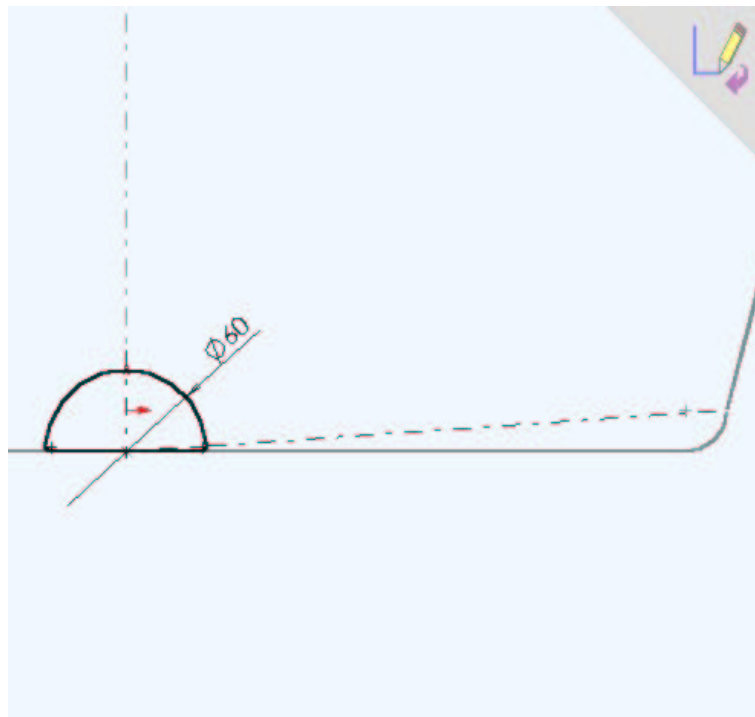


Figure C.49: Fifth nose model “nose shaper” cross section.

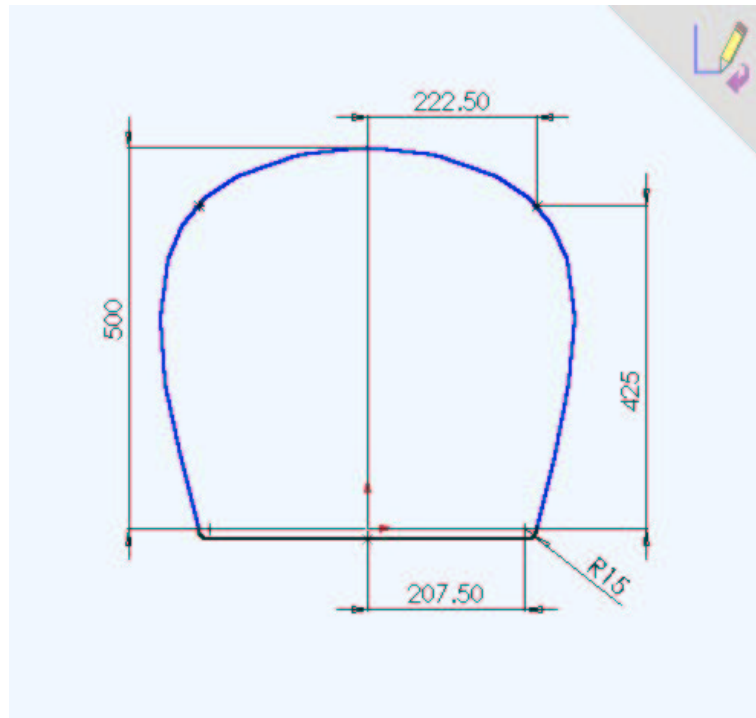


Figure C.50: Fifth nose model “bulkhead” cross section.

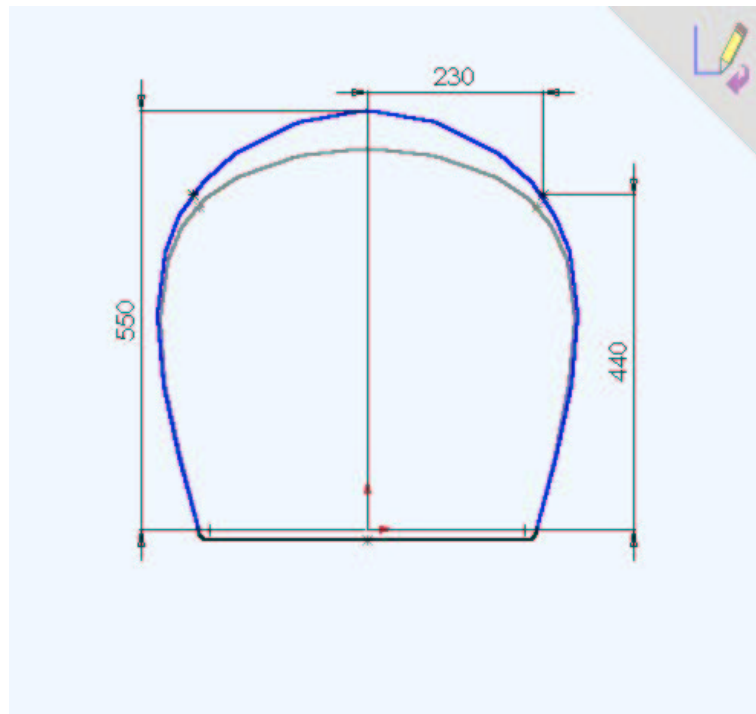


Figure C.51: Fifth nose model “kneebox” cross section.

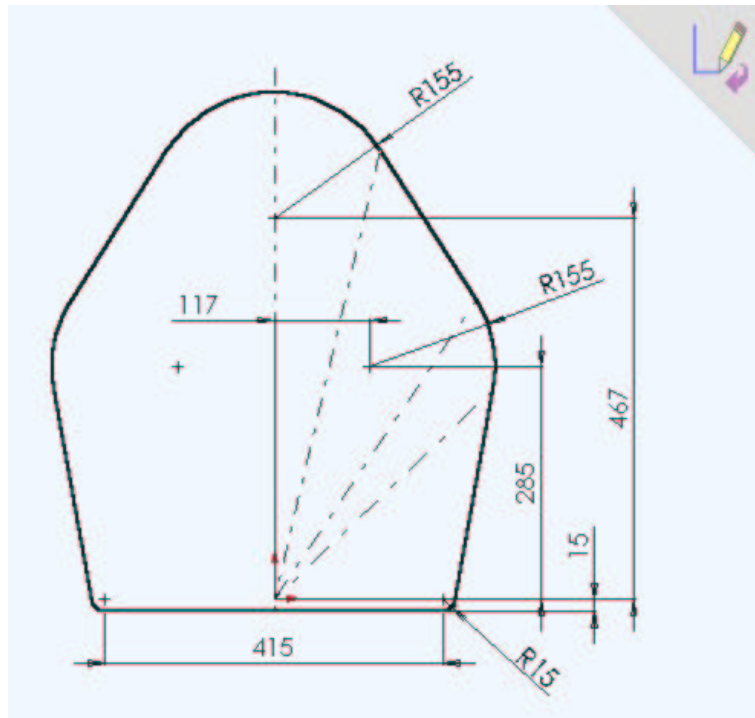


Figure C.52: Fifth nose model “front hoop” cross section.

C.4.7 Nose 6

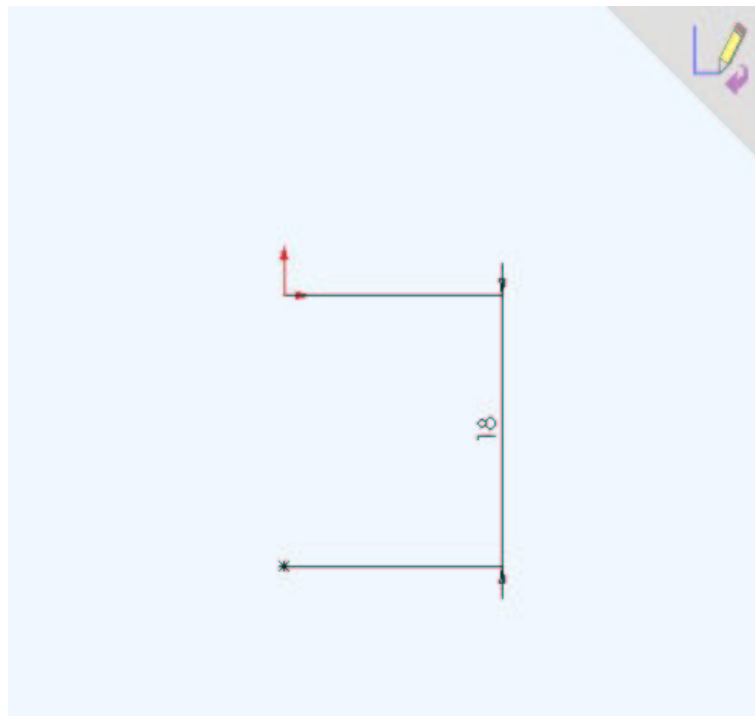


Figure C.53: Sixth nose model “nose point” cross section.

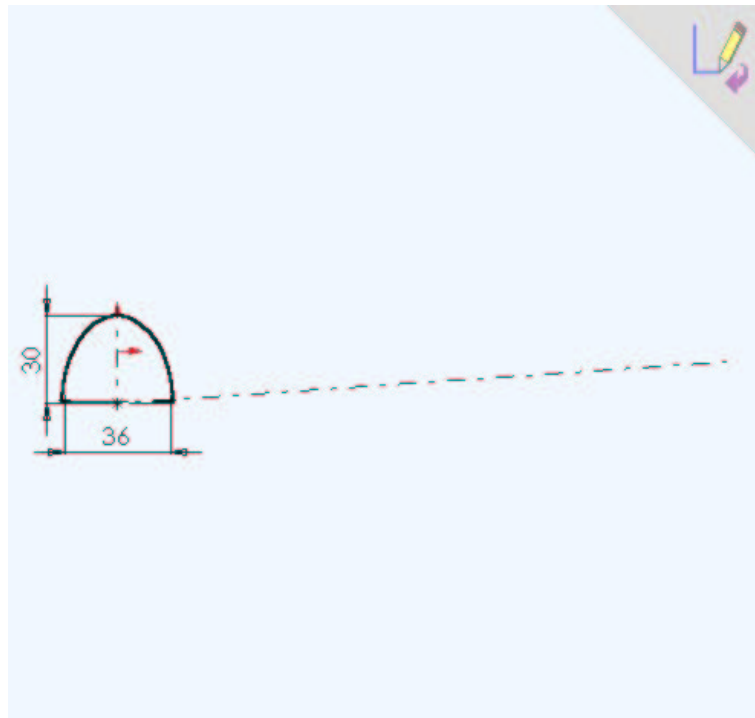


Figure C.54: Sixth nose model “nose shaper” cross section.

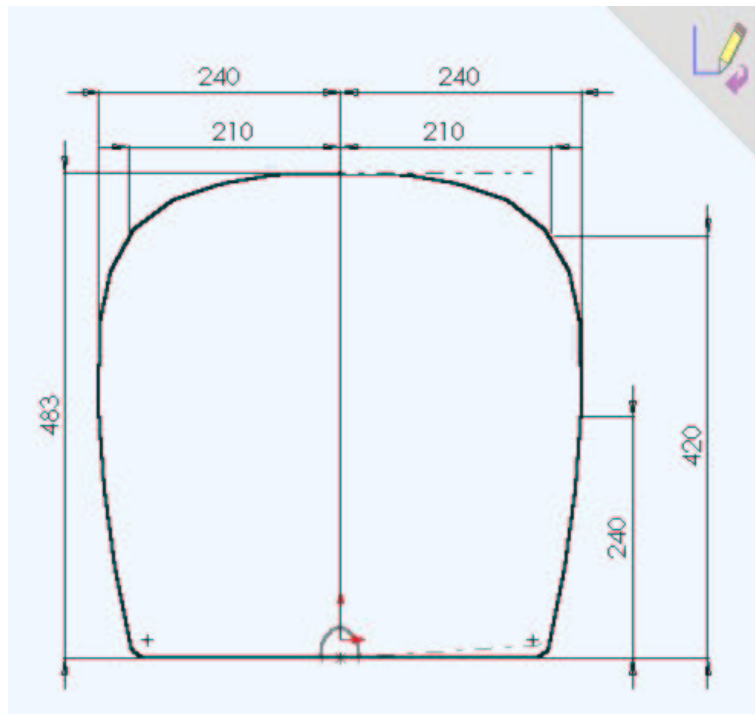


Figure C.55: Sixth nose model “bulkhead” cross section.

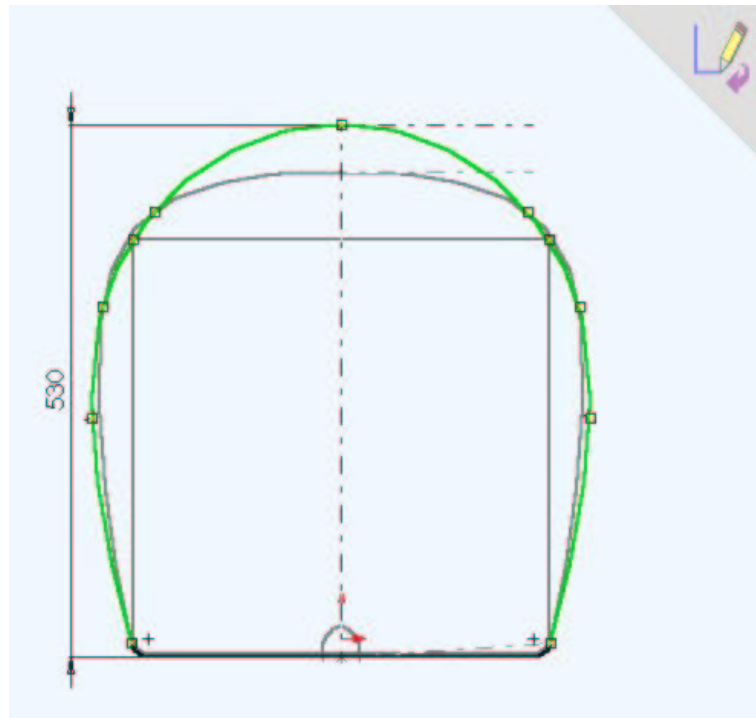


Figure C.56: Sixth nose model “kneebox” cross section.

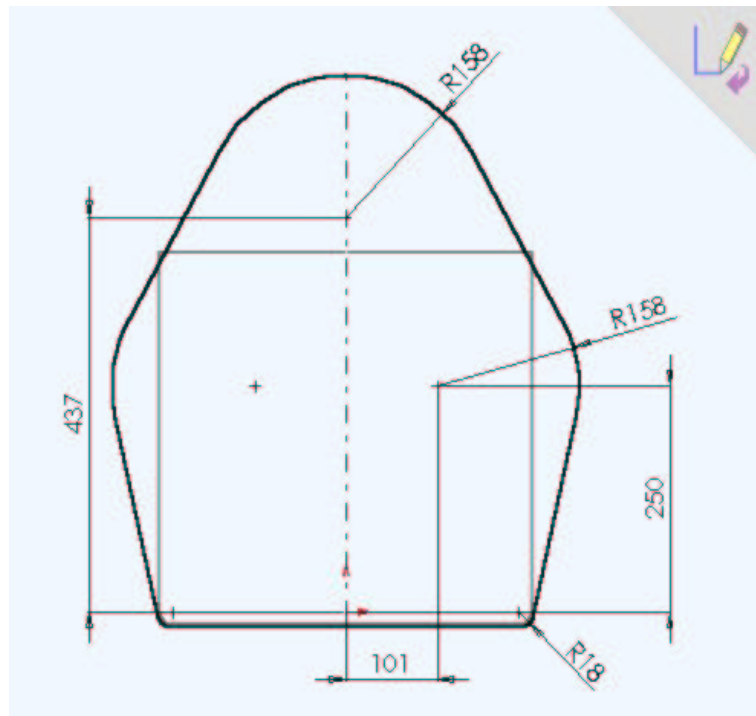


Figure C.57: Sixth nose model “front hoop” cross section.

C.4.8 The Final Model

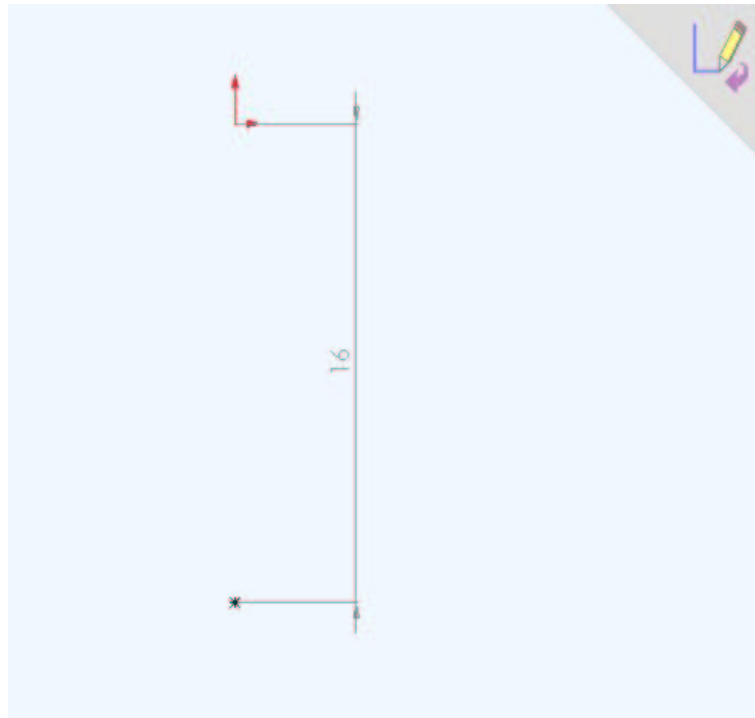


Figure C.58: Final nose model “nose point” cross section.

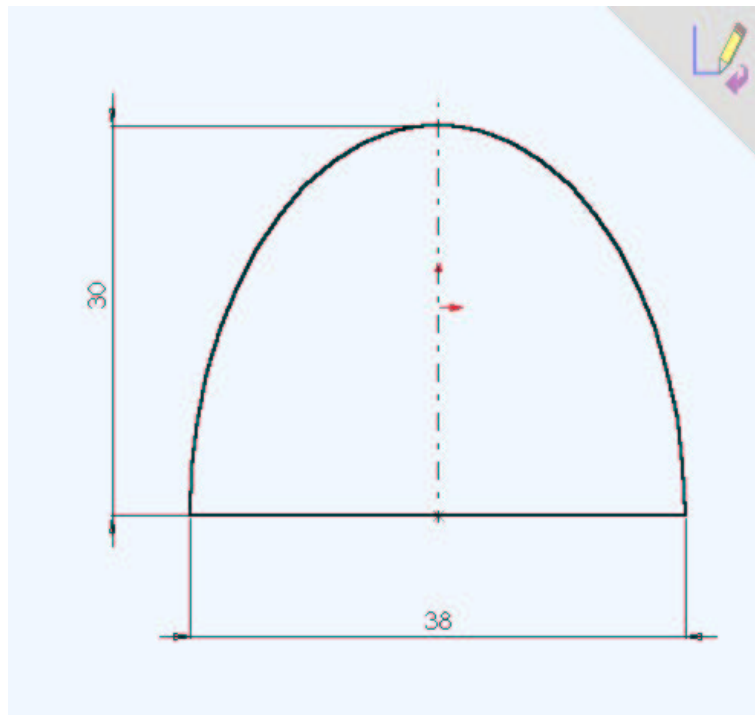


Figure C.59: Final nose model “nose shaper” cross section.

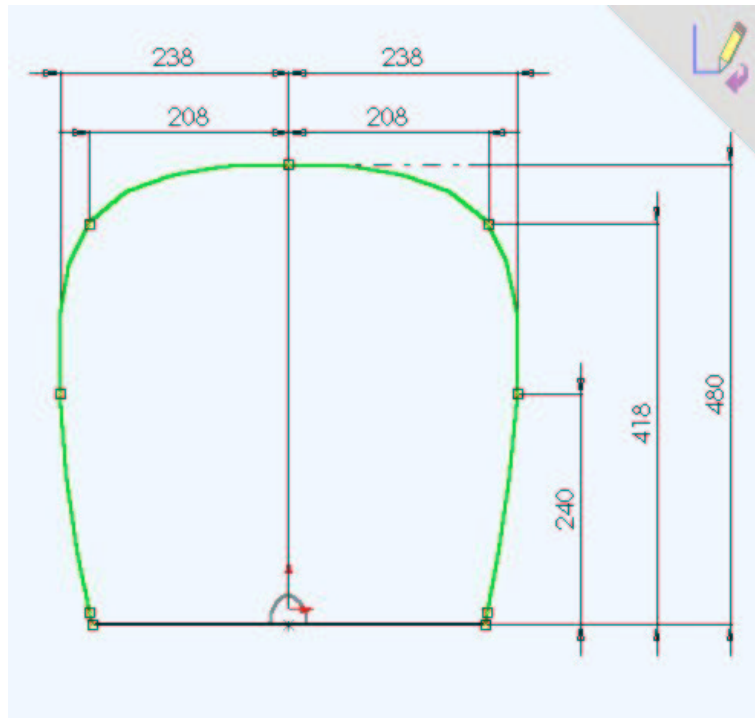


Figure C.60: Final nose model “bulkhead” cross section.

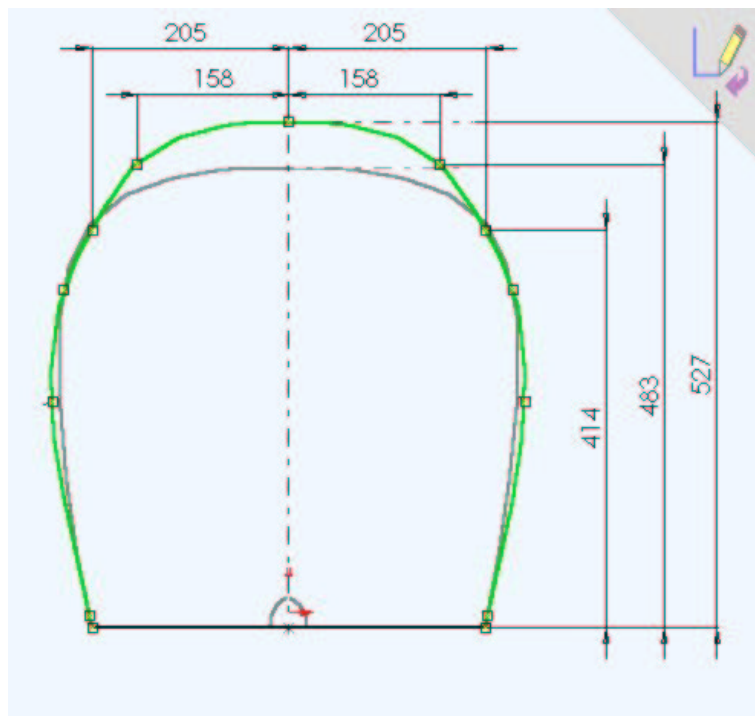


Figure C.61: Final nose model “kneebox” cross section.

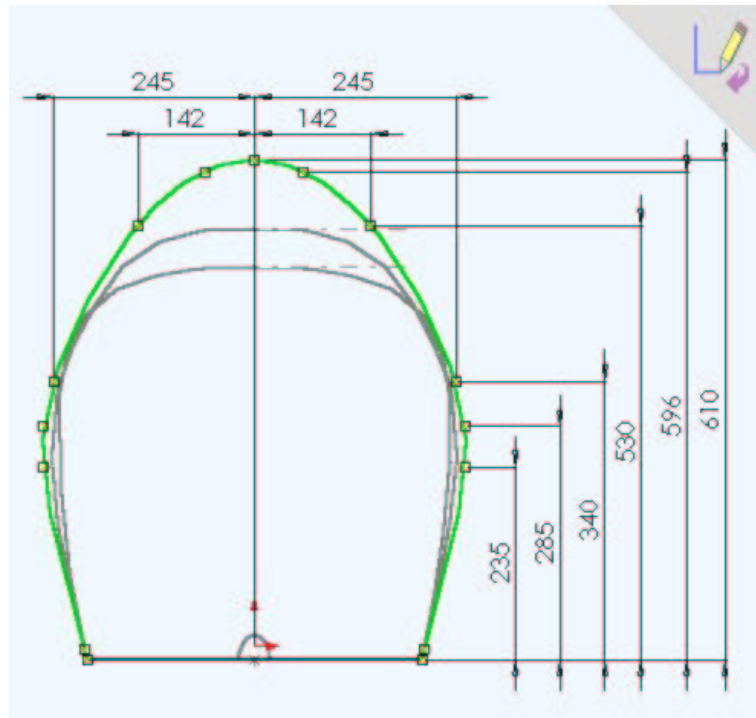


Figure C.62: Final nose model "front hoop" cross section.

Appendix D

Cost Report

D.1 Introduction to this Appendix

This appendix contains a cost report on the construction of the bodywork of the car, at a production volume of 5 units per day.

Name: Nose (1 off)

Materials:

Part	Amount	Unit	Description	\$/unit	Cost (\$)
Fibreglass	0.672	kg	chopped strand fibreglass mat	6.00	4.03
Resin	9.00	L	Epoxy resin + hardener	8.92	80.28
Materials Subtotal					\$84.31

Labour:

Description	Qty.	Amount	Unit	Manning	\$/Unit	Cost (\$)
Apply separator	1	5	min	2	0.583	5.83
First resin	1	5	min	2	0.583	5.83
Lay mat	6	10	min	2	0.583	69.96
Resin over mat	6	5	min	2	0.583	34.98
Final rolling	1	15	min	2	0.583	17.49
Extract mould	1	5	min	2	0.583	5.83
Trim edges	1	7	min	1	0.583	4.08
Drill hole	2		hole	1	0.350	0.70
Labour Subtotal						\$144.70

Name: Side Panels (2 off)

Materials:

Part	Amount	Unit	Description	\$/unit	Cost (\$)
Fibreglass	0.540	kg	chopped strand fibreglass mat	6.00	3.24
Resin	7.25	L	Epoxy resin + hardener	8.92	64.67
Materials Subtotal		(1 off)			\$67.91

Labour:

Description	Qty.	Amount	Unit	Manning	\$/Unit	Cost (\$)
Apply seperator	1	2	min	2	0.583	2.33
First resin	1	3	min	2	0.583	3.50
Lay mat	6	1	min	2	0.583	7.00
Resin over mat	6	3	min	2	0.583	20.99
Final rolling	1	7	min	2	0.583	8.16
Extract mould	1	8	min	2	0.583	9.33
Trim edges	1	7	min	1	0.583	4.08
Drill hole	2		hole	1	0.350	0.70
Labour Subtotal		(1 off)				\$56.09

Nose Total	\$229.01
Side Panel Total	\$247.99
GRAND TOTAL	\$477.00

The moulds were constructed at Buchanan Advanced Composites (BAC), Toowoomba, by team members, and materials and the use of their CNC milling machine were kindly donated by BAC.